

การศึกษาทางทฤษฎีของอนุพันธ์ไทอาคาลิกซ์[4]เอรีนและ  
สารประกอบเชิงซ้อนกับสังกะสี(II)



นาย บรรจบ วันโน

สถาบันวิทยบริการ

วิทยานิพนธ์นี้เป็นส่วนหนึ่งของการศึกษาตามหลักสูตรปริญญาวิทยาศาสตรดุษฎีบัณฑิต

สาขาวิชาเคมี ภาควิชาเคมี

คณะวิทยาศาสตร์ จุฬาลงกรณ์มหาวิทยาลัย

ปีการศึกษา 2549

ลิขสิทธิ์ของจุฬาลงกรณ์มหาวิทยาลัย

**THEORETICAL STUDY OF THIALIX[4]ARENE DERIVATIVES AND  
THEIR ZINC(II) COMPLEXES**



**Mr. Banchob Wanno**

**สถาบันวิทยบริการ**  
**จุฬาลงกรณ์มหาวิทยาลัย**

**A Dissertation Submitted in Partial Fulfillment of the Requirements for  
the Degree of Doctor of Philosophy Program in Chemistry**

**Department of Chemistry**

**Faculty of Science Chulalongkorn University**

**Academic year 2006**

**Copyright of Chulalongkorn University**

**Thesis Title**                      **Theoretical Study of Thiocalix[4]arene Derivatives and Their Zinc(II) Complexes**  
**By**                                        **Mr. Banchob Wann**  
**Field of Study**                      **Chemistry**  
**Thesis Advisor**                    **Associate Professor Vithaya Ruangpornvisuti, Dr.rer.nat.**

---

Accepted by the Faculty of Science, Chulalongkorn University in Partial Fulfillment of the Requirements for the Doctoral Degree

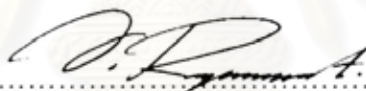


.....Dean of the Faculty of Science  
(Professor Piamsak Menasveta, Ph.D.)

Thesis Committee



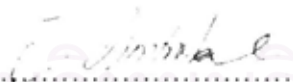
.....Chairman  
(Associate Professor Sirirat Kokpol, Ph.D.)



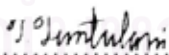
..... Thesis Advisor  
(Associate Professor Vithaya Ruangpornvisuti, Dr.rer.nat.)



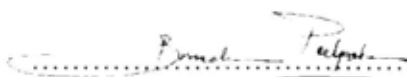
..... Member  
(Professor Supot Hannongbua, Dr.rer.nat.)



..... Member  
(Professor Jumras Limtrakul, Dr.rer.nat.)



..... Member  
(Associate Professor Thawatchai Tuntulani, Ph.D.)



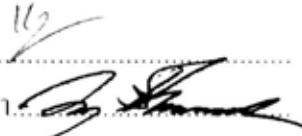
..... Member  
(Associate Professor Buncha Pulpoka, Ph.D.)

บรรจบ วันโน : การศึกษาทางทฤษฎีของอนุพันธ์ไทอาคาลิกซ์[4]เอรีนและสารประกอบ  
เชิงซ้อนกับสังกะสี(II). (THEORETICAL STUDY OF THIA CALIX[4]ARENE  
DERIVATIVES AND THEIR ZINC(II) COMPLEXES) อ. ที่ปรึกษา : รศ.ดร.  
วิทยา เรืองพรวิสุทธ์, 98 หน้า.

ได้คำนวณโครงสร้างทั้งสี่แบบของอนุพันธ์ไทอาคาลิกซ์[4]เอรีน และ ซัลโฟนิลคาลิกซ์[4]เอรีน  
โดยใช้ทฤษฎีฟังก์ชันความหนาแน่น (DFT) ที่ระดับ B3LYP/6-31G(d) ผลการคำนวณพบว่าโครงสร้างที่  
เสถียรที่สุดคือแบบโคนสำหรับอนุพันธ์ไทอาคาลิกซ์[4]เอรีนและแบบ 1,3-อัลเทอร์เนตสำหรับอนุพันธ์  
ซัลโฟนิลคาลิกซ์[4]เอรีน โดยพันธะไฮโดรเจนภายในโมเลกุลเป็นตัวแปรที่สำคัญที่มีต่อความเสถียรของ  
โครงสร้าง ได้คำนวณอิทธิพลของตัวทำละลายได้แก่ น้ำ คลอโรฟอร์ม และ ไดคลอโรโรมีเทน ที่มีต่อความ  
เสถียรของอนุพันธ์ซัลโฟนิลคาลิกซ์[4]เอรีน โดยใช้แบบจำลอง CPCM ร่วมกับวิธี DFT พบว่าตัวทำ  
ละลายทั้งหมดมีผลกระทบต่อความเสถียรของโครงสร้างเพียงเล็กน้อย นอกจากนี้ได้ทำนายการ  
เปลี่ยนโครงสร้างระหว่างแบบโคนกับแบบพาร์เซียลที่ระดับของทฤษฎี B3LYP/6-31G(d) พบว่าชนิดของ  
หมู่เชื่อมต่อกาลิกซ์มีผลต่อการเปลี่ยนโครงสร้างเป็นอย่างมาก โดยที่พลังงานด้านการหมุนของหมู่  
เชื่อมต่อกาลิกซ์ (-SO<sub>2</sub>-) ของอนุพันธ์ซัลโฟนิลคาลิกซ์[4]เอรีน มีค่าประมาณสองเท่าของหมู่เชื่อมต่อก  
ซัลเฟอร์ (-S-) ของอนุพันธ์ไทอาคาลิกซ์[4]เอรีน ได้ศึกษาการเกิดสารประกอบเชิงซ้อนระหว่างไอออน  
สังกะสี(II)กับโครงสร้างแบบโคนของไทอาคาลิกซ์[4]เอรีนและซัลโฟนิลคาลิกซ์ที่ระดับของทฤษฎี  
B3LYP/6-31G(d) พบว่าปฏิกิริยาการเกิดสารประกอบทั้งหมดเป็นแบบคายพลังงานความร้อน พลังงาน  
ของการเกิดสารประกอบเชิงซ้อนที่สูงที่สุดเป็นของสารประกอบระหว่างสังกะสี(II)กับไทอาคาลิกซ์[4]เอ  
รีน ซึ่งเป็นผลมาจากการเกิดปรากฏการณ์การส่งผ่านประจุระหว่างโลหะกับลิแกนด์ (MLTC) ที่พบใน  
สารประกอบนี้

ได้ศึกษาสารประกอบเชิงซ้อนระหว่างตัวรับไทอาคาลิกซ์[4]เอรีนและคาลิกซ์[4]เอรีนกับ  
คาร์บอกซิเลทชนิดต่างๆ (อะซิเตต ออกซาเลต มาโลเนต ซักซิเนต กลูทาเรต อะดิเปต และ พิเมเลต)โดย  
ใช้ระเบียบวิธีแบบ ONIOM(B3LYP/6-31G(d):AM1) คำนวณพลังงานของโครงสร้างของ  
สารประกอบที่ค้นหามาได้ทั้งหมดด้วยระเบียบวิธีแบบ B3LYP/6-31G(d) พบว่าความเสถียรสัมพัทธ์  
สำหรับสารประกอบของไทอาคาลิกซ์[4]เอรีนและสารประกอบของคาลิกซ์[4]เอรีนเรียงตามลำดับเป็น  
ดังนี้ มาโลเนต > ออกซาเลต > ซักซิเนต > กลูทาเรต และ ออกซาเลต > มาโลเนต > ซักซิเนต > กลูทา  
เรต > อะดิเปต > พิเมเลต ตามลำดับ

ภาควิชา.....เคมี.....  
สาขาวิชา.....เคมี.....  
ปีการศึกษา.....2549.....

ลายมือชื่อนิสิต.....  
ลายมือชื่ออาจารย์ที่ปรึกษา.....  


# # 4573820923: MAJOR CHEMISTRY

KEY WORD: CALIX[4]ARENE / THIALCALIX[4]ARENE / SULFONYLCALIX[4]ARENE / PROTON AFFINITY / ZINC COMPLEX / CARBOXYLATE / DFT / ONIOM

BANCHOB WANNO: THEORETICAL STUDY OF THIALCALIX[4]ARENE DERIVATIVES AND THEIR ZINC(II) COMPLEXES. THESIS ADVISOR: ASSOC. PROF. VITHAYA RUANGPORNVISUTI, 98 pp.

The four typical conformers of thiacalix[4]arene and sulfonylcalix[4]arene derivatives have been studied using the density functional theory (DFT) at B3LYP/6-31G(d) level of theory. The most stable conformer is found to be *cone* for thiacalix[4]arene derivatives and *1,3-alternate* for sulfonylcalix[4]arene derivatives in which an intramolecular hydrogen bond plays an important factor for the conformational stability. Effect of solvents, i.e., water, chloroform and dichloromethane on stability of sulfonylcalix[4]arene derivatives has been computed using the CPCM solvation model combined with DFT method. It is found that all solvents are slightly effect to their stability. The interconversion between *cone* and *partial cone* conformers found in each derivative has been predicted at B3LYP/6-31G(d) level of theory. It is clearly seen that bridge types of calix[4]arene show a strongly effect to the interconversion whereas the interconversion barrier of sulfonyl (-SO<sub>2</sub>-) bridges of sulfonylcalix[4]arene derivatives is higher than that of sulfur (-S-) bridges of thiacalix[4]arene derivatives approximately twice times. The complexations between zinc(II) ion and the *cone* conformer of thiacalix[4]arene and sulfonylcalix[4]arene derivatives have been investigated at B3LYP/6-31G(d) level of theory. The result shows that all of complexations are an exothermic process. Furthermore, the complexation between the Zinc(II) ion and thiacalix[4]arene yields the highest energy which results from the metal-ligand charge transfer (MLCT) effect found on its complex.

The host – guest complex of thiacalix[4]arene (tatbtc4a) and calix[4]arene (tatbc4a) receptors with a series of carboxylate guests (acetate, oxalate, malonate, succinate, glutarate, adipate, and pimelate) has been studied using the ONIOM(B3LYP/6-31G(d):AM1) method. All optimized structures are carried out by the B3LYP/6-31G(d) single point calculation. The relative stabilities of the tatbtc4a and tatbc4a complexes with carboxylates in order are malonate > oxalate > succinate > glutarate and oxalate > malonate > succinate > glutarate > adipate > pimelate, respectively.

Department.....Chemistry.....

Field of study.....Chemistry.....

Academic year.....2006.....

Student's signature..........

Advisor's signature..........

## ACKNOWLEDGEMENTS

I would like to take this opportunity to thank all those who have contributed to this work. Firstly, I especially thank Associate Professor Vithaya Ruangpornvisuti for his expert guidance as well as his tremendous personal support and encouragement.

I would like to acknowledge the committee, Associate Professor Dr. Sirirat Kokpol, Professor Dr. Supot Hannongbua, Professor Dr. Jumras Limtrakul, Associate Professor Dr. Thawatchai Tuntulani, and Associate Professor Dr. Buncha Pulpoka for their valuable suggestions and comments. I am very grateful to Professor Dr. Sean C. Smith and Dr. Aijun Du for their support.

Special thanks to all members in Supramolecular Chemistry Research Unit for their help. I also would like to thank all my friends at Chulalongkorn University for their friendship throughout my study.

I would like to acknowledge the grant and funding supports provided by Maharakham University, the Commission on Higher Education and the Royal Golden Jubilee (RGJ) grant (No. PHD47K0164).

I am very grateful to the Molecular Modeling and Computational Chemistry Research Group (MMCCRG) of Supramolecular Chemistry Research Unit (SCRU) at the Chulalongkorn University and the Centre for Computational Molecular Science (CCMS) at the University of Queensland for their facility of computer time.

Finally, I would like to thank my family who always encourage and support me.

สถาบันวิทยบริการ  
จุฬาลงกรณ์มหาวิทยาลัย

# CONTENTS

	<b>Page</b>
<b>ABSTRACT IN THAI</b> .....	<b>iv</b>
<b>ABSTRACT IN ENGLISH</b> .....	<b>v</b>
<b>ACKNOWLEDGEMENTS</b> .....	<b>vi</b>
<b>CONTENTS</b> .....	<b>vii</b>
<b>LIST OF FIGURES</b> .....	<b>ix</b>
<b>LIST OF TABLES</b> .....	<b>xiv</b>
<b>LIST OF ABBREVIATIONS</b> .....	<b>xvi</b>
<b>CHAPTER I INTRODUCTION</b> .....	<b>1</b>
1.1 Introduction of calix[4]arenes.....	1
1.2 Thiacalix[4]arene derivatives.....	2
1.3 Experimental study on calix[4]arenes and calix[4]arene complexes.....	4
1.4 Theoretical study on thiacalix[4]arenes and thiacalix[4]arene complexes.....	4
1.5 Overall objectives.....	6
<b>CHAPTER II THEORETICAL METHOD</b> .....	<b>7</b>
2.1 Density functional theory.....	8
2.1.1 The Hohenberg-Kohn theory.....	9
2.1.2 The Kohn-Sham equations.....	9
2.1.3 DFT exchange and correlations.....	11
2.1.4 Hybrid functions.....	12
2.2 Semi-empirical methods.....	13
2.2.1 The extended Hückel method.....	14
2.2.2 Neglect of differential overlap.....	14
2.2.3 Neglect of diatomic differential overlap.....	15
2.3 Hybrid methods.....	15
2.4 Basis sets.....	16
2.4.1 Split valence basis sets.....	17
2.4.2 Polarized basis sets.....	17
2.4.3 Diffuse basis sets.....	18
2.5 Basis set superposition error (BSSE).....	18

	<b>Page</b>
2.6 Molecular properties.....	19
2.6.1 Geometry optimization.....	19
2.6.2 Normal mode analysis or frequency calculation.....	22
2.7 Thermochemistry.....	24
2.7.1 Partition functions.....	24
2.7.2 Thermodynamic properties.....	26
2.8 Polarizable continuum solvent model.....	27
<b>CHAPTER III: RESULTS AND DISCUSSION.....</b>	<b>28</b>
3.1 Theoretical study of thiacalix[4]arene derivatives.....	29
3.1.1 Computational method.....	29
3.1.2 Comparison geometrical structure with calix[4]arene.....	30
3.1.3 Geometrical structure and energetic stability.....	31
3.1.4 Inversion barrier for <i>cone</i> – <i>partial cone</i> interconversion.....	49
3.1.5 Frontier molecular orbital energy gaps.....	51
3.1.6 Molecular electrostatic potential surface.....	53
3.1.7 Proton affinity.....	56
3.2 Complexation of thiacalix[4]arene and sulfonylcalix[4]arene derivative with zinc(II) ion .....	58
3.2.1 Computational method.....	58
3.2.2 Complexation properties.....	59
3.3 Host–guest complexes of thiacalix[4]arene and sulfonylcalix[4]arene derivatives with carboxylate and dicarboxylates study.....	67
3.3.1 Computational method.....	68
3.3.2 Complexation properties of amino- <i>p-tert</i> -butylthiacalix[4]arene	73
3.3.3 Complexation properties of amino- <i>p-tert</i> -butylcalix[4]arene.....	77
<b>CHAPTER IV CONCLUSIONS AND SUGGESTIONS.....</b>	<b>82</b>
<b>REFERENCES.....</b>	<b>84</b>
<b>APPENDICES.....</b>	<b>91</b>
<b>APPENDIX I.....</b>	<b>92</b>
<b>APPENDIX II.....</b>	<b>95</b>
<b>BIOGRAPHY.....</b>	<b>98</b>



## LIST OF FIGURES

Figure	Page
1.1 Chemical structures of (a) calix[4]arene, <b>C4A</b> and (b) four conformational isomers of calix[4]arene derivatives, where R and R' are any substituted groups.....	2
1.2 Chemical structures of thiacalix[4]arene and sulfonylcalix[4]arene derivatives.....	3
1.3 Proposed coordination manners of thiacalix[4]arene derivatives with (a) – (g) metal ions and (h) inclusion complex.....	4
2.1 Newton-Raphson steps (in one dimension) for optimizing geometries.....	21
3.1 Comparison of (a) classical calix[4]arene ( <b>C4A</b> ) and <b>1</b> and (b) <b>C4A</b> and <b>7</b> structures obtained at the B3LYP/6-31G(d) level of theory. Hydrogen bonds are displayed in dashed lines.....	31
3.2 Atomic labeling of (a) thiacalix[4]arene, (b) mercaptothiacalix[4]arene and (c) aminothiacalix[4]arene and their zinc(II) complexes .....	32
3.3 Atomic labeling of (a) sulfonylcalix[4]arene, (b) mercaptosulfonylcalix[4]arene and (c) aminosulfonylcalix[4]arene and their zinc(II) complexes.....	33
3.4 Conformational geometries of typical conformers of thiacalix[4]arenes ( <b>1</b> ) optimized at the B3LYP/6-31G(d) level of theory.....	35
3.5 Conformational geometries of typical conformers of <i>p-tert</i> -butylthiacalix [4]arenes ( <b>2</b> ) optimized at the B3LYP/6-31G(d) level of theory.....	35
3.6 Conformational geometries of typical conformers of mercaptothiacalix[4]arenes ( <b>3</b> ) optimized at the B3LYP/6-31G(d) level of theory.....	36
3.7 Conformational geometries of typical conformers of mercapto- <i>p-tert</i> -butylthiacalix [4]arenes ( <b>4</b> ) optimized at the B3LYP/6-31G(d) level of theory.....	36
3.8 Conformational geometries of typical conformers of aminothiacalix[4]arenes ( <b>5</b> ) optimized at the B3LYP/6-31G(d) level of theory.....	37
3.9 Conformational geometries of typical conformers of amino- <i>p-tert</i> -butylthiacalix[4] arenes ( <b>6</b> ) optimized at the B3LYP/6-31G(d) level of theory.....	37

<b>Figure</b>	<b>Page</b>
3.10 Conformational geometries of typical conformers of sulfonylcalix[4]arenes (7) optimized at the B3LYP/6-31G(d) level of theory.....	40
3.11 Conformational geometries of typical conformers of <i>p-tert</i> -butylsulfonyl calix[4] arenes (8) optimized at the B3LYP/6-31G(d) level of theory.....	40
3.12 Conformational geometries of typical conformers of mercaptosulfonyl calix[4] arenes (9) optimized at the B3LYP/6-31G(d) level of theory.....	41
3.13 Conformational geometries of typical conformers of mercapto- <i>p-tert</i> -butyl sulfonyl calix[4]arenes (10) optimized at the B3LYP/6-31G(d) level of theory.....	41
3.14 Conformational geometries of typical conformers of aminosulfonylcalix[4] arenes (11) optimized at the B3LYP/6-31G(d) level of theory.....	42
3.15 Conformational geometries of typical conformers of amino- <i>p-tert</i> -butyl sulfonylcalix[4]arenes (12) optimized at the B3LYP/6-31G(d) level of theory.....	42
3.16 Relative energies computed at the B3LYP/6-31G(d)// B3LYP/6-31G(d) level of theory phase of <i>cone</i> , <i>partial cone</i> , <i>1,2-alternate</i> and <i>1,3-alternate</i> conformers in gas phase of thiacalix[4]arene derivatives for (a) smaller compound series and (b) bigger compound series ( <i>p-tert</i> -butyl derivatives).	45
3.17 Relative energies computed at the B3LYP /6-31G(d)//B3LYP /6-31G(d) level of theory phase of <i>cone</i> , <i>partial cone</i> , <i>1,2-alternate</i> and <i>1,3-alternate</i> conformers in gas phase of sulfonylcalix[4]arene derivatives for (a) smaller compound series and (b) bigger compound series ( <i>p-tert</i> -butyl derivatives).	46
3.18 Relative energies computed at the CPCM/B3LYP/6-31G(d) level of theory of <i>cone</i> , <i>partial cone</i> , <i>1,2-alternate</i> and <i>1,3-alternate</i> conformers in gas phase (●), water (▲), chloroform (■) and dichloromethane (▼) of the (a) sulfonyl calix[4]arene, (b) mercaptosulfonylcalix[4]arene and (c) amino-sulfonylcalix[4]arene.....	48

<b>Figure</b>	<b>Page</b>
3.19 The energy profiles for interconversion reactions between <i>cone</i> (left) and <i>partial cone</i> (right) conformers of thiacalix[4]arene ( <b>1</b> , <b>3</b> , and <b>5</b> ) and sulfonylcalix[4] arene ( <b>7</b> , <b>9</b> , and <b>11</b> ) derivatives obtained at level B3LYP/6-31G(d)//B3LYP/6-31G(d) of theory.....	50
3.20 The intermediate structures of <i>cone</i> - <i>partial cone</i> interconversion reactions for compounds <b>1</b> , <b>3</b> , <b>5</b> , <b>7</b> , <b>9</b> , and <b>11</b> obtained at level B3LYP/6-31G(d) of theory.....	50
3.21 Localization the LUMO (above) and HOMO (bottom) orbitals in the <i>cone</i> conformers of thiacalix[4]arene derivatives ( <b>1</b> to <b>6</b> ).....	51
3.22 The frontier molecular orbital energy gaps of cone conformers of thiacalix[4]arene and sulfonylcalix[4]arene derivatives .....	52
3.23 Localization the LUMO (above) and HOMO (bottom) orbitals in the <i>cone</i> conformers of sulfonylcalix[4]arene derivatives ( <b>7</b> to <b>12</b> ).....	53
3.24 The molecular electrostatic potential (in au) presented over electronic isodensity, $\rho=0.05 \text{ e } \text{\AA}^{-3}$ of the cone conformers of the thiacalix[4]arene derivatives ( <b>1</b> to <b>6</b> ).....	54
3.25 The molecular electrostatic potential (in au) presented over electronic isodensity, $\rho=0.05 \text{ e } \text{\AA}^{-3}$ of the <i>cone</i> conformers of the sulfonylcalix[4]-arene derivatives ( <b>7</b> to <b>12</b> ) .....	55
3.26 The B3LYP/6-31G(d)-optimized structures of (a) the sulfonylcalix[4]arene (designated as LH <sub>2</sub> ), its deprotonated species (b) LH <sup>-</sup> and (c) L <sub>b</sub> <sup>2-</sup> . Three types of hydrogen bonds are presented and their bond distances are in \AA....	56
3.27 The B3LYP/6-31G(d)-optimized structures of (a) the mercaptosulfonyl calix[4]arene (designated as LH <sub>2</sub> ), its deprotonated species (b) LH <sup>-</sup> , (c) L <sub>a1</sub> <sup>2-</sup> , (d) L <sub>a2</sub> <sup>2-</sup> and (e) L <sub>b</sub> <sup>2-</sup> . The hydrogen bond distances, Type 1 and 2 are in \AA.....	57
3.28 The B3LYP/6-31G(d)-optimized structures of (a) the aminosulfonylcalix [4]arene (designated as L), its protonated species (b) LH <sup>+</sup> , (c) L <sub>a</sub> H <sub>2</sub> <sup>2+</sup> , (d) L <sub>b</sub> H <sub>2</sub> <sup>2+</sup> , (e) LH <sub>3</sub> <sup>3+</sup> and (f) LH <sub>4</sub> <sup>4+</sup> . The hydrogen bond distances, type 1 and 3 are in \AA.....	57

<b>Figure</b>	<b>Page</b>
3.29 The B3LYP/6-31G(d)-optimized structures of the Zn(II) ion complexes of the cone conformers of thiacalix[4]arene derivatives ( <b>1</b> to <b>6</b> ).....	61
3.30 The B3LYP/6-31G(d)-optimized structures of the Zn(II) ion complexes of the cone conformers of sulfonylcalix[4]arene derivatives ( <b>7</b> to <b>12</b> ).....	62
3.31 Graphic inter-relation between the complexation energies ( $\Delta E_{\text{BSSE}}$ ) of thiacalix[4] arene and aminosulfonylcalix[4]arene complexes and the average distance of Zn-Y1 and Zn-Y2 bonds (Y1 = Y2 = O, S or N as shown in Figures 3.2 and 3.3).....	66
3.32 Localization the LUMO and HOMO orbitals in the cone conformers of zinc(II) complexes with thiacalix[4]arene derivatives ( <b>1</b> to <b>6</b> ).....	66
3.33 Localization the LUMO and HOMO orbitals in the cone conformers of zinc(II) complexes with sulfonylcalix[4]arene derivatives ( <b>7</b> to <b>12</b> ).....	67
3.34 Real molecule (top) and model system (bottom) of hosts a tatbtc4a and b tatca4a. The bold atoms of the real molecules of hosts were treated at the higher level of theory used in the ONIOM(MO:MO) calculation.....	69
3.35 Atom labeling of tatbtc4a/oxalate complex as a representative of a host–guest system.....	70
3.36 Geometrical structures of tetraamino- <i>tert</i> -butylthiacalix[4]arene (tatbtc4a) complex with oxalate optimized at a B3LYP/6-31G, b ONIOM(B3LYP/6-31G(d):AM1), (c) ONIOM(B3LYP/6-31G(d):PM3), and (d) ONIOM(B3LYP/6-31G(d):MNDO) levels of theory.....	71
3.37 ONIOM(B3LYP/6-31G(d ):AM1)-optimized geometries of tetraamino- <i>p-tert</i> -butylthiacalix[4]arene (tatbtc4a) with carboxylate guests. Binding energies $\Delta E$ are in kcal/mol.....	76
3.38 Plots of preorganization energies of tatbtc4a receptor and carboxylates (guests) and their complexation and binding energies against the size of the carboxylate guests, based on the ONIOM(B3LYP/6-31G(d ):AM1) method.....	77
3.39 ONIOM(B3LYP/6-31G(d):AM1)-optimized geometries of amino- <i>p-tert</i> -butylcalix[4]arene (tatbc4a) with carboxylate guests. Binding energies $\Delta E$ are in kcal/mol.....	80

Figure	Page
3.40 Plots of preorganization energies of tatbc4a receptor and carboxylates (guests) and their complexation and binding energies against the size of the carboxylate guests, based on the ONIOM(B3LYP/6-31G(d):AM1) method.....	81



สถาบันวิทยบริการ  
จุฬาลงกรณ์มหาวิทยาลัย

## LIST OF TABLES

Table	Page
1.1 Compound names for thiacalix[4]arene derivatives.....	3
3.1 Geometrical data for the structure of <i>cone</i> conformer of thiacalix[4]arene derivatives ( <b>1</b> to <b>6</b> ) computed at the B3LYP/6-31G(d) level of theory.....	38
3.2 Geometrical data for the structure of <i>cone</i> conformer of sulfonylcalix[4]arene derivatives ( <b>7</b> to <b>12</b> ) computed at the B3LYP/6-31G(d) level of theory.....	43
3.3 Geometrical data for the structure of <i>1,3-alternate</i> conformer of thiacalix[4]arene derivatives computed at B3LYP/6-31G(d) level of theory .....	44
3.4 Protonation energies of <i>cone</i> conformers of the sulfonylcalix[4]arene ( <b>7</b> ), mercaptosulfonylcalix[4]arene ( <b>9</b> ) and aminosulfonylcalix[4]arene ( <b>11</b> ).....	58
3.5 Complexation energies of zinc(II) ion with the <i>cone</i> conformers of thiacalix[4]arene and sulfonylcalix[4]arene derivatives obtained at B3LYP/6-31G(d) level of theory.....	63
3.6 Geometrical data for zinc(II) complexes of <i>cone</i> conformer of thiacalix[4]arene derivatives computed at B3LYP/6-31G(d) level of theory.....	64
3.7 Geometrical data for zinc(II) complexes of <i>cone</i> conformer of sulfonylcalix[4]arene derivatives computed at B3LYP/6-31G(d) level of theory.....	65
3.8 Geometrical data for the geometries of amino- <i>p-tert</i> -butylthiacalix[4]arene (tatbtc4a) complex with oxalate optimized at the B3LYP/6-31G(d), ONIOM(B3LYP/6-31G(d):AM1), ONIOM(B3LYP/6-31G(d):PM3), and ONIOM(B3LYP/6-31G(d):MNDO) levels of theory.....	72
3.9 Binding energies, enthalpies, and free energies of association of amino- <i>p-tert</i> -butyl thiacalix[4]arene ( <b>6</b> , tatbtc4a) and various anionic guests.....	74
3.10 Preorganization energies, corresponding thermodynamics of amino- <i>p-tert</i> -butylthia calix[4]arene ( <b>6</b> , tatbtc4a) receptor (host), carboxylates (guest), and their complexation energies derived from the ONIOM (B3LYP/6-31G(d):AM1) calculations.....	74

<b>Table</b>	<b>Page</b>
3.11 Binding energies of association of the amino- <i>p-tert</i> -butylthiacalix[4]arene (6, tatbtc4a) and various anionic guests and their BSSE corrections values derived from the B3LYP/6-31G(d)//ONIOM (B3LYP/6-31G(d):AM1) calculations and their BSSE corrected values.....	75
3.12 Binding energies, enthalpies, and free energies of association of amino- <i>p-tert</i> -butylcalix[4]arene (tatbc4a) and various anionic guests.....	78
3.13 Preorganization energies, corresponding thermodynamics of Tetraamino- <i>tert</i> -butylthiacalix[4]arene (tatbc4a) receptor (host), carboxylates (guest), and their complexation energies derived at ONIOM (B3LYP/6-31G(d):AM1) calculations.....	79
3.14 Binding energies of association of the tetraamino- <i>p-tert</i> -butylcalix[4]arene (tatbc4a) and various anionic guests and their BSSE corrections values derived from the B3LYP/6-31G(d)//ONIOM (B3LYP/6-31G(d):AM1) calculations and their BSSE corrected values.....	79
S1 Relative energies, $\Delta E_{rel}$ of thiacalix[4]arene derivatives obtained at the B3LYP/6-31G(d)//B3LYP/6-31G(d) level of theory.....	92
S2 Relative energies, $\Delta E_{rel}$ of sulfonylcalix[4]arene derivatives obtained at the B3LYP/6-31G(d)//B3LYP/6-31G(d) level of theory derivatives.....	93
S3 Relative energies, $\Delta E_{rel}$ (in kcal/mol) of the B3LYP/6-31G(d)-optimized conformers of sulfonylcalix[4]arene derivatives obtained at different levels of theory, the total energies (in au) of the most stable conformer are shown in parentheses.....	94
S4 Dipole moments (in debye) of the B3LYP/6-31G(d)-optimized conformers of sulfonylcalix[4]arene derivatives obtained at different levels of theory..	95
S5 The $E_{LUMO}$ and $E_{HOMO}$ energies and frontier molecular orbital energy gap, $\Delta E_{HOMO-LUMO}$ of typical conformers of thiacalix[4]arene derivatives computed at B3LYP/6-31G(d,p)//B3LYP/6-31G(d) level of theory.....	96
S6 The $E_{LUMO}$ and $E_{HOMO}$ energies and frontier molecular orbital energy gap, $\Delta E_{HOMO-LUMO}$ of typical conformers of thiacalix[4]arene derivatives computed at B3LYP/6-31G(d,p)//B3LYP/6-31G(d) level of theory.....	97

## LIST OF ABBREVIATIONS

$\Delta$	Delta
AM1	Austin model 1
B3LYP	Becke's three parameter hybrid functional using the LYP correlation function
BLYP	Beck-Lee-Yang-Parr function
BSSE	Basis set superposition error
CP	Counterpoise method
DFT	Density functional theory
ECP	Effective core potential
G	Gibbs free energy
GGA	Generalized gradient approximation
H	Enthalpy
HF	Hartree-Fock
HOMO	Highest occupied molecular orbital
IMOMO	Integrated molecular orbital-molecular orbital
KS	Kohn-Sham
LCAO	Linear combination of atomic orbitals
LDA	Local density approximation
LSD	Local spin density approximation
HOMO	Highest occupied molecular orbital
LYP	Lee-Yang-Parr functional
MM	Molecular mechanics
MNDO	Modified neglect of differential overlap
MO	Molecular orbital
ONIOM	Our own <i>N</i> -layered integrated molecular orbital and molecular mechanics
QM	Quantum mechanics
QM/MM	Quantum mechanical/molecular mechanical
SCF	Self-consistent field
STO	Slater type orbital
STO-3G	Slater type orbital approximated by 3 gaussian type orbitals



UV	Ultraviolet
VWN	Vosko-Wilk-Nusair functional
ZPE	Zero-point energy



สถาบันวิทยบริการ  
จุฬาลงกรณ์มหาวิทยาลัย

# CHAPTER I

## INTRODUCTION

In supramolecular chemistry, a wide variety of macrocyclic receptors are able to recognize or selectively interact with neutral, anionic and cationic species to form host-guest complexes which are extremely important in chemistry. Recognition is related to selective host-guest receptors and is strongly dependent on the host-guest intermolecular interactions. The one family of model systems in supramolecular host-guest chemistry is calix[n]arenes. [1-3]

### 1.1 Introduction of calix[4]arenes

Calix[4]arenes (C4A) are macrocyclic compounds which consist of four phenol rings connected via methylene bridges located ortho position to the hydroxyl groups (see Figure 1.1a). These rings cannot be coplanar but adopt an orientation which makes the molecule appear like a cup. They have been used increasingly in supramolecular chemistry as building blocks for larger molecules which are designed for the complexation of cations or neutral molecules. [1-3] The important characteristic of the calix[4]arene structure is its  $\pi$ -rich electron cavity, which favors the inclusion of charged guest compounds, which are stabilized by noncovalent binding forces related to cation- $\pi$  electron interactions.[3-5] The calix[4]arene have four characteristic non-planar conformations, designated as *cone* (C), *partial cone* (PC), *1,2-alternate* (1,2-A), and *1,3-alternate* (1,3-A) (see Figure 1.1b). Partial functionalizations of calixarenes have been performed at their lower (phenolic OH groups) and/or upper rims. In addition, calix[4]arenes are highly useful cyclic compounds in which the introduction of functional groups in the narrow or in the wide rims can be designed to favor interactions with specific guest systems. This can lead to the construction of very sophisticated molecular sensors.

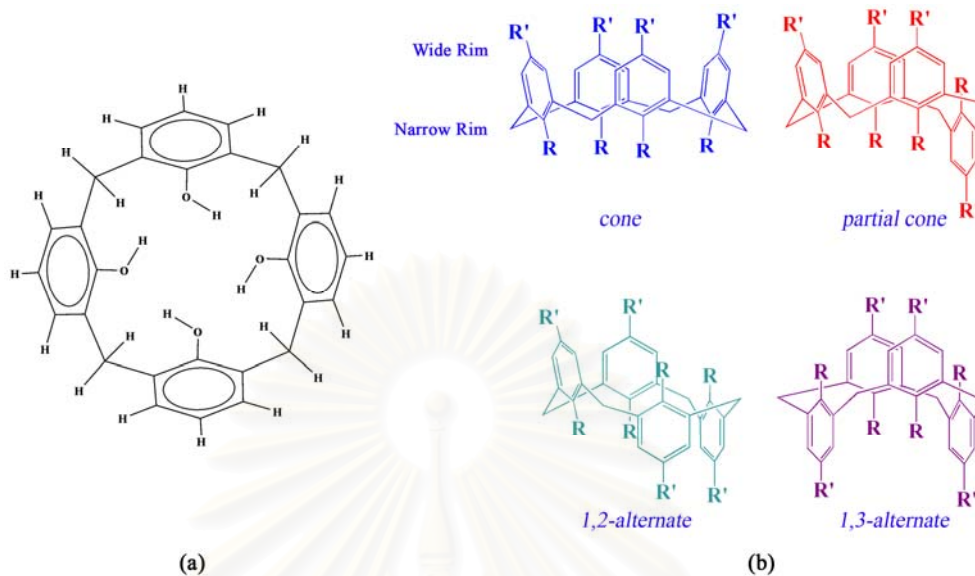


**Figure 1.1** Chemical structures of (a) calix[4]arene, **C4A** and (b) four conformational isomers of calix[4]arene derivatives, where R and R' are any substituted groups.

## 1.2 Thiacalix[4]arene derivatives

The well known thiacalix[4]arenes (**1** to **6**) are the replacement of the bridging  $\text{CH}_2$  groups of calix[4]arene by S atoms whereas sulfonylcalix[4]arenes (**7** to **12**) and sulfinylcalix[4]arenes (**13** to **18**) are the replacement of the bridging  $\text{CH}_2$  groups by  $\text{SO}_2$  and SO groups, respectively (see Figure 1.2 and Table 1.1). All thiacalix[4]arene derivatives are interesting because of the affinity of sulfur atoms and/or oxygen atoms. Thiacalix[4]arene favors transition metal ions while sulfonylcalix[4]arene prefers alkaline earth metal ions. Interestingly, sulfinylcalix[4]arene can coordinate to both groups of these metal ions. The increasing number of coordination sites leads to significant changes of thiacalix[4]arene chemistry and a large diversity on their host-guest properties, especially the inclusion complexes with ions of alkali and transition metals. Further more, the cavity size is enlarged and the chemical reactivity and chelating property are modified. [12,13] The replacement of OH groups at the narrow rim of **1** and **7** with SH or  $\text{NH}_2$  groups is also attractive in recognition systems. The proposed binding modes of thiacalix[4]arene and sulfonylcalix[4]arene derivatives are presented in Figure 1.3.

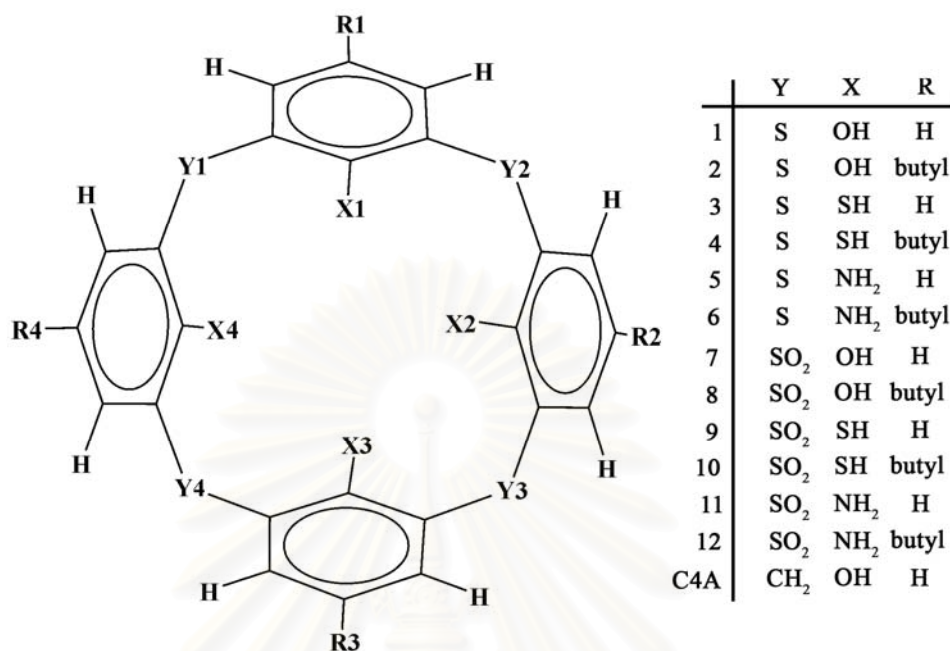


**Figure 1.2** Chemical structures of thiacalix[4]arene and sulfonylcalix[4]arene derivatives.

**Table 1.1** Compound names for thiacalix[4]arene derivatives

Compounds	Names	Y	X	R
1	thiacalix[4]arene	S	OH	H
2	<i>p-tert</i> -butyl thiacalix[4]arene	S	OH	Butyl
3	tetramercapto thiacalix[4]arene	S	SH	H
4	tetramercapto- <i>p-tert</i> -butyl thiacalix[4]arene	S	SH	Butyl
5	tetraamino thiacalix[4]arene	S	NH <sub>2</sub>	H
6	tetraamino- <i>p-tert</i> -butylthiacalix[4]arene	S	NH <sub>2</sub>	Butyl
7	sulfonylcalix[4]arene	SO <sub>2</sub>	OH	H
8	<i>p-tert</i> -butyl sulfonylcalix[4]arene	SO <sub>2</sub>	OH	Butyl
9	tetramercapto sulfonylcalix[4]arene	SO <sub>2</sub>	SH	H
10	tetramercapto- <i>p-tert</i> -butyl sulfonylcalix[4]arene	SO <sub>2</sub>	SH	Butyl
11	tetraamino sulfonylcalix[4]arene	SO <sub>2</sub>	NH <sub>2</sub>	H
12	tetraamino- <i>p-tert</i> -butyl sulfonylcalix[4]arene	SO <sub>2</sub>	NH <sub>2</sub>	Butyl
13	sufinylcalix[4]arene	SO	OH	H
14	<i>p-tert</i> -butyl sufinylcalix[4]arene	SO	OH	Butyl
15	tetramercapto sufinylcalix[4]arene	SO	SH	H
16	tetramercapto- <i>p-tert</i> -butyl sufinylcalix[4]arene	SO	SH	Butyl
17	tetraamino sufinylcalix[4]arene	SO	NH <sub>2</sub>	H
18	tetraamino- <i>p-tert</i> -butyl sufinylcalix[4]arene	SO	NH <sub>2</sub>	Butyl
C4A	calix[4]arene	CH <sub>2</sub>	OH	H
Butyl-C4A	<i>p-tert</i> -butyl calix[4]arene	CH <sub>2</sub>	OH	Butyl

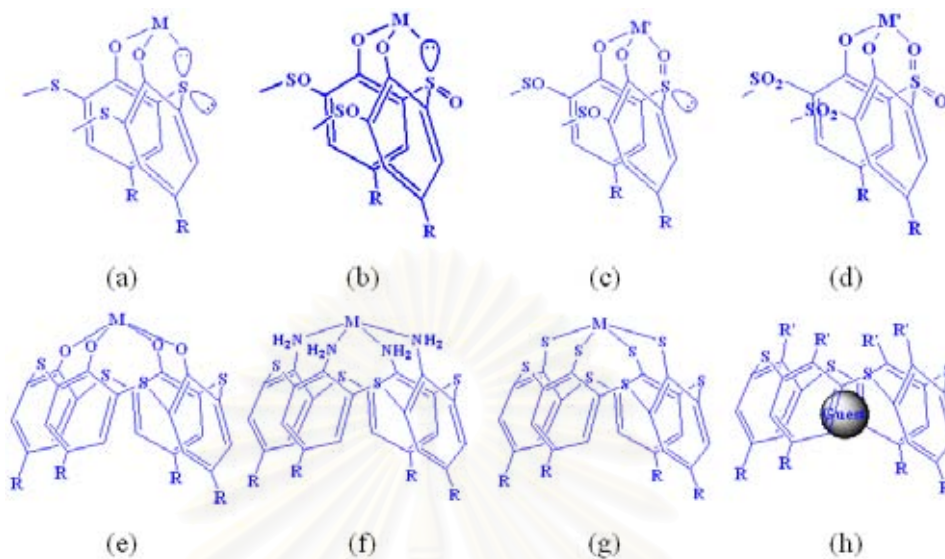


**Figure 1.3** Proposed coordination manners of thiacalix[4]arene derivatives with (a) – (g) metal ions and (h) inclusion complex.

### 1.3 Experimental study on calix[4]arenes and calix[4]arene complexes

Several studies have been reported in which the relative stability of calix[4]arene conformations could be determined using experiments and theoretical calculation methods. The increasing numbers of coordination sites lead to significant changes of their chemistry and a large diversity in their host–guest properties, [14-19] especially the inclusion complexes formed with alkali metal ions [16-23] such as  $\text{Mg}^{2+}$ ,  $\text{Ca}^{2+}$ , and  $\text{Ba}^{2+}$ , and transition metal ions, such as  $\text{Co}^{2+}$ ,  $\text{Ni}^{2+}$ ,  $\text{Cu}^{2+}$ ,  $\text{Pd}^{2+}$ ,  $\text{Ti}^{4+}$ , and  $\text{Zn}^{2+}$ . Due to the hydrophobicity of calixarene cavity, some organic solvents could be included within the cavity to form the inclusion complexes, and their X-ray structures have been determined.[14-15, 24-25]

### 1.4 Theoretical study on thiacalix[4]arenes and thiacalix[4]arene complexes

Determination of three-dimensional arrangement of such supramolecular entities in the solid state, usually single-crystal X-ray structure determination is regarded as ultimately structural proof. However, this methodology strongly depends on the accessibility of single-crystalline material. If such crystalline material is not

available,  $^{13}\text{C}$  CP-MAS NMR, vibrational spectroscopy or thermochemical methods are employed. In solution, NMR titration experiments have widely used for characterization of inclusion process. The use of single-crystal structure analysis gives directly access to the three-dimensional coordinates of the supramolecular systems. Most spectroscopic methodologies depend on the interpretations and sometimes on chemical intuitions. Computational approach is the one of the high progressional supramolecular chemistry. This approach can lead to the microscopic insight into the structural and thermodynamical features involved in the processes of molecular recognition and supramolecular organization. Further more, computational approach has been widely used to support and interpret the experimental results. Several molecular and quantum mechanics studies have been focused on calixarenes, especially to study their conformational preference, proton affinity and complexation ability with some ions or guest molecules. [1 - 5]

During the last decade, many theoretical studies have been applied successfully for theoretical investigation of calixarenes.[1, 2] However, only the part of theoretical studies in thiacalix[4]arenes (**1**) were found. Bernardino and Costa Cabral reported the structure and conformational equilibrium of thiacalix[4]arene (**1**) using HF/3-21G, HF/3-21G(d,p), B3LYP/3-21G and B3LYP/6-31G(d,p) levels of theory for geometry optimization. [26] Several single point energy calculations were performed using different methods. The conformation stability was predicted in the decreasing order to be: *cone* > *partial cone* > *1,3-alternate* > *1,2-alternate*. Surprisingly, Ruangpornvisuti has been optimized four main conformers of **1** (and its *p*-*tert*-butyl derivative, compound **2**), using semiempirical AM1 method and computed their conformation energies using single point calculation at B3LYP/6-31G(d) level of theory. The result showed that the stability order was as same as Bernardino and Costa Cabral. [27]

Ruangpornvisuti research group also reported the structural investigation of sulfonylcalix[4]arene (**7**), *p*-*tert*-butyl sulfonylcalix[4]arene (**8**).[28] Two different types of hydrogen bonds in *cone* and *partial cone* conformers of **7**, and cone conformer of **8** have been found. Complexation between the most stable conformer and zinc(II) ion was processed by the exothermic reaction. Suwattanamala et al. studied structural and conformational equilibriums of tetramercaptothiacalix[4]arene

(3) and tetraamino thiacalix[4]arene (5) using DFT methods. [29] The results showed that cone conformer was the most stable conformer of both compounds and substituted groups in the narrow rim. For example, -SH and -NH<sub>2</sub> groups were not effective to the stability order. In addition, intramolecular bonds between hydrogen atoms and sulfur bridges were a dominant factor in stabilizing all conformers rather than hydrogen bonds between the groups of the lower rim.

### 1.5 Overall objectives

The aim of this study is to investigate the geometrical structures of typical conformers of thiacalix[4]arene (1 to 6) and sulfonylcalix[4]arene (7 to 12) derivatives as shown in Figure 1.2, their proton affinities, relative stabilities, complexations with zinc(II) ion and the relative energies using the density functional theory (DFT) method at B3LYP/6-31G(d) level of theory. The electronic properties, HOMO–LUMO molecular orbital energy gaps and isodensity surface of typical conformers of thiacalix[4]arene and sulfonylcalix[4]arene derivatives, their zinc(II) complexes have been determined. The binding interactions between carboxylates and thiacalix[4]arene (5, 6) derivatives receptors have been investigated theoretically by using ONIOM methods to obtain their binding energies and thermodynamic data for their interactions.

สถาบันวิทยบริการ  
จุฬาลงกรณ์มหาวิทยาลัย

## CHAPTER II

### THEORETICAL METHOD

A branch of chemistry that uses the results of theoretical chemistry incorporated into efficient computer programs to calculate the structures and properties of molecules is called computational chemistry (also called molecular modeling). Examples of such properties are energy and interaction energy, charges, dipoles and higher multipole moments, vibrational frequencies, reactivity or other spectroscopic quantities. The main theoretical methods available belong to five broad classes as described below. [30-34]

Molecular mechanics (MM) is based on a model of a molecule as a collection of balls (atoms) held together by springs (bonds). If we know the normal spring lengths and the angles between them, and how much energy it takes to stretch and bend the springs, we can calculate the energy of a given collection of balls and springs i.e., of a given molecule; changing the geometry until the lowest energy is found enable us to do a geometry optimization, i.e., to calculate a geometry for the molecule. Molecular mechanics is fast: a fairly large molecule like calix[4]arene [ $C_{28}H_{28}O_4$ ] can be optimized in seconds on a powerful desktop computer.

*Ab initio* calculations (also called *ab initio* quantum mechanics: *ab initio* is from the Latin: “from the first principle”) are based on the Schrödinger equation. This is one of the fundamental equations of modern physics and describes, among other things, how the electrons in molecule behave. The *ab initio* method solved the Schrödinger equation for a molecule and gives us the molecule’s energy and wave function. The wave function is a mathematic function that can be used to calculate the electron distribution (and, in theory at least, any things else about the molecule). From the electron distribution we can tell things like how polar the molecule is, and which parts of it are likely to be attracted by nucleophiles or electrophiles. The Schrödinger equation cannot be solved exactly for any molecule with more than one electron. Thus approximation are used.

Semiempirical (SE) calculations are, like *ab initio*, based on the Schrödinger equation. However, more approximation are made in solving it and the very complicated integrals that must be calculated in the *ab initio* method are not actually



evaluated in SE calculations. On the other hand, the program draws on a kind of library of integrals that was compiled by finding the best fit of some calculated entity like geometry or energy (heat of formation) to the experimental values. This plugging of experimental values into a mathematical procedure to get the best calculation values is called parameterization (or parametrization). It is the combination of the theory and experiment that makes the method semiempirical: It is based on the Schrödinger equation, but parameterized with experimental values (empirical means experimental). Semiempirical calculations are slower than MM but much faster than *ab initio* calculations.

Density functional calculations (often called density functional theory (DFT) calculations) are, like *ab initio* and SE calculations, based on the Schrödinger equation. However, unlike the other two methods, the DFT does not calculate a wave function, but rather derives the electron distributions (electron density functions) directly. A functional is a mathematical entity related to a function. Density functional calculations are usually faster than *ab initio*, but slower than SE.

Molecular dynamics (MD) calculations apply the laws of motion to the molecules. Thus one can simulate the motion of an enzyme as it changes shape on binding to the substrate, or the motion of a swarm of water molecules around a molecule of solute. This section provides the introduction of the theoretical methods used in this study. [35-37]

## 2.1 Density functional theory

Density functional theory (DFT) is an entirely different approach to computational quantum chemistry from the wavefunction methods. [35-38] It involves expressing the energy of a system as a functional of the electron density,  $\rho$ , rather than of a wavefunction,  $\psi$ . This is based on the proof of Hohenberg and Kohn that There exists a universal functional of the density,  $F[\rho(r)]$ , independent of  $v(r)$  [the external potential due to the nuclei], such that the expression  $E = \int v(r)\rho(r)dr + F[\rho(r)]$  has as its minimum the correct ground state energy associated with  $v(r)$ . Density Functional Theory is thus formally an exact theory given that the mathematical form of this universal functional is known. Unfortunately, in practice it is not known, nor can it be

precisely determined or systematically improved. Approximate functionals have therefore been proposed, often on the basis of fits which give the correct results for certain well characterized systems. Density functional theory is, therefore, a semi-empirical theory. It is important to note, however, that as DFT is based upon the actual electron density, both dynamical and non-dynamical correlation are implicitly accounted for in DFT calculations.

### 2.1.1 The Hohenberg-Kohn theorem

Within a Born-Oppenheimer approximation, the ground state of the system is a result of the positions of the nuclei. In the quantum mechanics Hamiltonian equation the kinetic energy of electrons ( $\hat{T}_e$ ) and the electron-electron interaction ( $\hat{V}_{ee}$ ) adjust themselves to the external potential ( $\hat{V}_{ext}$ ) to get the lowest total energy. Thus, the external potential can be uniquely determined from knowledge of the electron density. The Hohenberg-Kohn theorem (1964) states that if  $N$  interacting electrons move in an external potential  $V_{ext}$ , the ground-state electron density  $\rho_0(r)$  minimizes the functional

$$E[\rho] = F[\rho] + \int \rho(r)V_{ext}(r)dr \quad 2.1$$

In equation (2.1)  $F[\rho]$  is a universal functional of  $\rho(r)$  and the minimum value of the functional  $E$  is  $E_0$ , the exact ground-state electronic energy.

$$\hat{F} = \hat{T}_e + \hat{V}_{ee} = \sum_i -\frac{1}{2}\nabla_i^2 + \sum_{i \neq j} \frac{1}{|r_i - r_j|} \quad 2.2$$

and by using the variation principle, the density can be obtained.

### 2.1.2 The Kohn-Sham equations

Kohn and Sham (1965) introduced a method based on the Hohenberg-Kohn theorem that allows one to minimize the functional  $E[n(r)]$  by varying  $\rho(r)$  over all the densities containing  $N$  electrons. They derived a coupled set of differential equations

enabling the ground state density  $\rho_0(r)$  to be found. Kohn and Sham separated  $F[\rho(r)]$  in equation (2.1) into three distinct parts, so that the functional  $E$  becomes

$$E[\rho(r)] = T_s[\rho(r)] + \frac{1}{2} \iint \frac{\rho(r)\rho(r')}{|r-r'|} drdr' + E_{xc}[\rho(r)] + \int \rho(r)V_{ext}(r)dr \quad 2.3$$

where  $T_s[\rho(r)]$  is defined as the kinetic energy of a non-interacting electron gas with density  $\rho(r)$ ,

$$T_s[\rho(r)] = -\frac{1}{2} \sum_i \psi_i^*(r) \nabla^2 \psi_i(r) dr \quad 2.4$$

and  $E_{xc}[\rho(r)]$  is the exchange-correlation energy functional. Introducing a normalization constraint on the electron density,  $\int \rho(r)dr = N$ , by the Lagrange's method of undetermined multiplier, we obtain

$$\delta \left\{ E[\rho(r)] - \mu \left[ \int \rho(r)dr - N \right] \right\} = 0 \quad 2.5$$

where  $\mu$  is an undetermined Lagrange multiplier. The number of electrons in the system is constant so  $\delta N = 0$ . Then equation (2.5) reduces to

$$\delta E[\rho(r)] - \mu \delta \left( \int \rho(r)dr \right) = 0 \quad 2.6$$

Using the definition of the differential of the functional  $\delta F = \int \frac{\delta F}{\delta f(x)} \delta f(x) dx$ , and the fact that the differential and the integral signs may be interchanged,

$$\int \frac{\delta E[\rho(r)]}{\delta \rho(r)} \delta \rho(r) dr - \mu \int \delta \rho(r) dr = 0 \quad 2.7$$

$$\int \left\{ \frac{\delta E[\rho(r)]}{\delta \rho(r)} - \mu \right\} \delta \rho(r) dr = 0 \Rightarrow \frac{\delta E[\rho(r)]}{\delta \rho(r)} = \mu \quad 2.8$$

Equation (2.8) may now be rewritten in terms of an effective potential,  $V_{eff}(r)$ ,

$$\frac{\delta T_s[\rho(r)]}{\delta \rho(r)} + V_{eff}(r) = \mu \quad 2.9$$

where

$$V_{eff}(r) = V_{ext}(r) + \int \frac{\rho(r')}{|r-r'|} dr' + V_{xc}(r) \quad 2.10$$

and

$$V_{xc}(r) = \frac{\delta E_{xc}[\rho(r)]}{\delta \rho(r)} \quad 2.11$$

To find the ground state energy,  $E_0(r)$ , and the ground state density,  $\rho_0(r)$ , the one electron Schrödinger equation

$$\left( -\frac{1}{2} \nabla_i^2 + V_{eff}(r) \right) \phi_i(r) = \varepsilon_i \phi_i(r) \quad 2.12$$

should be solved self-consistently with

$$\rho(r) = \sum_{i=1}^N |\phi_i(r)|^2 \quad 2.13$$

Similar to the SCF procedure in the Hartree-Fock method, the density  $\rho(r)$  can be solved iteratively. A self-consistent solution is required due to the dependence of  $V_{eff}(r)$  on  $\rho(r)$ .

### 2.1.3 DFT exchange and correlations

The form of  $E_{xc}$  is in general unknown and its exact value has been calculated for only a few very simple systems. In the density functional theory, the exchange energy is defined as

$$E_X[\rho] = \langle \phi[\rho] | \hat{V}_{ee} | \phi[\rho] \rangle - U[\rho] \quad 2.14$$

when  $U[\rho]$  is the Hartree piece of the columbic potential. The correlation term is defined as the remaining unknown piece of the energy:

$$E_C[\rho] = F[\rho] - T_s[\rho] - U[\rho] - E_X[\rho] \quad 2.15$$

Due to the definition of  $F[\rho]$ , the correlation energy consists of two separate contributions:

$$E_C[\rho] = T_C[\rho] + U_C[\rho] \quad 2.16$$

when  $T_C[\rho]$  and  $U_C[\rho]$  are the kinetic contribution and the potential contribution, respectively, of the correlation energy.

In electronic structure calculations,  $E_{xc}$  is most commonly approximated within the local density approximation or generalized-gradient approximation. Ziegler (1991) In the local density approximation (LDA), the value of  $E_{xc}[\rho(r)]$  is

approximated by the exchange-correlation energy of an electron in homogeneous electron gas of the same density  $\rho(r)$ , *i.e.*

$$E_{XC}^{LDA}[\rho(r)] = \int \epsilon_{XC}(\rho(r))\rho(r)dr \quad 2.17$$

The most accurate data for  $\epsilon_{XC}(\rho(r))$  is calculated from Quantum Monte Carlo calculations. For systems with slowly varying charge densities this approximation generally gives very good results. An obvious approach to improving the LDA, so called generalized gradient approximation (GGA), is to include gradient corrections by making  $E_{XC}$  a functional of the density and its gradient:

$$E_{XC}^{GGA}[\rho(r)] = \int \epsilon_{XC}(\rho(r))\rho(r)dr + \int F_{XC}[\rho(r), |\nabla\rho(r)|]dr \quad 2.18$$

where  $F_{XC}$  is a correction chosen to satisfy one or several known limits for  $E_{XC}$ . Clearly, there is no unique recipe for the  $F_{XC}$ , and several functions have been proposed in the literature. The development of improved functions is currently a very active area of research and although incremental improvements are likely, it is far from clear whether the research will be successful in providing the substantial increase in accuracy that is desired.

### 2.1.4 Hybrid functions

From the Hamiltonian equation and the definition of the exchange-correlation energy, an exact connection can be made between the  $E_{xc}$  and the corresponding potential connecting the non-interacting reference and the actual system. The resulting equation is called the Adiabatic connection formula (ACF) and involves an integration over the parameter  $\lambda$  which turns on the electron-electron interaction

$$E_{XC} = \int_0^1 \langle \psi_\lambda | V_{XC}(\lambda) | \psi_\lambda \rangle d\lambda \quad 2.19$$

In the  $\lambda=0$  limit, the electrons are non-interacting and there is consequently no correlation. Since the Kohn-Sham wavefunction is simply a single Slater determinant of orbitals then if the KS orbitals are identical to the HF orbitals, the exact exchange energy is precisely the HF exchange energy:

$$E_x[\phi_i; \lambda = 0] = -\frac{1}{2} \sum_{\sigma} \sum_{i,j} \int d^3 r \int d^3 r' \frac{\phi_{i\sigma}^*(r) \phi_{j\sigma}^*(r') \phi_{i\sigma}(r') \phi_{j\sigma}(r)}{|r - r'|} = E_x^{exact} \quad 2.20$$

The approximation of exchange-correlation can be made by summing  $E_{XC}$  terms of different values of  $\lambda$  within the limit  $\lambda = 0$  to 1. The choice of terms is arbitrary. Hybrid functionals includes a mixture of Hartree-Fock Exchange with DFT exchange-correlation.

B3LYP functional uses Becke's exchange functional with part of the Hartree-Fock exchange mixed in and a scaling factor on the correlation part but using the LYP correlation function. The exchange-correlation energy has the form of

$$AE_X^{Slater} + (1-A)E_X^{HF} + B\Delta E_X^{Beck} + (1-C)E_C^{VWN} + CE_C^{LYP} \quad 2.21$$

where the exchange includes the Slater exchange  $E_X^{Slater}$ , or local spin density exchange, along with corrections involving the gradient of the density and the correlation is provided by the LYP and VWN correlations. The constants  $A$ ,  $B$ , and  $C$  are those determined by fitting to the G1 molecule set. The values of the three parameters are determined by fitting to the 56 atomization energies, 42 ionization potentials, 8 proton affinities, and 10 first-row atomic energies in the G1 molecule set, computing values of  $A=0.80$ ,  $B=0.72$ , and  $C=0.81$ .

## 2.2 Semi-empirical methods

Semi-empirical methods increase the speed of computation by using approximations of *ab initio* techniques (e.g., by limiting choices of molecular orbitals or considering only valence electrons) which have been fitted to experimental data (for instance, structures and formation energies of organic molecules). [30-34] Until recently, the size of many energetic molecules placed them beyond the scope of *ab initio* calculations, so preliminary theoretical studies were performed using semi-empirical techniques. However, semi-empirical methods have been calibrated to typical organic or biological systems and tend to be inaccurate for problems involving hydrogen-bonding, chemical transitions or nitrated compounds. Several semi-empirical methods are available and appear in commercially available computational

chemistry software packages. Some of the more common semi-empirical methods can be grouped according to their treatment of electron-electron interactions.

### **2.2.1 The extended Hückel method**

Extended Hückel calculations neglect all electron-electron interactions, making them computationally fast but not very accurate. The model provides a qualitative estimate of the shapes and relative energies of molecular orbitals, and approximates the spatial distribution of electron density. Extended Hückel models are good for chemical visualization and can be applied to frontier orbital treatments of chemical reactivity.

### **2.2.2 Neglect of differential overlap**

The neglect of differential overlap (NDO) models neglect some but not all of the electron-electron interactions. The Hartree-Fock Self-Consistent Field (HF-SCF) method is used to solve the Schrödinger equation with various approximations:

The complete NDO (CNDO) the product of two atomic orbitals on different atoms is set equal to zero everywhere. In this case, repulsion between electrons in different orbitals depends only upon the nature of the atoms involved, and not 3 Obviously, n is constantly increasing as computing power is improved. on the particular orbitals. Because CNDO neglects almost all description of electron exchange properties, it does not differentiate between states that have the same electronic configuration, but different values of electron spin.

Intermediate NDO (INDO) differential overlap between orbitals on the same atom are taken into account in the description of electron-electron repulsion, but differential overlap between orbitals on different atoms is neglected.

Modified INDO, version 3 (MINDO/3) reparameterized version of INDO optimized to predict good enthalpies of formation and reasonable molecular geometries for a range of chemical systems, in particular, sulphur-containing compounds, carbocations, and polynitro organic compounds.

Zerner's INDO methods (ZINDO/1 and ZINDO/S) Michael Zerner's (University of Florida) versions of INDO developed for use with molecular systems containing transition metals. ZINDO/1 is optimized to predict molecular geometries and ZINDO/S is optimized to predict UV spectra.

### 2.2.3 Neglect of diatomic differential overlap

The neglect of diatomic differential overlap (NDDO) methods build upon the INDO model by including the overlap density between two orbitals on one atom interacting with the overlap density between two orbitals on the same or another atom.

Modified NDO (MNDO) a method introduced to correct some of the problems associated with MINDO/3. The MNDO does not work well for sterically crowded molecules, four-membered rings, hydrogen bonding, hypervalent compounds, nitro groups and peroxides. In general, MNDO overestimates activation barriers to chemical reactions.

Austin Method, version 1 (AM1) a reparameterized version of MNDO which includes changes in nuclear repulsion terms. Although more accurate than MNDO, AM1 does not handle phosphorus-oxygen bonds, nitro compounds and peroxide bonds. [14]

Parameterization Model, version 3 (PM3) a second reparameterization of MNDO, functionally similar to AM1, but with some significant improvements. PM3 is a recently developed semi-empirical method that may contain as yet undiscovered defects.

## 2.3 Hybrid methods

The combine high level quantum mechanical calculations on a small part of a system with a lower-level method on the rest of the system. Thus for large clusters or macromolecules, accurate calculations can be carried out on the area of interest without ignoring or making unnecessary assumptions about the remainder of the system.



Three methods have been developed and extensively used by Morokuma et al. at Emory University (Atlanta, GA). These methods and their applications are likely to receive increasing attention in the next few years:

Integrated Molecular Orbital and Molecular Mechanics (IMOMM) - a two-layer method in which a high level MO calculation is combined with molecular mechanics [39]. For example, the IMOMM method has been used to investigate organometallic catalyzed polymerization reactions [40,41].

Integrated Molecular Orbital and Molecular Orbital (IMOMO) - a two-layer method which combines high level and low-level MO calculations [42]. This method can be used for calculating bond dissociation energies of large molecules.

Our own *N*-layered Integrated molecular Orbital molecular Mechanics (ONIOM) method” - a technique that has largely superseded IMOMM and IMOMO, which are in fact, subsets of ONIOM. ONIOM is a three-level general method, allowing the combination of any high-level method with any low- or medium-level method. [43] ONIOM has been applied to calculations of bond breaking in fullerenes. [44]

## 2.4 Basis sets

In general, a basis set is an assortment of mathematical functions used to solve a differential equation. In quantum chemical calculations, the term ‘basis set’ which applied to a collection of contracted Gaussians representing atomic orbitals, are optimized to reproduce the desired chemical properties of a system. [31-33]

Standard *ab initio* software packages generally provide a choice of basis sets that vary both in size and in their description of the electrons in different atomic orbitals. Larger basis sets include more and a greater range of basis functions. Therefore, larger basis sets can better refine the approximation to the ‘true’ molecular wave function, but require correspondingly more computer resources. Alternatively, accurate wave functions may be obtained from different treatments of electrons in atoms. For instance, molecules containing large atoms ( $Z > 30$ ) are often modeled using basis sets incorporating approximate treatments of inner-shell electrons which account for relativistic phenomena.

Minimal basis sets contain the minimum number of AO basis functions needed to describe each atom (*e.g.*, 1s for H and He; 1s, 2s, 2p<sub>x</sub>, 2p<sub>y</sub>, 2p<sub>z</sub> for Li to Ne). An example of a minimal basis sets is STO-3G, which uses three Gaussian-type functions (3G) per basis function to approximate the atomic Slater-type orbitals. Although minimal basis sets are not recommended for consistent and accurate predictions of molecular energies, their simple structure provides a good tool for visualizing qualitative aspects of chemical bonding. Improvements on minimal basis sets are described below.

#### 2.4.1 Split valence basis sets

In split valence basis sets, additional basis functions (one contracted Gaussian plus some primitive Gaussians) are allocated to each valence atomic orbital. The resultant linear combination allows the atomic orbitals to adjust independently for a given molecular environment. Split valence basis sets are characterized by the number of functions assigned to valence orbitals. Double zeta basis sets use two basis functions to describe valence electrons, triple zeta use three functions, and so forth. Basis sets developed by Pople and coworkers are denoted by the number of Gaussian functions used to describe inner and outer shell electron. Thus '6-31G' describes an inner shell atomic orbital with a contracted Gaussian composed of six primitive Gaussians, an inner valence shell with a contracted Gaussian composed of three primitives, and an outer valence shell with one primitive. Other split-valence sets include 3-21G, 4-31G, and 6-31G.

#### 2.4.2 Polarized basis sets

Polarization functions can be added to basis sets to allow for non-uniform displacement of charge away from atomic nuclei, thereby improving descriptions of chemical bonding. Polarization functions describe orbitals of higher angular momentum quantum number than those required for the isolated atom (*e.g.*, *p*-type functions for H and He, and *d*-type functions for atoms with  $Z > 2$ ), and are added to the valence electron shells. For example, the 6-31G(d) basis set is constructed by

adding six *d*-type Gaussian primitives to the 6-31G description of each non-hydrogen atom. The 6-31G(d,p) is identical to 6-31G(d) for heavy atoms, but adds a set of Gaussian *p*-type functions to hydrogen and helium atoms. The addition of *p*-orbitals to hydrogen is particularly important in systems where hydrogen is bridging atom.

### 2.4.3 Diffuse basis sets

Species with significant electron density far removed from the nuclear centers (*e.g.*, anions, lone pairs and excited states) require diffuse functions to account for the outermost weakly bound electrons. Diffuse basis sets are recommended for calculations of electron affinities, proton affinities, inversion barriers and bond angles in anions. The addition of diffuse *s*- and *p*-type Gaussian functions to non-hydrogen atoms is denoted by a plus sign-as in 3-21+G. Further addition of diffuse functions to both hydrogen and larger atoms is indicated by a double plus.

### 2.5 Basis set superposition error (BSSE)

A consequence of using finite (and hence incomplete) atom-centered basis sets in calculations of interaction energies (including covalent bonding, hydrogen bonding and van der Waals interactions) is the presence of basis set superposition error. Briefly stated, this is the phenomenon whereby, given an interacting system *AB*, the moiety *A* can be stabilized by the nearby presence of the basis functions belonging to moiety *B* (in addition to any true interaction between *A* and *B*) and vice versa. This is because these additional basis functions compensate for the incompleteness of *A*'s own basis, thus improving the description of *A* and lowering its energy. Thus the system is not only stabilized by any true interaction between *A* and *B* but also by this superposition effect.

An estimate of the magnitude of this effect (and hence a possible correction for it) can be obtained via the counterpoise method of Boys and Bernardi.[45] This involves calculating the energy of each moiety (atom or fragment) both with its own basis functions,  $E_A$ ,  $E_B$ , and in the presence of the basis functions of the entire system  $E_{A|B}$ ,  $E_{|A}B$ . The counterpoise corrections for *A* and *B* then given by:

$$\Delta E_A^{CP} = A_{A[B]} - E_A \quad 2.22$$

$$\Delta E_B^{CP} = A_{[A]B} - E_B \quad 2.23$$

The sum of these counterpoise corrections,  $\Delta E_A^{CP} + \Delta E_B^{CP}$ , therefore represents the total correction to the interaction energy and thus the counterpoise corrected interaction energy is given by:

$$\Delta E_{AB}^{corrected} = E_A + E_B - E_{AB} + \Delta E_A^{CP} + \Delta E_B^{CP} \quad 2.24$$

It should be noted that  $E_{A[B]}$  and  $E_{[A]B}$  are evaluated at the geometry optimized for  $AB$ , that is, the geometry used to calculate  $E_{AB}$ . If  $A$  and/or  $B$  are molecular fragments, these geometries may be different from their equilibrium geometries (those used to calculate  $E_A$  and  $E_B$ ); this may be a potential source of inaccuracy in  $\Delta E_A^{CP} + \Delta E_B^{CP}$ . This further highlights the approximate nature of the counterpoise correction.

## 2.6 Molecular properties

### 2.6.1 Geometry optimization

A molecule with  $N$  atoms has  $3N-6$  internal degrees of freedom ( $3N-5$  if linear) in a Cartesian coordinate system. [31] These correspond to three degrees of freedom for each of the  $N$  atoms less the three degrees of freedom associated with translations of the (rigid) molecule and the three (or two) degrees of freedom corresponding to molecular rotation. The potential energy surface (PES) of the molecule,  $E(\mathbf{R})$ , is therefore a function of these  $3N-6$  ( $3N-5$ ) internal distortions of the molecule.

In most chemical applications one is interested in energies and other properties of molecules at their equilibrium geometries, which represent minima on this PES, and at transition state geometries, which correspond to first order saddle points. A local minimum on the PES is characterized by the energy gradient,  $F$ , being zero with respect to all geometric parameters:

$$F_i = \frac{\partial E(\mathbf{R})}{\partial R_i} = 0 \quad \forall i \quad 2.25$$

Furthermore, it is also required that the Hessian,  $H$ , be positive definite; that is, have all its eigenvalues greater than zero. The  $H$  is the second derivative matrix with matrix elements:

$$H_{ij} = \frac{\partial^2 E(R)}{\partial R_i \partial R_j} \quad 2.26$$

For a transition state (a first order saddle point) the gradient is also zero, while the Hessian has one negative eigenvalue. This corresponds to a geometry where the energy is a minimum with respect to all geometric parameters except one, the reaction coordinate, for which it is at a maximum.

In order to successfully find an equilibrium structure or transition state on the potential energy surface it is necessary to start with a molecular configuration,  $R_0$ , which is in the neighborhood of the appropriate local minimum or saddle point geometry,  $R_e$ . The PES,  $E(R)$ , can then be expanded as a Taylor series around  $R_0$ :

$$\begin{aligned} E(R) &= E(R_0) + \sum_i \frac{\partial E(R)}{\partial R_i} (R_i - R_i^0) + \frac{1}{2} \sum_{i,j} \frac{\partial^2 E(R)}{\partial R_i \partial R_j} (R_i - R_i^0) (R_j - R_j^0) + \dots \\ &= E(R_0) + \Delta R^T F + \frac{1}{2} \Delta R^T H \Delta R + \dots \end{aligned} \quad 2.27$$

where  $\Delta R_i = R_i - R_i^0$ .

The geometry corresponding to the minimum of the above quadratic expression (Equation (2.27)) is obtained by solving

$$\frac{\partial E(R)}{\partial R_i} = \frac{\partial E(R)}{\partial R_i} \Big|_{R=R_0} + \frac{\partial^2 E(R)}{\partial R_i \partial R_j} \Big|_{R=R_0} (R_j - R_j^0) = 0 \quad \forall i \quad 2.28$$

that is,

$$F + H \Delta R = 0 \quad 2.29$$

where the gradient vector,  $F$ , and Hessian,  $H$ , are evaluated at  $R_0$ .

The solution for the required change in geometry is therefore given by

$$\Delta R = -H^{-1} F \quad 2.30$$

The truncation of the Taylor expansion at second order means that the PES has been

approximated by a parabolic surface with the same gradient and curvature as the PES at  $R_0$  (Figure 2.1). Correcting  $R_0$  by  $\Delta R$  moves the geometry to the stationary point of this quadratic surface,  $R_1$ , which, if the starting geometry is within the local region of the stationary point sought, will be closer to  $R_e$ . This process is repeated at the new geometry thus found until the elements of the gradient vector are below some preset convergence threshold, at which point the geometry is said to be converged and the equilibrium geometry has been found. This iterative process is known as the Newton-Raphson method; it represents a second order local model, since in a given search it aims to find the closest stationary point.

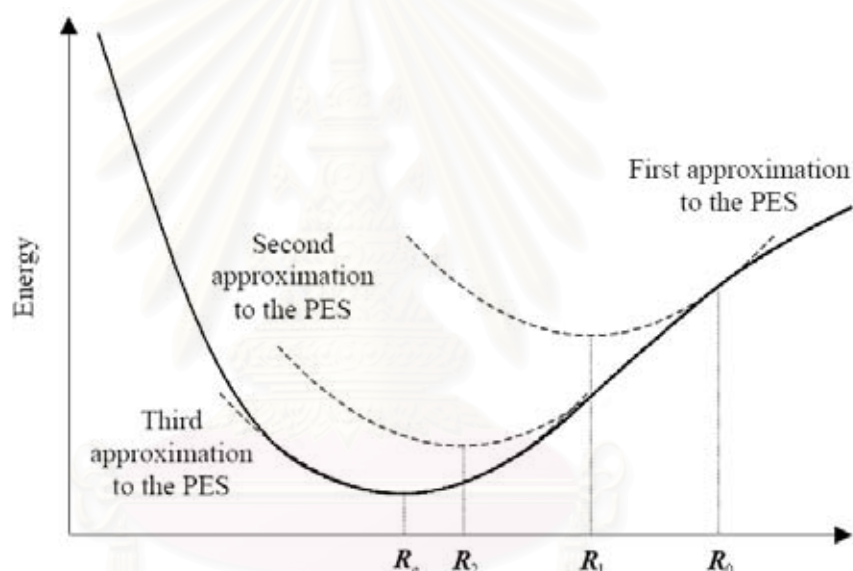


**Figure 2.1** Newton-Raphson steps (in one dimension) for optimizing geometries.

In practice calculating the Hessian in each step is quite expensive and, if possible, it is avoided. This can be done by making a reasonable initial guess of the diagonal elements on the basis of computed force constants and using the gradient information to improve the approximate Hessian during the optimization procedure. While this process works well for equilibrium geometries, the local region is generally much smaller for transition state structures and thus much more accurate Hessians are required. If the starting geometry is close enough to  $R_e$  it is sufficient to

only calculate the Hessian fully in the first Newton-Raphson step; for more difficult cases, however, it may be necessary to calculate it at every step.

While gradients and Hessians are initially calculated with respect to the Cartesian coordinates of the atoms, it is usually more convenient for the purposes of geometry optimization to perform a conversion such that they are expressed in terms of the  $3N-6$  (or  $3N-5$ ) internal coordinates of the molecule. This approach also allows experimental or empirical force constants to be more readily utilized for the construction of approximate Hessians.

Sometimes it is desirable to perform a geometry optimization where various constraints have been applied. These constraints are particularly useful when mapping potential energy surfaces where one geometric parameter is systematically varied while the others are allowed to relax in response. In such situations the Hessian needs to be calculated with respect to the molecular internal coordinates. The Lagrange method can be applied in order to obtain derivatives with the constraints embedded in them; these can then be used to aid in the location of critical points as described above.

### 2.6.2 Normal mode analysis or frequency calculation

By definition the Hessian matrix is the matrix of force constants. When expressed in terms of internal coordinates, its elements are the harmonic force constants for the  $3N-6$  ( $3N-5$ ) internal degrees of freedom of the molecule of interest. These determine the molecule's harmonic vibrational frequencies. The latter, by definition, correspond to the normal vibrational modes; these can be determined by a unitary transformation of the Hessian such that the classical potential ( $V$ ) and kinetic ( $T$ ) energies of the system are in a diagonal representation. In the Cartesian representation  $V$  and  $T$  are given by:

$$V = X^+ H X \quad 2.31$$

$$T = \frac{1}{2} \dot{X}^+ M \dot{X} \quad 2.32$$

where  $H$  is the Hessian matrix,  $M$  is the (diagonal) matrix of atomic masses and  $X$  is the vector of Cartesian displacements of the atoms with time derivative,  $\dot{X}$ .

The normal modes,  $Q$ , are related to  $X$  via a linear transformation:

$$X = AQ \quad 2.33$$

In the normal mode representation  $V$  and  $T$  are therefore given as:

$$V = Q^+ A^+ H A Q \quad 2.34$$

$$T = \frac{1}{2} \dot{Q}^+ A^+ H A \dot{Q} \quad 2.35$$

Thus, if  $A$  satisfies the generalized eigenvalue equations

$$H A = M A \Lambda \quad 2.36$$

where  $\Lambda$  is the diagonal matrix of eigenvalues, one obtains:

$$V = Q^+ \Lambda Q \quad 2.37$$

$$T = \frac{1}{2} \dot{Q}^+ \dot{Q} \quad 2.38$$

The normal mode frequencies are simply proportional to the square roots of the elements of  $\Lambda$ . If the geometry of interest corresponds to a minimum on the PES,  $H$  is positive definite and thus all diagonal elements of  $\Lambda$  will be positive and all frequencies will be real. If the geometry is a transition state or higher order saddle point, one or several of the elements of  $\Lambda$  will be negative and will thus return imaginary frequencies.

The total zero-point energy (ZPE) of the molecular system in the harmonic approximation can be readily obtained from the vibrational frequencies by summing over the zero-point energies of all modes:

$$ZPE = \frac{1}{2} \sum_i h \nu_i \quad 2.39$$

where  $h$  is Planck's constant.

In reality the harmonic approximation does not provide a true representation of the vibrational modes since bond stretches are much better represented by Morse type potentials and bending/torsional modes are periodic. Nevertheless, so long as the vibrational amplitudes are small, the harmonic approximation can be demonstrated to be valid for at least the lowest energy vibrations. An anharmonic treatment or at least anharmonic corrections need to be applied in situations where this harmonic approximation fails, such as in the computation of vibrational overtones.



## 2.7 Thermochemistry

The calculation of theoretical heats of formation is essential for many of the applications of quantum chemistry, in particular for aiding in the interpretation of experimental results and for the prediction of reaction kinetics. Unfortunately, however, this requires the computation of the reaction enthalpy for the formation of a molecule relative to the standard states of its constituent elements; in many cases these standard states are liquids or solids for which direct calculation of the energy is not feasible. Given that accurate experimental values are available for the enthalpies of formation of free atoms, a practical alternative is to use these in conjunction with a theoretical prediction of the atomization energy,  $\sum D_0$ , to predict the heat of formation for the molecule of interest. Thus, given an atomization energy at 0 K,

$$\sum D_0 = \sum_{atoms} E_{atom} - E_{molecule} \quad 2.40$$

(where the total molecular energy includes the zero-point vibrational energy), Hess' law can be applied to obtain the  $\Delta_f H_0^0$ :

$$\Delta_f H_0^0(molecule) = \sum_{atoms} \Delta_f H_0^0(atom) - \sum D_0 \quad 2.41$$

Heats of formation at other temperatures ( $\Delta_f H_T^0$ ) as well as entropies ( $S_T^0$ ) and Gibbs free energies of formation ( $\Delta_f G_T^0$ ) can then be calculated using the standard methods of statistical mechanics.

### 2.7.1 Partition functions

The first step in determining the thermal contributions to the enthalpies and entropies of a molecule is to determine its partition function,  $q$ ; this is a measure of the number of states accessible to the molecule (translational, rotational, vibrational and electronic) at a particular temperature. [46,47]

Given the energies,  $E_i$ , of the available quantum states of a molecule,  $q$  is defined as:

$$q = \sum_{i=1}^{\infty} g_i e^{-\beta E_i} \quad 2.42$$

where  $g_i$  is the degeneracy of the  $i^{\text{th}}$  state and

$$\beta = \frac{1}{k_B T} \quad 2.43$$

where  $k_B$  is Boltzmann's constant and  $T$  is the temperature of interest. The summation in Equation (2.42) is over all possible quantum states of the system.

It is assumed that the translational ( $T$ ), rotational ( $R$ ), vibrational ( $V$ ) and electronic ( $E$ ) modes of the system can be separated, thus allowing the energy of each level,  $E_i$ , to be separated into  $T$ ,  $R$ ,  $V$  and  $E$  contributions:

$$E_i = E_i^T + E_i^R + E_i^V + E_i^E \quad 2.44$$

While the translational modes are truly independent from the rest, the separations of the other modes are based on approximations, in particular the Born-Oppenheimer approximation for electronic and (ro-) vibrational motion and the Rigid Rotor Approximation (which assumes that the geometry of the molecule does not change as it rotates) for vibrational and rotational modes. Within these approximations, the total molecular partition function can therefore be factorized into translational, rotational, vibrational and electronic contributions:

$$q = q^T q^R q^V q^E \quad 2.45$$

The translational partition function is given by:

$$q^T = \frac{V}{\Lambda^3} \quad 2.46$$

$$\Lambda = h \left( \frac{\beta}{2\pi m} \right)^{1/2} \quad 2.47$$

where  $h$  is Planck's constant,  $m$  is the mass of the molecule, and  $V$  is the volume available to it; for a gas phase system this is the molar volume at the specified temperature and pressure (usually determined by the ideal gas equation).

The formulation for rotational partition functions depends on whether or not the molecule is linear. For linear molecules

$$q^R = \frac{k_B T}{\sigma h c B} \quad 2.48$$

and for non-linear molecules

$$q^R = \frac{1}{\sigma} \left( \frac{k_B T}{h c} \right)^{3/2} \left( \frac{\pi}{ABC} \right)^{1/2} \quad 2.49$$

where  $\sigma$  is the rotational symmetry number of the molecule,  $c$  is the speed of light and  $A$ ,  $B$  and  $C$  are the rotational constants. The vibrational partition function in the harmonic approximation is

$$q^V = \prod_i \frac{1}{1 - e^{-\beta h c \tilde{\nu}_i}} \quad 2.50$$

where  $\tilde{\nu}_i$  are the harmonic vibrational frequencies (expressed as wavenumbers) and the product is taken over all ( $3N-6$  or  $3N-5$ ) vibrational modes (excluding the reaction coordinate for transition states). For the electronic partition function it is usually assumed that there will be no thermal excitation into higher electronic states so that the partition function,  $q^E$ , is simply given by the degeneracy of the appropriate electronic state.

### 2.7.2 Thermodynamic properties

The thermal contributions to thermodynamic properties such as enthalpy, entropy, free energy, heat capacity, etc. are all derived from the molecular partition functions. [46] For a system of  $N$  molecules the internal energy (relative to internal energy at 0 K) is given by

$$U_T^0 - U_0^0 = -N \left( \frac{\partial \ln q}{\partial \beta} \right) \quad 2.51$$

where the derivative is taken at constant volume. The enthalpy is therefore

$$\begin{aligned} H_T^0 - H_0^0 &= (U_T^0 - U_0^0) + p\Delta V \\ &= (U_T^0 - U_0^0) + Nk_B T \end{aligned} \quad 2.52$$

The entropy of the system is given by

$$S^0 = \frac{(U_T^0 - U_0^0)}{T} + Nk_B \ln q \quad 2.53$$

so that the change in Gibbs free energy is

$$\begin{aligned} (G_T^0 - G_0^0) &= (H_T^0 - H_0^0) - TS^0 \\ &= Nk_B T - Nk_B T \ln q \end{aligned} \quad 2.54$$

The Gibbs free energy change for a reaction is, of course, related to the equilibrium constant for the reaction:

$$\Delta_r G^0 = -Nk_B T \ln K_{eq} \quad 2.55$$

## 2.8 Polarizable continuum solvent model

In a polarizable continuum model (PCM), the molecule is surrounded by a dielectric medium, the polarizable continuum, with a given dielectric constant,  $\epsilon$ . [32-34] This medium is polarized in response to the charge distribution (nuclei and electrons) that it experiences and produces an electric field, called a reaction field, which in turn polarizes the molecule. The resulting slightly changed charge distribution alters the reaction field somewhat, which again leads to further polarization of the molecule. This process continues until equilibrium is reached. In the PCM implemented in the Gaussian program, the reaction field is represented through charges located on the surface of the molecular cavity. The molecular cavity can be created in several ways, but is generally based on interlocking van der Waals-spheres centered at atomic positions. The surface of this cavity is smoothed (for numerical reasons) and in the PCM model approximated by many small planar surface elements of given area. Charges are then placed on each of the surface elements to represent the reaction field of the dielectric medium. The extent to which the medium can be polarized and hence the ultimate strength of the reaction field is controlled by the magnitude of the dielectric constant.

## CHAPTER III

### RESULTS AND DISCUSSION

In this chapter, the study is divided into three parts. In the first part, geometrical structures, relative energies, and electronic properties of four typical conformers as called *cone* (*C*), *partial cone* (*PC*), *1,2-alternate* (*1,2-A*) and *1,3-alternate* (*1,3-A*) of six compounds of thiacalix[4]arene derivatives (tetrahydroxythiacalix[4]arene (**1**), tetrahydroxy-*p-tert*-butylthiacalix[4]arene (**2**), tetramercaptothiacalix[4]arene (**3**), tetramercapto-*p-tert*-butylthiacalix[4]arene (**4**), tetraaminothiacalix[4]arene (**5**), and tetraamino-*p-tert*-butylthiacalix[4]arene (**6**)) and six compounds of sulfonylcalix[4]arene derivatives (tetrasulfonylcalix[4]arene (**7**), tetrahydroxy-*p-tert*-butylsulfonylcalix[4]arene (**8**), tetramercapto sulfonylcalix[4]arene (**9**), tetramercapto-*p-tert*-butylsulfonylcalix[4]arene (**10**), tetraaminosulfonylcalix[4]arene (**11**), and tetraamino-*p-tert*-butylsulfonylcalix[4]arene (**12**)) (tetra and tetrahydroxy prefixes are further omitted for simplicity) have been studied using the density functional theory (DFT) method at B3LYP/6-31G(d) level of theory. [48-49] Due to the computation cost, three selected compounds, **7**, **9** and **11** are chosen for the protonation study under the single point calculation at B3LYP/6-31G(d)//B3LYP/6-31G(d), B3LYP/6-31G(d)//B3LYP/6-31G(d,p) and B3LYP/6-31G(d)//B3LYP/6-311G(d,p) levels of theory. The effect of common solvents used in experimental studies, i.e., water, chloroform and dichloromethane on relative stabilities of **7**, **9** and **11** has been computed under the conductor-like polarizable continuum model (CPCM) combined with the DFT method at B3LYP/6-31G(d) level of theory. [50,51] Further more, inversion barriers between *cone* and *partial cone* of the corresponding compounds of **1**, **3**, **5**, **7**, **9**, and **11** have been studied at the B3LYP/6-31G(d) level of theory.

In the second part, the complexation properties, the HOMO–LUMO molecular orbital energy gaps and electronic of the zinc(II) complexes of the cone conformer of 12 compounds (**1-12**) with zinc(II) ion have been studied by using the density functional theory (DFT) method at B3LYP/6-31G(d) level of theory.

Finally, the host–guest interactions between carboxylate guests and amino-*p*-*tert*-butylthiacalix[4]arene hosts have been investigated using ONIOM method to obtain complexation energies and thermodynamic data. [42]

### 3.1 Theoretical study of thiacalix[4]arene and sulfonylcalix[4]arene derivatives

#### 3.1.1 Computational method

Geometry optimizations of all investigated compounds, thiacalix[4]arene and sulfonylcalix[4]arene derivatives have been computed by density functional theory. The DFT calculation has been performed with the Becke's three-parameter exchange functional with the Lee–Yang–Parr correlation functional (B3LYP). [48-49] All geometry optimizations have been carried out using the 6-31G(d) basis set. In addition, the *cone* conformer of calix[4]arene are studied using the same level of theory for comparison to the title compounds.

To study the effect of solvents and basis sets on the energetically stability of the host compounds, the smaller sulfonylcalix[4]arene derivatives as **7**, **9** and **11** are chosen. The B3LYP/6-31G(d,p) and B3LYP/6-311G(d,p) levels of theory are employed for the single-point energetically calculations of the B3LYP/6-31G(d)-optimized geometries of the involved species. The solvent effect has been investigated by single-point computations on the B3LYP/6-31G(d)-optimized gas-phase structures using the conductor-like polarizable continuum model (CPCM) at B3LYP/6-31G(d)//B3LYP/6-31G(d) level of theory. [50, 51] All calculations have been performed with the Gaussian 03 program. [52] The molden 4.3 program [53] is utilized to display the molecular structure, monitor the geometrical parameters and observe the molecular geometry convergence through out the Gaussian output files. The molecular graphics of all related species are generated with the Gauss View 3.0 [54] and molekel 4.3 programs. [55]

The chemical hardness ( $\eta$ ), Mulliken electronegativity ( $\chi$ ) and electronic chemical potential ( $\mu$ ) for all conformers of sulfonylcalix[4]arene, mercapto sulfonylcalix[4]arene, aminosulfonylcalix[4]arene have been computed using orbital energies of the highest occupied molecular orbital (HOMO) and the lowest unoccupied molecular orbital (LUMO) at the B3LYP/6-31G(d) level. The chemical hardness, Mulliken electronegativity and electronic chemical potential are derived

from the first ionization potential ( $I=E(N-1)-E(N)$ ) and electron affinity ( $A=E(N)-E(N+1)$ ) [56] of the  $N$ -electron molecular system with a total energy ( $E$ ) and external potential using the relations:

$$\eta = \left( \frac{\partial^2 E}{\partial N^2} \right)_{v(r)} \cong \frac{1}{2}(I - A) \quad 3.1$$

$$\chi = - \left( \frac{\partial E}{\partial N} \right)_{v(r)} = -\mu \cong \frac{1}{2}(I + A). \quad 3.2$$

According to the Koopmans theorem [57],  $I$  and  $A$  are computed from the HOMO and LUMO energies using the relations:  $I = -E_{HOMO}$  and  $A = -E_{LUMO}$ .

### 3.1.2 Comparison geometrical structure with calix[4]arene

The aim of this topic is to characterize thiacalix[4]arene (**1**) and sulfonylcalix[4]arene (**7**) with respect to the classical compound, calix[4]arene (**C4A**), to give some keys for designing new supramolecular structures. For the thiacalix[4]arenes compounds **1** to **6**, four of six thiacalix[4]arenes of the studied compounds have been experimentally achieved, namely the thiacalix[4]arene **1**, *p*-*tert*-butylthiacalix[4]arene **2**, mercapto-*p*-*tert*-butylthiacalix[4]arene **4**, amino-*p*-*tert*-butylthiacalix[4]arene **6**, whereas the synthesis of mercaptothiacalix[4]arene **3** and aminothiacalix[4]arene **5** has not been reported due to its synthetic difficulty. So the theoretical study will be used to predict their molecular properties.

When the DFT calculated structures of **C4A** and thiacalix[4]arene macrocycle, **1** are compared, it is interesting to note that O and H atoms of hydroxyl groups in the two structures in Figure 3.1 (a) are superimposed rather well. Moreover, the slightly larger size of **1** is responsible for the O...H...O bond angle which is smaller than 11.7 degrees. On the other hand the Figure 3.1 (b) shows that when the DFT calculated structures of **C4A** and sulfonylcalix[4]arene, **7** are compared, only the O atoms of hydroxyl groups in the two structures are superimposed. However, the H atoms of hydroxyl group point to the oxygen atoms of sulfonyl (-SO<sub>2</sub>-) bridges to form new hydrogen bonds. The calix[4]arene macrocycle thus seems to be somewhat better preorganized for the narrow rim hydrogen bonding. In addition, when methylene bridges are changed to sulfur bridges the cavity sized can be increased approximately 9%. Moreover, when methylene (-CH<sub>2</sub>-) bridges are changed to sulfonyl (-SO<sub>2</sub>-)

bridges the cavity sized can be increased approximately 10%. The diversity of their cavity sizes could contain the different guest molecules.

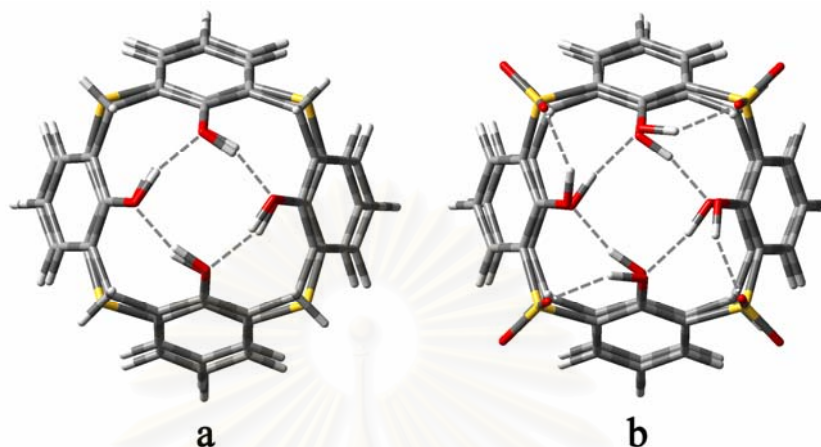


**Figure 3.1** Comparison of (a) classical calix[4]arene (**C4A**) and **1** and (b) **C4A** and **7** structures obtained at the B3LYP/6-31G(d) level of theory. Hydrogen bonds are displayed in dashed lines.

### 3.1.3 Geometrical structure and energetic stability

This part will consider here only four main conformations which are cone, partial cone, *1,2*-alternate and *1,3*-alternate. In order to facilitate the description of the results it is convenient to put forward a naming picture for the atoms in the molecule, so that in what follows they may be referred to easily. Such a naming convention is pictorially described in Figures 3.2 and 3.3. The conformational geometries of four typical conformers obtained at the B3LYP/6-31G(d) level of theory of thiacalix[4]arene (**1** to **6**) and sulfonylcalix[4]arene (**7** to **12**) derivatives are shown in Figures 3.4 to 3.9 and Figures 3.10 to 3.15, respectively. The symmetries of cone conformers of smaller compounds; **1**, **3**, **5**, **7**, **9** and **11** are  $C_4$ ,  $C_2$ ,  $C_{2V}$ ,  $C_4$ ,  $C_2$ , and  $C_{4V}$ , respectively. It should be noted that the replacement of four OH groups with SH or  $NH_2$  groups can reduce the symmetries of cone conformers. Except for **11** the replacement of OH group with  $NH_2$  group increases the conformation symmetry because it is the formation of hydrogen bonds between amino proton and sulfonyl oxygen (see Figure 3.12). However, an introduction of *tert*-butyl groups onto the smaller derivatives to form the larger compounds (**2**, **4**, **6**, **8**, **10** and **12**) is slightly effective to their conformational symmetries and their geometrical structures.



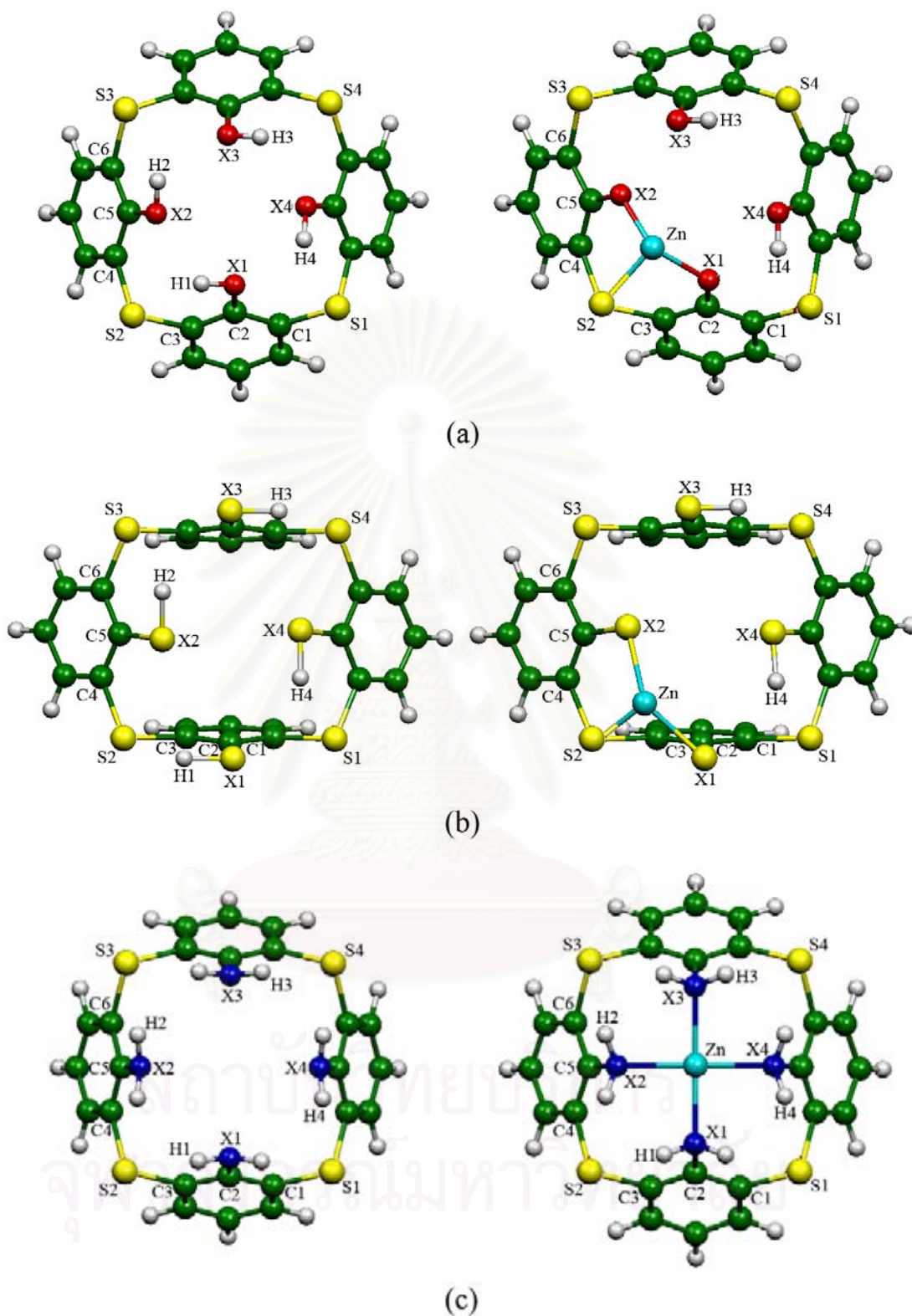


**Figure 3.2** Atomic labeling of (a) thiactalix[4]arene, (b) mercaptothiactalix[4]arene and (c) aminothiactalix[4]arene and their zinc(II) complexes.

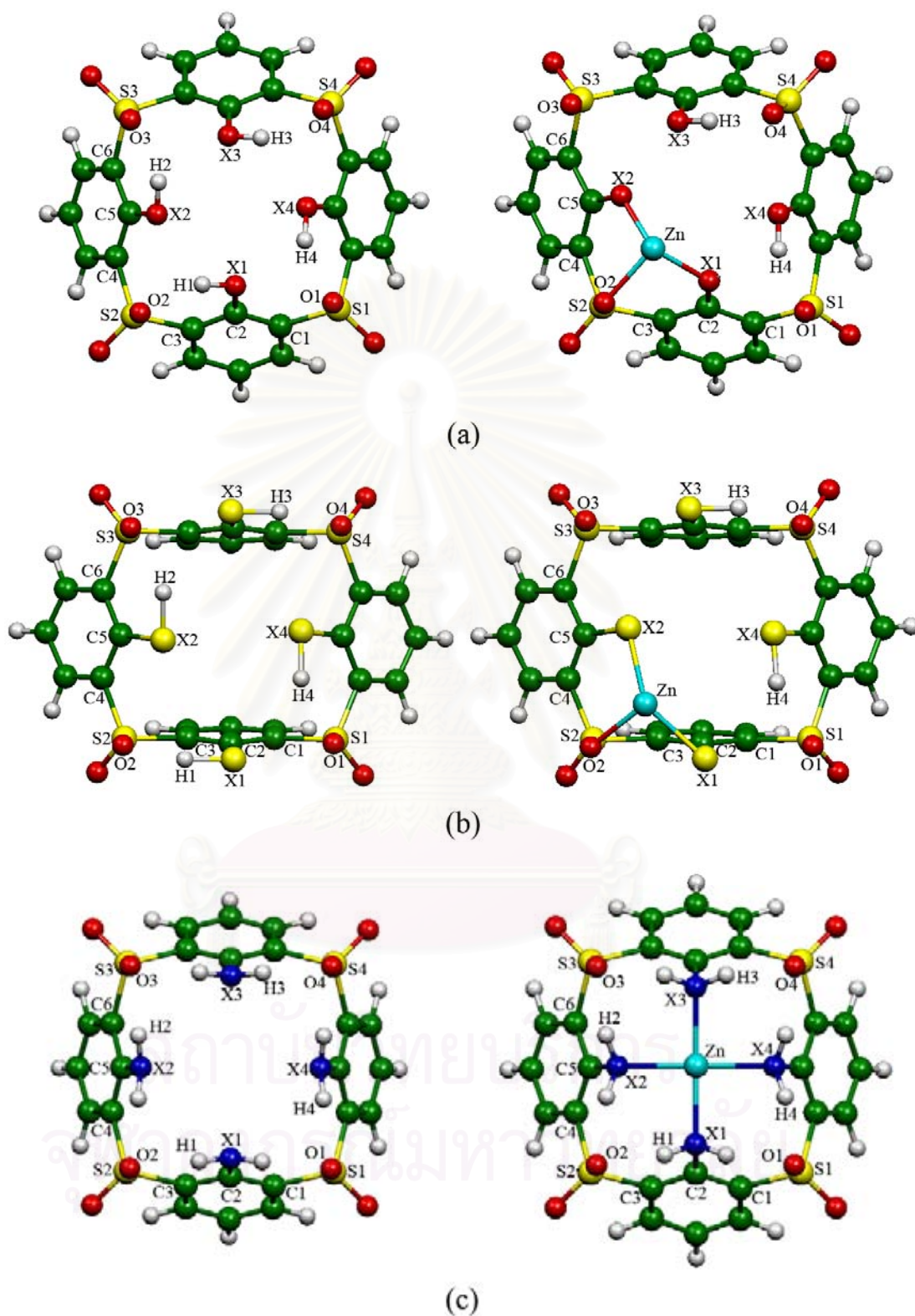


**Figure 3.3** Atomic labeling of (a) sulfonylcalix[4]arene, (b) mercaptosulfonylcalix[4]arene and (c) aminosulfonylcalix[4]arene and their zinc(II) complexes.

For thiacalix[4]arene compounds, the intra hydrogen bonds (displayed in dash lines at the top view of each structure) between narrow rim substituted groups (-OH, -SH and -NH<sub>2</sub>) of the *cone* conformers are obviously apparent. Further more, the cone conformer of thiacalix[4]arene **1** shows the highest symmetry,  $C_4$ , whereas *partial cone* conformer shows the lowest symmetry,  $C_1$ . A number of hydrogen bonds caused by the interaction between phenolic proton and adjacent phenolic oxygen are four in *cone* in which hydrogen bond distances are identical and equivalent to 1.829 Å and number of hydrogen bond decreases to two in *partial cone*, *1,2-alternate* and non in *1,3-alternate*. This results are also found in compounds **2** to **6**. The optimized geometrical parameters of cone conformers are collected in Table 3.1. It should be note here that the hydrogen bond distances in *cone* conformer computed at B3LYP/6-31G(d) level of thiacalix[4]arene (1.829 Å) are longer than those of the calix[4]arene (1.699 Å) and *p-tert-butylcalix[4]arene* (1.697 Å).

The substituted groups at narrow rim (-NH<sub>2</sub>, -SH) of the *cone* conformer are slightly effective to the cavity sizes, defined as the bond distances between the neighbored sulfur atoms (S1-S2 and S2-S3 distances), of thiacalix[4]arene bridges but they are strongly sensitive to their C-X and X-X distances (X=S or N, the narrow rim substituted atoms, see Figures 3.4 to 3.9). The average cavity sizes of compounds **1** to **6** are about 5.602 Å. However, it is clearly seen that the steric effect break down the  $C_4$  symmetrical structures of compounds **2** to **6** produced the  $C_2$  or  $C_{2v}$  symmetrical structures containing two stronger hydrogen bonds. Further more, the X1-X2 and X2-X3 distances (X=S or N) of the cone conformers of compounds **3** to **6** are not identical. The dihedral angles between two opposite benzene rings are also not consistent (see Table 3.1). The identical X1-X2 and X2-X3 distances (X=O) of compounds **1** and **2** are about 2.740 Å. The non identical X1-X2 and X2-X3 distances (X=N) are about 3.785 and 3.258 Å, respectively for compounds **3** and **4**. The non identical X1-X2 and X2-X3 distances (X=S) are about 3.909 and 3.258, respectively for compounds **5** and **6**.

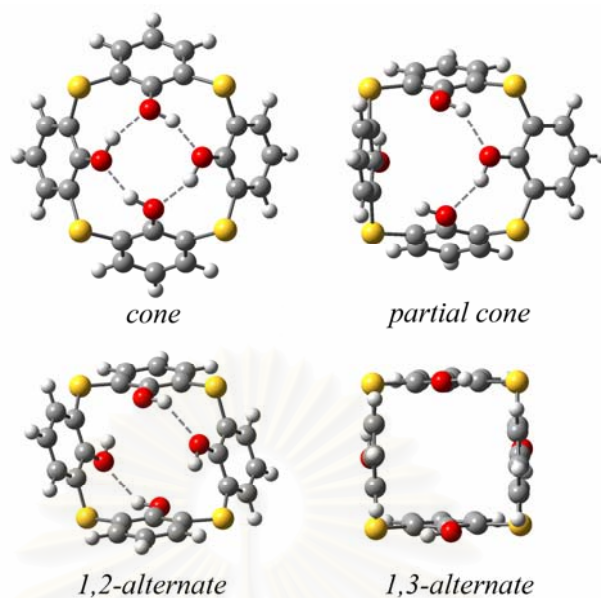


**Figure 3.4** Conformational geometries of typical conformers of thiacalix[4]arene (**1**) optimized at the B3LYP/6-31G(d) level of theory.

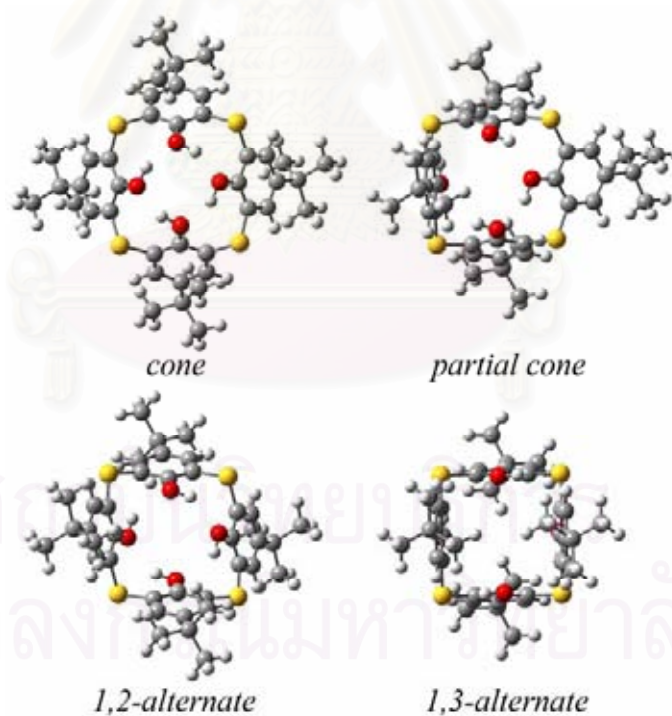


**Figure 3.5** Conformational geometries of typical conformers of *p*-tert-butylthiacalix[4]arene (**2**) optimized at the B3LYP/6-31G(d) level of theory.

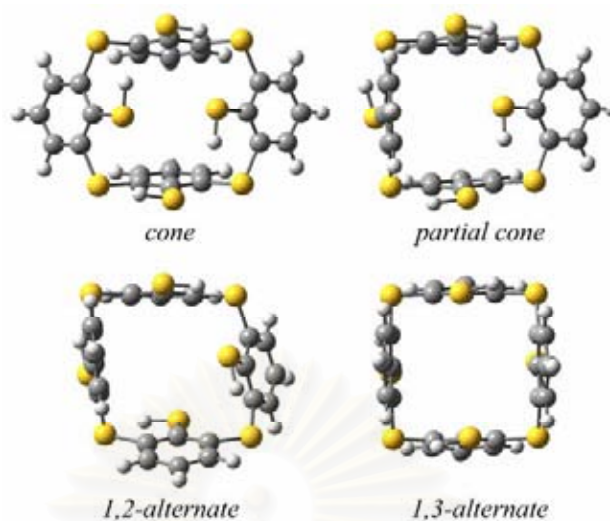


**Figure 3.6** Conformational geometries of typical conformers of mercaptothiacalix[4]arene (**3**) optimized at the B3LYP/6-31G(d) level of theory.

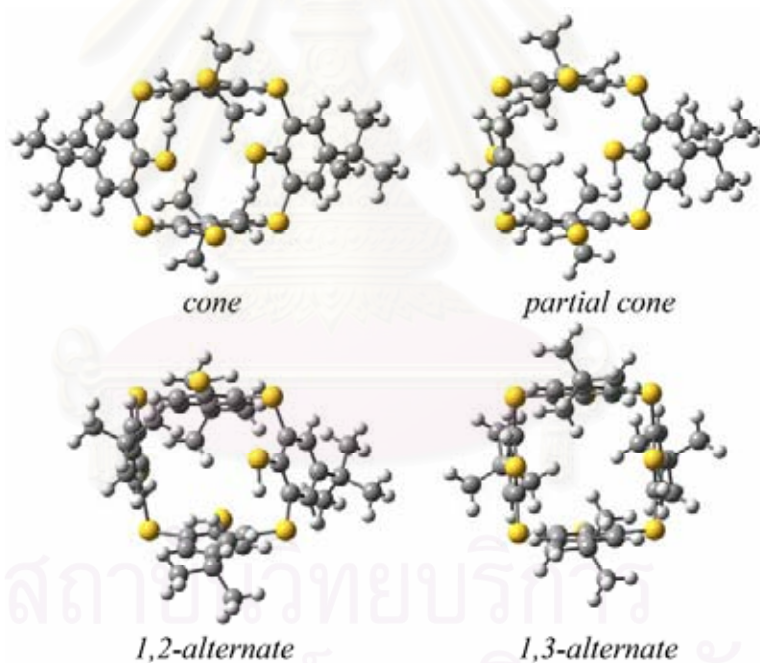


**Figure 3.7** Conformational geometries of typical conformers of mercapto-*p*-*tert*-butylthiacalix[4]arene (**4**) optimized at the B3LYP/6-31G(d) level of theory.

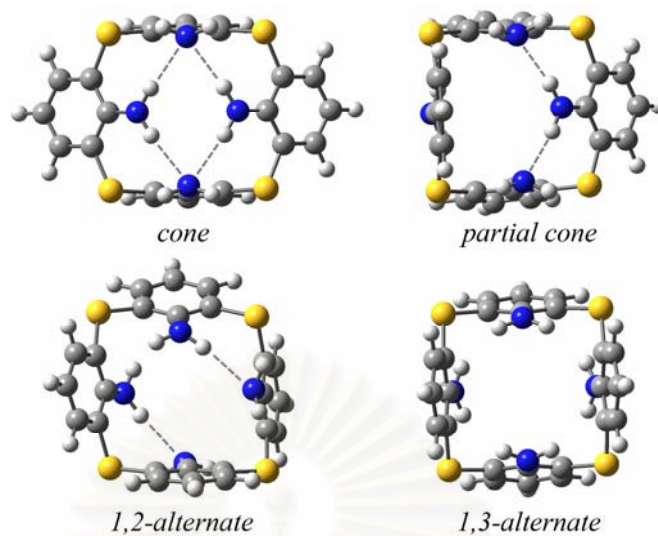


**Figure 3.8** Conformational geometries of typical conformers of aminothiocalix[4]arene (**5**) optimized at the B3LYP/6-31G(d) level of theory.

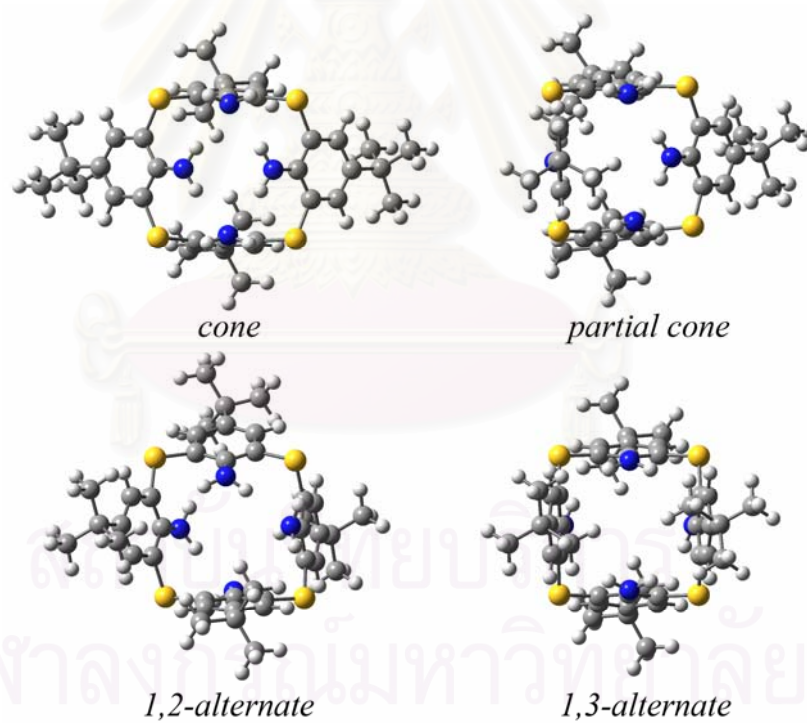


**Figure 3.9** Conformational geometries of typical conformers of amino-*p*-*tert*-butylthiocalix[4]arene (**6**) optimized at the B3LYP/6-31G(d) level of theory.

**Table 3.1** Geometrical data for the structure of cone conformer of thiacalix[4]arene derivatives computed at the B3LYP/6-31G(d) level of theory

Parameter <sup>a</sup>	1	2	3	4	5	6
Distance (Å)						
S1-S2	5.582	5.581	5.641	5.641	5.586	5.584
S2-S3	5.582	5.581	5.630	5.649	5.643	5.640
S1-S3	7.895	7.892	7.947	7.917	7.940	7.937
S2-S4	7.895	7.894	7.991	8.046	7.940	7.937
S1-C1	1.802	1.803	1.813	1.814	1.808	1.809
C3-S2	1.802	1.803	1.814	1.815	1.808	1.809
S2-C4	1.802	1.803	1.804	1.809	1.801	1.803
C2-X1	1.357	1.358	1.784	1.783	1.404	1.405
C5-X2	1.357	1.358	1.767	1.767	1.361	1.364
X1-X2	2.743	2.740	3.822	3.748	3.263	3.253
X2-X3	2.743	2.741	3.958	3.861	3.262	3.254
X1-X3	3.880	3.879	6.827	6.599	5.373	5.339
X2-X4	3.880	3.874	3.717	3.784	3.616	3.647
X1-H1	0.988	0.988	1.352	1.352	1.015	1.015
H1-X2 <sup>b</sup>	1.829	1.823	3.160	3.057	3.282	3.261
X2-H2	0.988	0.988	1.351	1.351	1.010	1.011
H2-X3 <sup>b</sup>	1.829	1.823	2.751	2.635	2.262	2.250
Angle (Å)						
S1-C1-C2	120.7	120.7	120.9	120.9	120.0	120.0
C1-C2-X1	118.1	118.5	118.2	118.8	120.6	120.9
C2-C3-S2	120.8	120.7	122.3	122.7	120.0	120.0
C2-X1-H1	110.7	110.7	95.1	95.0	113.7	113.5
C3-S2-C4	104.3	104.2	100.2	100.3	102.7	102.7
S2-C4-C5	120.7	120.7	121.4	121.3	121.6	121.6
C4-C5-X2	118.1	118.4	117.8	118.0	121.5	121.8
Dihedral angle (Å)						
S1-C1-C2-C3	-175.8	-175.9	175.4	174.7	178.4	178.0
S1-C1-C2-X1	3.7	3.2	-5.4	-7.9	3.5	3.0
C1-C2-C3-S2	173.9	174.1	-175.1	-172.3	-178.4	-178.1
C1-C2-X1-H1	164.0	163.6	168.1	168.9	-157.8	-157.5
C2-C3-S2-C4	89.0	88.6	125.4	118.8	111.7	110.4
C3-S2-C4-C5	-87.5	-86.9	-70.9	-77.2	-71.4	-73.0
S2-C4-C5-C6	-175.8	-175.9	172.0	174.3	179.5	179.6
S2-C4-C5-X2	3.7	3.3	-8.1	-6.4	-1.3	-1.6
C4-C5-C6-S3	173.9	174.0	-172.0	-176.0	-179.5	-179.7
C4-C5-X2-H2	164.0	163.5	-177.8	-179.6	170.3	167.5

<sup>a</sup> X = O for **1**, **2**, X = S for **3**, **4**, and X = N for **5**, **6**, see Figure 3.2. <sup>b</sup> Hydrogen bond distance.

For the sulfonylcalix[4]arene derivatives, the B3LYP/6-31G(d) optimized structures of the four conformers named *cone*, *partial cone*, *1,2-alternate* and *1,3-alternate* of compounds **7** to **12** are presented in Figures 3.10 to 3.15, respectively. The selected geometrical data for their *cone* conformers are collected in Tables 3.2. A large number of hydrogen bonds are found in sulfonylcalix[4]arene derivatives. In contrast to thiacalix[4]arene derivatives, three types of hydrogen bonds are observed. Type I of hydrogen bond is the intra interactions of narrow rim substituted groups, Type II is the interaction between narrow rim substituted protons and adjacent

sulfonyl bridge oxygens and Type III is the interaction between narrow rim substituted protons and adjacent benzyl protons. The average cavity sizes of the *cone* conformers of sulfonylcalix[4]arene compounds **7** to **12** are as same as for thiacalix[4]arenes at about 5.694 Å. The wide rim substituted (*tert*-butyl) groups show slightly effect to main geometrical structures for all sulfonylcalix[4]arene compounds. Their cavity sizes are very close to those of thiacalix[4]arene derivatives. In addition, the *cone* conformer of compound **7** shows the highest symmetry,  $C_4$ , whereas *partial cone* conformer shows the lowest symmetry,  $C_1$ , as found in compound **1**. Interestingly, the *cone* conformers of compound **11** (the -NH<sub>2</sub> substituted compound) show the highest symmetrical structure as  $C_{4v}$ . It is higher than compound **7**,  $C_4$  symmetry. This may be due to the formation of symmetrical hydrogen bonds between amino and sulfonyl groups. The computed geometrical data of *1,3-alternate* conformers of **7**, **9** and **11** compared to the experimental data of **7** are listed in Table 3.3. The results show that computed structures are good agreement to experimental data. In cone conformer, the replacement of the -OH group with the -NH<sub>2</sub> and -SH groups at narrow rim of compounds **7** and **8** given compounds **9** to **12**, the old types of intra hydrogen bonds are disappeared. At the results, the new intra hydrogen bonds between the narrow rim substituted groups (-OH, -SH and NH<sub>2</sub>) and sulfonyl bridge oxygens are apparently. The bond distances between the sulfur bridge atoms are about 5.694 Å. The symmetry of compound **7** and **8** is nearly  $C_4$ -symmetry (see Figures 10 and 11). As shown in Figures 12, 13 and 15, the steric effects break down the  $C_4$ -symmetrical structures of compounds **9**, **10** and **12** to produce  $C_2$ -symmetrical structures. In contrast, compounds **7** to **10** and **12**, the new intra hydrogen bonds between the narrow rim substituted groups and the sulfonyl bridge oxygens of compound **11** can yield the  $C_{4v}$ -symmetries (see Figure 3.14). Then the identical X1-X2 and X2-X3 distances (X=O) of compounds **7** and **8** are about 2.920 Å. The non identical X1-X2 and X2-X3 distances (X=S) are about 3.820 and 4.000 Å, respectively for both compounds **9** and **10**. The identical X1-X2 and X2-X3 distances (X=N) are about 5.950 Å, for compound **11** and the non identical X1-X2 and X2-X3 distances (X=N) are about 5.659 and 3.908 Å, respectively for compound **12**.



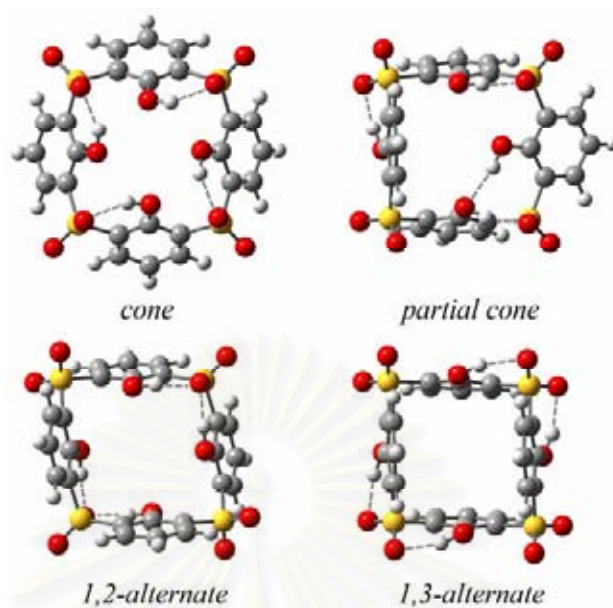


**Figure 3.10** Conformational geometries of typical conformers of sulfonylcalix[4]arene (**7**) optimized at the B3LYP/6-31G(d) level of theory.

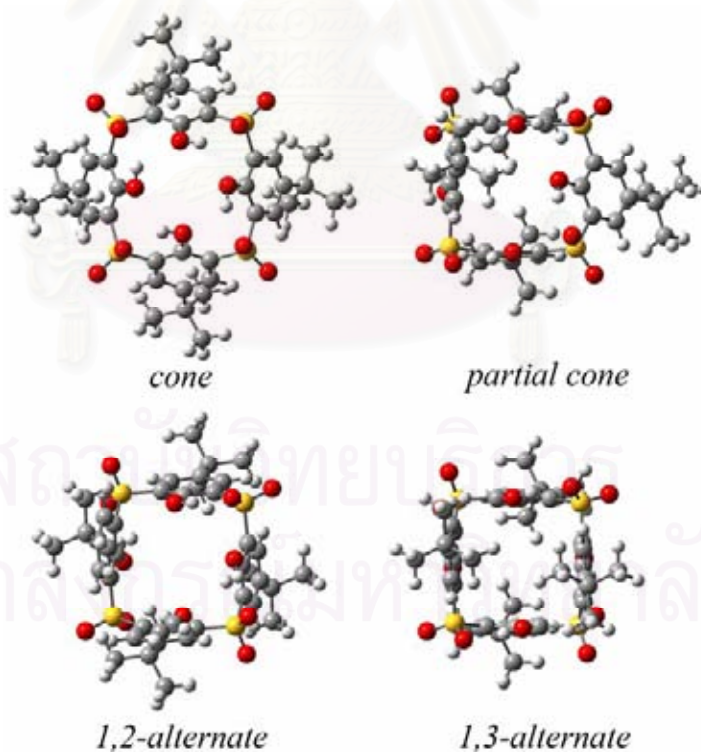


**Figure 3.11** Conformational geometries of typical conformers of *p*-*tert*-butylsulfonylcalix[4]arene (**8**) optimized at the B3LYP/6-31G(d) level of theory.

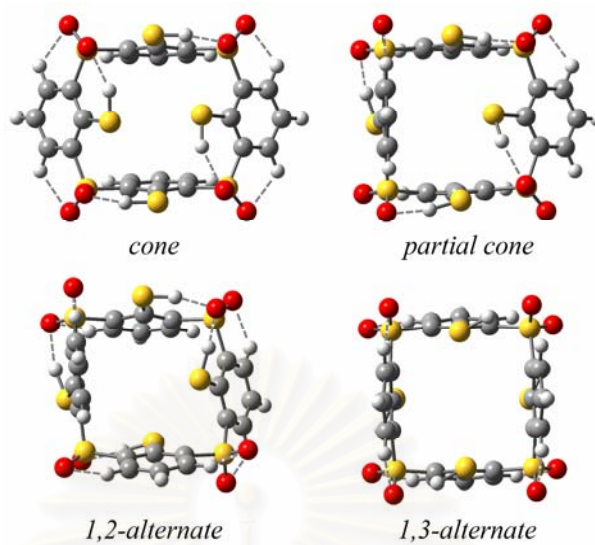


**Figure 3.12** Conformational geometries of typical conformers of mercaptosulfonylcalix[4]arene (**9**) optimized at the B3LYP/6-31G(d) level of theory.

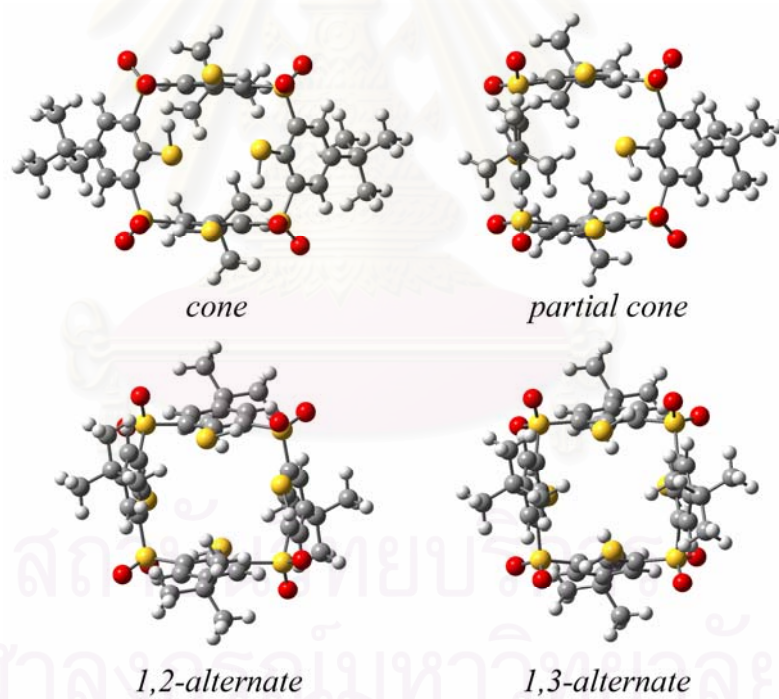


**Figure 3.13** Conformational geometries of typical conformers of mercapto-*p-tert*-butylsulfonylcalix[4]arene (**10**) optimized at the B3LYP/6-31G(d) level of theory.

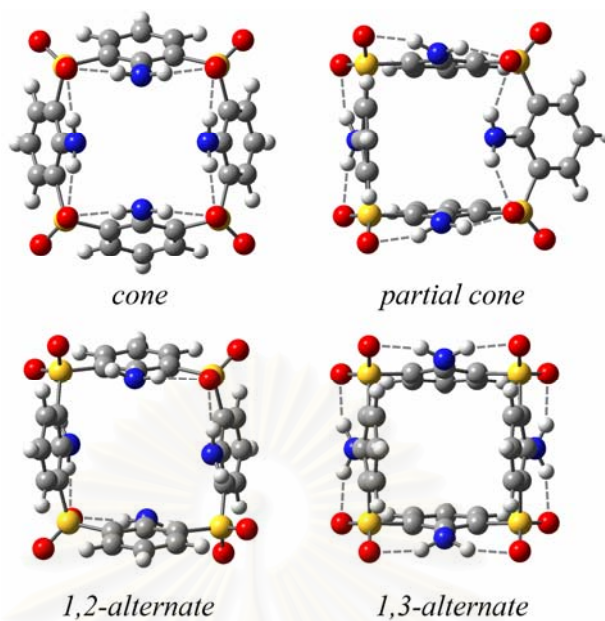


**Figure 3.14** Conformational geometries of typical conformers of aminosulfonylcalix[4]arene (**11**) optimized at the B3LYP/6-31G(d) level of theory.

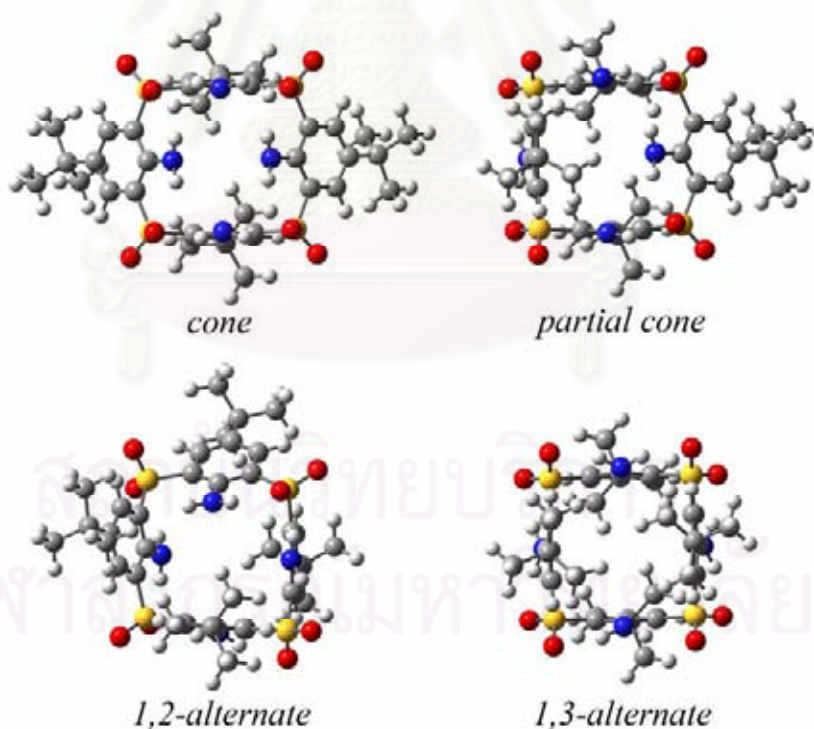


**Figure 3.15** Conformational geometries of typical conformers of amino-*p*-*tert*-butylsulfonylcalix[4]arenes (**12**) optimized at the B3LYP/6-31G(d) level of theory.

**Table 3.2** Geometrical data for the structure of *cone* conformer of sulfonylcalix[4]arene derivatives computed at the B3LYP/6-31G(d) level of theory

Parameter <sup>a</sup>	7	8	9	10	11	12
Distance (Å)						
S1-S2	5.637	5.630	5.818	5.806	5.702	5.708
S2-S3	5.637	5.631	5.710	5.727	5.700	5.619
S1-S3	7.976	7.970	8.104	8.128	8.062	8.009
S2-S4	7.968	7.955	8.198	8.173	8.062	8.010
S1-C1	1.809	1.809	1.826	1.825	1.806	1.808
C3-S2	1.802	1.802	1.836	1.837	1.807	1.805
S2-C4	1.809	1.808	1.824	1.826	1.806	1.801
C2-X1	1.338	1.339	1.778	1.779	1.359	1.366
C5-X2	1.337	1.339	1.769	1.770	1.359	1.365
X1-X2	2.922	2.917	3.825	3.817	3.516	3.461
X2-X3	2.914	2.903	4.003	4.004	3.515	3.470
X1-X3	4.127	4.119	6.810	6.636	5.002	5.659
X2-X4	4.127	4.112	3.805	3.773	4.941	3.908
X1-H1	0.986	0.985	1.352	1.351	1.012	1.013
H1-X2	2.332	2.319	3.368	3.295	-	-
X2-H2	0.986	0.985	1.349	1.348	1.012	1.013
H2-X3	5.317	2.303	2.899	2.857	-	-
O1-O2	2.561	5.326	5.799	5.813	5.549	5.452
O2-O3	5.316	5.330	5.991	5.950	5.552	5.606
S1-O1	1.476	1.476	1.473	1.474	1.487	1.486
S2-O2	1.476	1.477	1.474	1.475	1.487	1.486
H1-O2 <sup>b</sup>	1.882	1.890	1.832	1.843	1.954	1.919
H2-O3 <sup>b</sup>	1.882	1.901	2.021	2.012	1.958	2.146
Angle (Å)						
S1-C1-C2	122.6	122.5	125.4	125.6	123.4	123.7
C1-C2-X1	119.5	119.8	119.9	120.1	122.3	122.7
C2-C3-S2	120.9	120.7	127.7	127.4	123.4	123.6
C2-X1-H1	110.6	110.5	94.7	94.7	116.5	116.4
C3-S2-C4	106.3	106.3	103.0	103.8	105.8	105.0
S2-C4-C5	122.6	122.4	123.4	123.4	123.3	121.2
C4-C5-X2	119.5	120.0	119.3	119.1	122.3	122.5
O1-S1-C1	109.3	109.2	109.9	110.1	108.6	108.3
O2-S2-C4	109.3	109.3	108.8	108.6	108.6	107.7
Dihedral angle (Å)						
S1-C1-C2-C3	-179.2	-179.4	176.4	174.2	174.5	176.7
S1-C1-C2-X1	1.1	0.8	-6.7	-10.6	-5.4	-2.7
C1-C2-C3-S2	178.1	178.2	-176.1	-175.2	-174.6	-176.8
C1-C2-X1-H1	-169.6	-170.3	179.7	-179.0	-163.3	-163.6
C2-C3-S2-C4	86.9	86.8	117.7	113.7	93.4	110.2
C3-S2-C4-C5	-86.7	-86.5	-66.4	-71.5	-92.2	-71.0
S2-C4-C5-C6	-179.2	-179.4	173.3	173.6	174.6	176.5
S2-C4-C5-X2	1.1	1.0	-6.4	-8.0	-5.1	-0.4
C4-C5-C6-S3	178.1	178.1	-171.3	-171.6	-174.8	-176.3
C4-C5-X2-H2	-169.6	-170.4	-171.0	-178.0	-163.3	-162.3
O1-S1-C1-C2	27.7	28.3	-4.8	-1.3	23.1	4.6
O2-S2-C4-C5	27.6	27.8	52.0	47.1	24.2	44.4

<sup>a</sup> X = O for **7**, **8**, X = S for **9**, **10**, and X = N for **11**, **12**, see Figure 3.3. <sup>b</sup> Hydrogen bond distance.

**Table 3.3** Geometrical data for the structure of *1,3-alternate* conformer of sulfonylcalix[4]arene derivatives computed at B3LYP/6-31G(d) level of theory

Parameter <sup>a</sup>	<b>7</b>	<b>9</b>	<b>11</b>	X-ray <sup>b</sup>
Bond distances (Å)				
S2-C3	1.791	1.820	1.799	1.771
S2-O2	1.480	1.476	1.477	1.449
S1-S2	5.571	5.734	5.599	5.500
S1-S3	7.597	8.066	7.918	7.761
X1-C2	1.346	1.781	1.368	1.355
X1-H1	0.982	1.350	1.015	-
X2-H2	0.982	1.350	1.015	-
X1-X3	6.288	5.599	6.709	5.632
X2-X4	6.289	5.599	6.709	5.632
Bond angles (°)				
C1-C2-X1	119.9	120.4	122.3	118.6
C2-X1-H1	108.9	95.0	115.3	-
C2-C3-S2	119.3	124.1	120.9	119.9
C3-S2-O2	106.8	108.2	108.4	107.1
C3-S2-C4	106.5	107.4	103.8	104.0
C4-C5-X2	122.7	123.5	122.3	118.6
C5-X2-H2	108.9	95.0	115.3	-
Dihedral Angles (°) <sup>a</sup>				
C1-C2-X1-H1	-158.0	-154.0	-160.4	-
C1-C2-C3-S2	-174.3	-176.4	-170.8	-176.6
C2-C3-S2-O2	-41.8	-51.4	-39.9	-43.4
C2-C3-S2-C4	72.6	63.5	74.4	68.9
H1-X1-C2-C3	24.3	26.3	21.7	-
X1-C2-C3-S2	3.5	3.3	7.3	-
C3-S2-C4-C5	72.6	63.5	74.6	62.6
S2-C4-C5-X2	3.5	3.3	7.2	-0.8
S2-C4-C5-C6	-174.3	-176.4	-170.9	-179.4
C4-C5-X2-H2	24.3	26.3	160.4	-
C4-C5-C6-S3	173.4	178.8	170.8	176.6
C5-C6-S3-O3	175.6	179.9	170.7	173.6
C5-C6-S3-C7	-69.6	-64.8	-74.4	-68.9
X2-C5-C6-S3	-4.5	-1.0	-7.3	-1.8

<sup>a</sup> X = O for **7**, X = S for **9** and X = N for **11**, see Figure 3.3. <sup>b</sup> The X-ray structure of **7** taken from [13].

For thiacalix[4]arene derivatives, the relative energies,  $\Delta E_{rel}$  in gas phase of four typical conformers computed at the B3LYP/6-31G(d)//B3LYP/6-31G(d) level of theory are shown in Figure 3.16 and listed in Table S1 of Appendix I. The *cone* conformer is the most stable conformer in all thiacalix[4]arene derivatives (**1** to **6**) while interestingly, for the mercaptothiacalix[4]arene, compound **4**, it has two most stable conformers, *cone* and *1,3-alternate*. Figure 3.16a displays the relative stabilities of the four typical conformers for the smaller series, the relative stability of thiacalix[4]arene, compound **1** is in decreasing order: *cone* > *partial cone* > *1,2-alternate* ~ *1,3-alternate*. Whereas, mercaptothiacalix[4]arene **3** and aminothiacalix[4]arene **5**, their relative stabilities are in decreasing order: *cone* > *partial cone* > *1,3-alternate* > *1,2-alternate*. Figure 16b displays the relative stabilities of the four typical conformers which are the bigger compound series, *p-tert-butyl* derivatives.

The result shows that amino-*p-tert*-butylthiacalix[4]arene **6** has the same relative stability order as found in its smaller derivatives, **5**. Further more, relative stabilities for mercapto-*p-tert*-butylthiacalix[4]arene **4** is in decreasing order: *cone* ~ *1,3-alternate* > *partial cone* > *1,2-alternate* whereas *p-tert*-butylthiacalix[4]arene **2** is in decreasing order: *cone* > *partial cone* > *1,2-alternate* > *1,3-alternate*. As the conformational geometry plots shown in Figures 3.4 to 3.9, all cone conformers adopt the orientations that allow the formation of a cyclic array of four intramolecular hydrogen bonds in the cavity. So the high stability of the *cone* conformation is rationalized by the intramolecular hydrogen bonding array of -OH (for compounds **1** and **2**), -SH (for compounds **3** and **4**) and -NH<sub>2</sub> (for compounds **5** and **6**) groups.

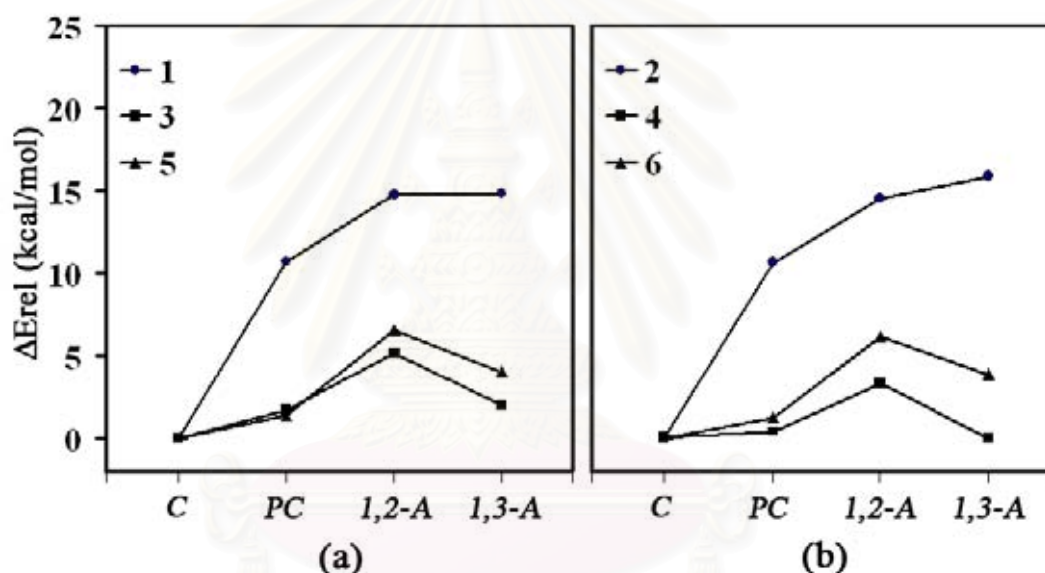


**Figure 3.16** Relative energies computed at the B3LYP/6-31G(d)//B3LYP/6-31G(d) level of theory phase of *cone*, *partial cone*, *1,2-alternate* and *1,3-alternate* conformers in gas phase of thiacalix[4]arene derivatives for (a) smaller compound series and (b) bigger compound series (*p-tert*-butyl derivatives).

For sulfonylcalix[4]arene derivatives (**7** to **12**), the relative energies,  $\Delta E_{rel}$  in gas phase of four typical conformers computed at the B3LYP/6-31G(d)//B3LYP/6-31G(d) levels of theory are shown in Figure 3.17 and listed in Table S2 of Appendix I. The relative stabilities of the four typical conformers for sulfonylcalix[4]arene **7** at the B3LYP/6-31G(d) level of theory are in the decreasing orders: *cone* ~ *partial cone* > *1,2-alternate* > *1,3-alternate* (see Figure 3.17b) The relative stabilities of those conformers are in decreasing order: *1,3-alternate* > *partial cone* > *1,2-alternate* >

*cone* for mercaptosulfonylcalix[4]arene **9** and *1,3-alternate* > *partial cone* > *cone* > *1,2-alternate* for aminosulfonylcalix[4]arene **11**. The result shows that the most stable conformer of compound **7** is *cone*, the same conformer as found in compound **11**. By contrast, the *1,3-alternate* is the most stable conformer for both compounds **9** and **11**, which are different from compounds **1** and **7**. The formation of eight hydrogen bonds in *1,3-alternate* conformer of sulfonylcalix[4]arene compounds **9** and **11** can be stabilized their geometrical structures (see Figures 3.10 to 3.15).

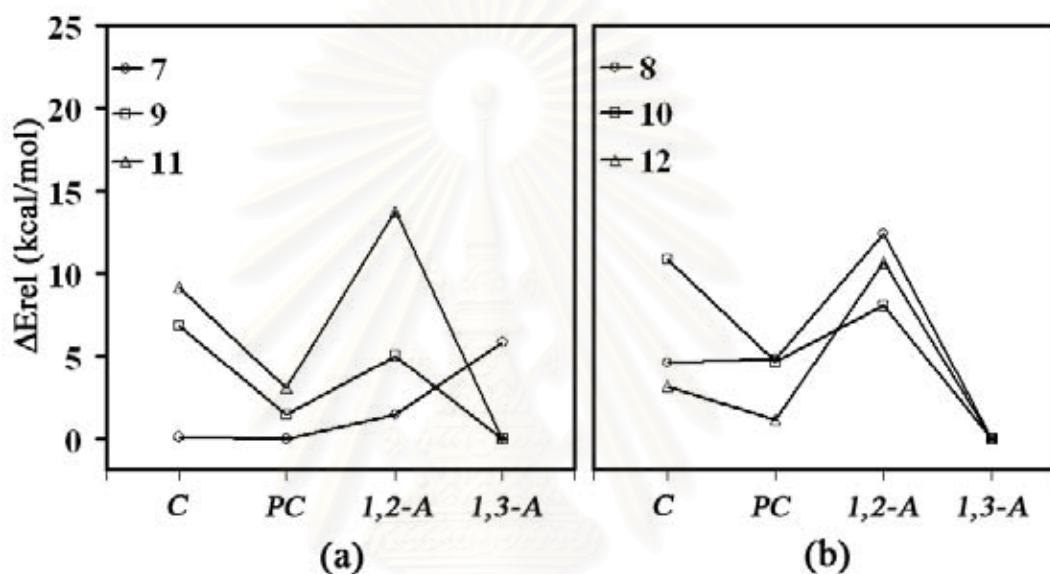


**Figure 3.17** Relative energies computed at the B3LYP /6-31G(d)//B3LYP /6-31G(d) level of theory phase of *cone*, *partial cone*, *1,2-alternate* and *1,3-alternate* conformers in gas phase of sulfonylcalix[4]arene derivatives for (a) smaller compound series and (b) bigger compound series (*p-tert-butyl* derivatives).

The solvation effects can be obtained and single point calculations have been also conducted on the gas-phase optimized geometries using a self-consistent reaction-field (SCRF) model. The SCRF model treats the solute at the quantum mechanical level, and the solvent is represented as a dielectric continuum. Specifically, the conductor-like polarizable continuum model (CPCM) is chosen to describe the bulk solvent. [50, 51] The CPCM represents the polarization of the liquid by a charge density appearing on the surface of the cavity created in the solvent, i.e., the solute/solvent interface. This cavity is built using a molecular shape algorithm. It should be emphasized that the reliability of this method to describe the solvation effects on the conformational equilibrium of calix[4]arene are recently proved.

In this part, the smaller sulfonylcalix[4]arene compounds namely sulfonylcalix[4]arene **7**, mercaptosulfonyl calix[4]arene **9** and aminosulfonylcalix[4]arene **11** are chosen to study for solvent effect. The relative energies,  $\Delta E_{rel}$  in gas phase, water, chloroform and dichloromethane of the main conformers computed at the B3LYP/6-31G(d)//B3LYP/6-31G(d) level of theory are plotted in Figure 3.18 and listed in Table S3. Further more, As shown in Figure 3.18, in gas phase, the relative stabilities of the four typical conformers of sulfonylcalix[4]arene at the B3LYP/6-31G(d) level of theory are in decreasing orders: *partial cone* > *cone* > *1,2-alternate* > *1,3-alternate*, and this order is also maintained at B3LYP/6-31G(d,p)//B3LYP/6-31G(d) and B3LYP/6-311G(d,p)//B3LYP/6-31G(d) levels of theory. In water, chloroform and dichloromethane, those stabilities computed using the CPCM-B3LYP/6-31G(d) method are in same decreasing order: *1,2-alternate* > *partial cone* > *cone* > *1,3-alternate*. The most stable conformers of the sulfonylcalix[4]arene in the vacuo and in solvents (water, chloroform and dichloromethane) are the *partial cone* and *1,2-alternate*, respectively. Nevertheless, the differences of relative energies for three conformers *cone*, *partial cone* and *1,2-alternate* are less than 2 kcal/mol. The relative stabilities of those conformers either in vacuo or solvents i.e., water, chloroform and dichloromethane) are in decreasing order: *1,3-alternate* > *partial cone* > *1,2-alternate* > *cone* for mercaptosulfonylcalix[4]arene and *1,3-alternate* > *partial cone* > *cone* > *1,2-alternate* for aminosulfonylcalix[4]arene. The most stable conformer of the mercaptosulfonylcalix[4]arene and aminosulfonylcalix[4]arene is the same conformer which is *1,3-alternate*. In addition, polarity orders reported in term of dipole moments of the conformers of sulfonylcalix[4]arene, mercaptosulfonylcalix[4]arene and aminosulfonylcalix[4]arene are in the same sequence: *cone* > *partial cone* > *1,2-alternate* > *1,3-alternate*, as reported in Table S4.



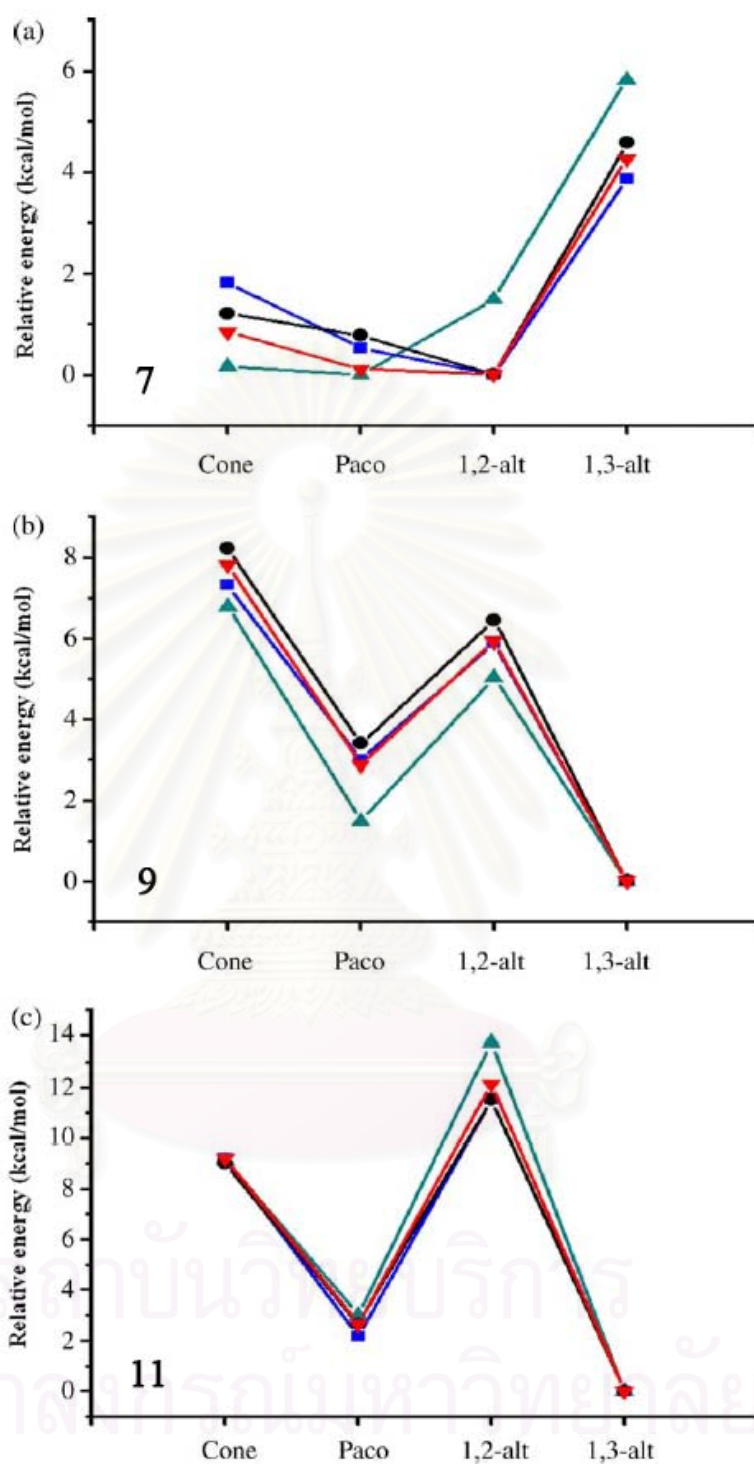


**Figure 3.18** Relative energies computed at the CPCM/B3LYP/6-31G(d) level of theory of *cone*, *partial cone*, *1,2-alternate* and *1,3-alternate* conformers in gas phase (●), water (▲), chloroform (■) and dichloromethane (▼) of the (a) sulfonylcalix[4]arene, (b) mercaptosulfonyl calix[4]arene and (c) aminosulfonyl calix[4]arene.

### 3.1.4 Inversion barrier for *cone* – *partial cone* interconversion

The cavity can, in principle, adopt four basic structures; *cone*, *partial cone*, *1,2-alternate* and *1,3-alternate*. Interconversion between the conformers is possible provided by the narrow rim substituent which is sufficiently small to pass through the annulus of the cavity. However, if the narrow rim substituted groups take a part in some specific interactions, certain conformations may be thermodynamically favored or disfavored. This is the case of thiacalix[4]arene and sulfonylcalix[4]arene derivatives in which hydroxyl, mercapto and amino groups form a circular array of four hydrogen bonds that stabilize the conical shape and occasionally, show disfavor other conformations forming a smaller number of hydrogen bonds. Another reason for conformational stability is inversion or rotational barriers of calix[4]arene bridges. According to effect of narrow rim substituted groups and bridge type on rotational energy barriers, the thiacalix[4]arene derivatives **1**, **3**, and **5** and sulfonylcalix[4]arene derivatives **7**, **9**, and **11** are chosen in this study. The interconversion has been predicted at B3LYP/6-31G(d) level of theory. Figure 3.19 displays the energy profiles for *cone* - *partial cone* interconversion reactions obtained at B3LYP/6-31G(d) level of theory and their intermediate structures are shown in Figure 3.20. For thiacalix[4]arene series, the *cone* conformer of compound **1** is more stable than its *partial cone* about 10.69 kcal/mol, whereas for compounds **3** and **5**, the *cone* conformer is more stable than *partial cone* only 1.76 and 1.39 kcal/mol, respectively. The rotational barriers of compounds **1**, **3** and **5**, are 53.88, 50.68 and 47.43 kcal/mol, respectively. For sulfonylcalix[4]arene series, stability of *cone* conformer of compound **7** is slightly different from its *partial cone* conformer, ca. 0.16 kcal/mol. In addition, the *cone* conformer of compounds **8** and **9** is less stable than *partial cone* 5.29 and 6.11 kcal/mol, respectively. The rotational barriers of compounds **7**, **9** and **11** are 103.76, 129.06 and 100.14 kcal/mol, respectively. From the results, it should be summarized that the narrow rim substituted groups have slightly effect to the rotational barriers while the calix[4]arene bridges have strongly effect. The rotational barriers of thiacalix[4]arene derivatives are approximately twice times higher than sulfonylcalix[4]arene derivatives. As the result, the smaller sulfur (-S-) bridges tend to rotate easier than the bigger sulfonyl (-SO<sub>2</sub>-) bridges. Moreover, the sulfur bridges can not form hydrogen bonds with the narrow rim substituted groups whereas sulfonyl

bridges can form a large number of hydrogen bonds with either the narrow rim substituted groups or benzyl protons (see Figures 3.10, 3.12 and 3.14).

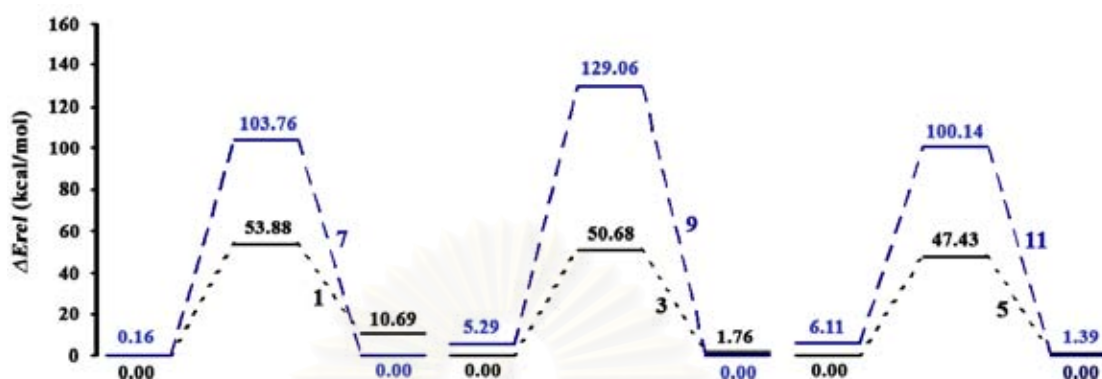


**Figure 3.19** The energy profiles for interconversion reactions between cone (left) and partial cone (right) conformers of thiacalix[4]arene (**1**, **3**, and **5**) and sulfonylcalix[4]arene (**7**, **9**, and **11**) derivatives obtained at B3LYP/6-31G(d)//B3LYP/6-31G(d) level of theory.

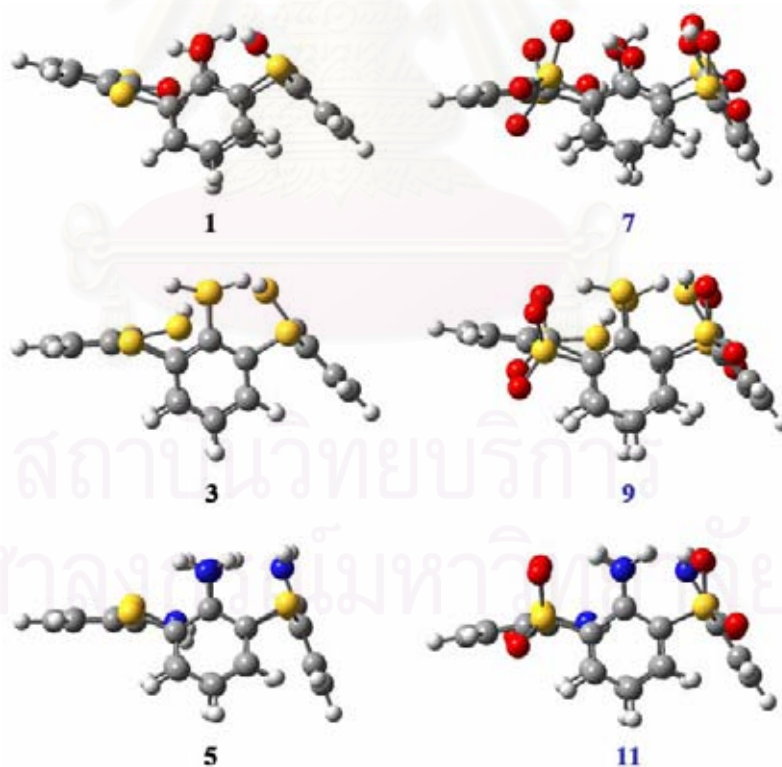


**Figure 3.20** The intermediate structures of *cone* - *partial cone* interconversion reactions for compounds **1**, **3**, **5**, **7**, **9** and **11** obtained at level B3LYP/6-31G(d) of theory.

### 3.1.5 Frontier molecular orbital energy gaps

The localizations of the lowest unoccupied molecular orbital (LUMO) and the highest occupied molecular orbital (HOMO) in the *cone* conformers of thiacalix[4]arene derivatives computed at the B3LYP/6-31G(d) level of theory are shown in Figure 3.21. It is clearly seen that all cyclic thiacalix[4]arenes are located by fine and symmetric dispersion of both LUMO and HOMO but their phases are quite different. The energies of the LUMO, HOMO and frontier molecular orbital energy gaps,  $\Delta E_{HOMO-LUMO}$  of all conformers of thiacalix[4]arene derivatives are listed in Table S5 in Appendix II, respectively. Average values of the frontier molecular orbital energy gaps of all conformers of compounds **1** to **6** are  $4.99 \pm 0.24$ ,  $4.89 \pm 0.18$ ,  $4.76 \pm 0.17$ ,  $4.71 \pm 0.15$ ,  $4.45 \pm 0.14$ , and  $4.39 \pm 0.14$  eV, respectively. The relative chemical reactivities for all thiacalix[4]arene derivatives indicated by their average energy gaps as shown in Table S5 are in increasing orders: **1** < **2** < **3** < **4** < **5** < **6**, respectively. Then it should be noted that the effect of narrow rim substituted group on reactivity is in increasing order: -OH < -SH < -NH<sub>2</sub>, respectively and the *p*-*tert*-butyl substituted groups can improve the reactivity of thiacalix[4]arene compounds (see Figure 3.22).

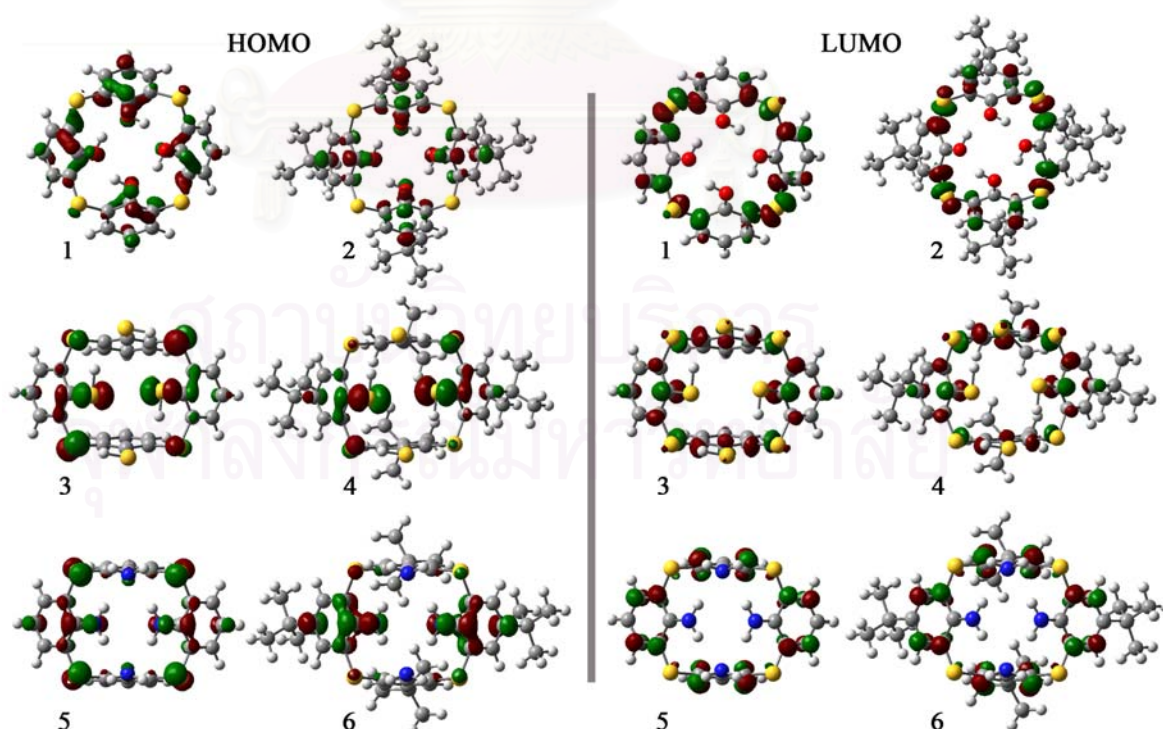


**Figure 3.21** Localization the LUMO (above) and HOMO (bottom) orbitals in the cone conformers of thiacalix[4]arene derivatives (**1** to **6**).

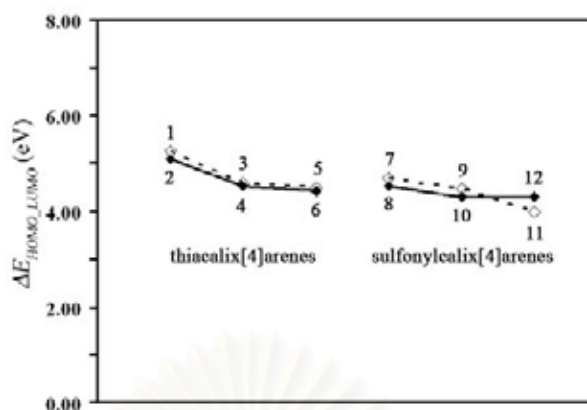


**Figure 3.22** The frontier molecular orbital energy gaps of cone conformers of thiacalix[4]arene and sulfonylcalix[4]arene derivatives.

The localizations of LUMO and HOMO in the *cone* conformers of sulfonylcalix[4]arene derivatives computed at the B3LYP/6-31G(d) level of theory are shown in Figure 3.23. Their LUMO and HOMO are also finely dispersed as found in thiacalix[4]arene derivatives. The energies of the LUMO, HOMO and frontier molecular orbital energy gaps,  $\Delta E_{HOMO-LUMO}$  of all conformers of sulfonylcalix[4]arene derivatives are presented in Table S6 of Appendix II. Average values of the frontier molecular orbital energy gaps of all conformers of compounds **7**, **8**, **9**, **10**, **11** and **12** are  $4.72 \pm 0.06$ ,  $4.63 \pm 0.08$ ,  $4.52 \pm 0.12$ ,  $4.46 \pm 0.20$ ,  $4.22 \pm 0.18$ , and  $4.26 \pm 0.04$  eV, respectively. The relative chemical reactivities for all sulfonylcalix[4]arene derivatives are in increasing orders: **7** < **8** < **9** < **10** < **11** ~ **12**, respectively. It is found that the narrow rim substituted and *p-tert*-butyl substituted groups of sulfonylcalix[4]arene derivatives provide the same trend of chemical reactivity as found in thiacalix[4]arene derivatives (see Figure 3.22).

In addition, as the hardness ( $\eta$ ) of thiacalix[4]arene and sulfonylcalix[4]arene derivatives is in a function of their energy gaps (see Tables S5 and S6), their hardness values are quite small. Therefore, these compounds have possibility to form complexes with  $Zn^{2+}$  or some metal cations. It is also found that di-deprotonated form of cone conformer of sulfonylcalix[4]arene prefers soft-to-intermediate metal ions (e.g.  $Zn^{2+}$ ,  $Cd^{2+}$ ,  $Hg^{2+}$ ). [12] As  $Zn^{2+}$  is soft-to-intermediate metal ion the zinc complex with cone conformer of sulfonylcalix[4]arene derivatives is found. Therefore, zinc complexes with novel mercaptosulfonylcalix[4]arene and aminosulfonyl calix[4]arene can be investigated.

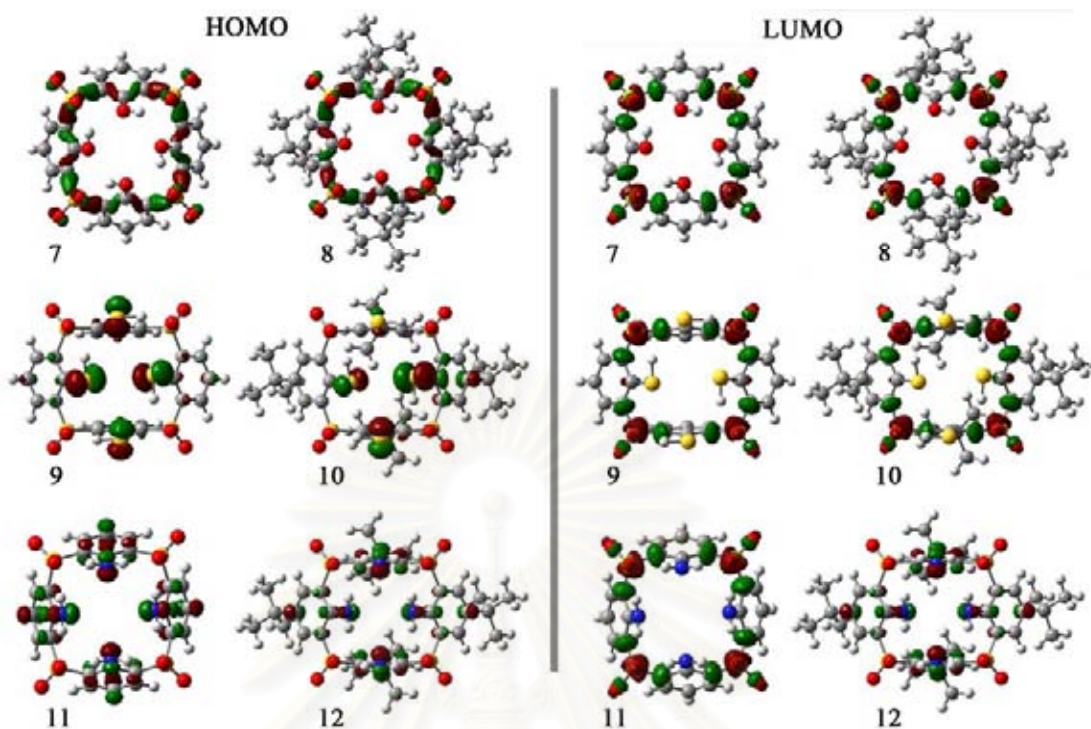


**Figure 3.23** Localization the LUMO (above) and HOMO (bottom) orbitals in the cone conformers of sulfonylcalix[4]arene derivatives (**7** to **12**).

### 3.1.6 Molecular electrostatic potential surface

Molecular electrostatic potential surfaces of the *cone* conformers of thiacalix[4]arene, **1** to **6** and sulfonylcalix[4]arene **7** to **12** derivatives generated from the Gaussian output files of their B3LYP/6-31G(d) computations with GFPRINT and POP=FULL keywords using the molekel 4.3 software [55] are shown in Figures 3.24 and 3.25, respectively. The most nucleophilic regions (negative electronic potential) are shown in red while the most electrophilic regions (positive electrostatic potential) are shown in blue. The molecular potentials presented over electronic isodensity ( $\rho = 0.05 \text{ e } \text{\AA}^{-3}$ ) as shown in Figures 3.24 and 3.25. Negative values contributing over the hetero atoms of all compounds, especially O, S and N atoms at narrow rim substituted groups and O atoms at sulfonyl bridges ( $-\text{SO}_2-$ ) are remarkably found. In addition, strong positive charges on the hydroxy, mercapto and amino protons are also found. This observation can be related with the interactions established with the metal ions.

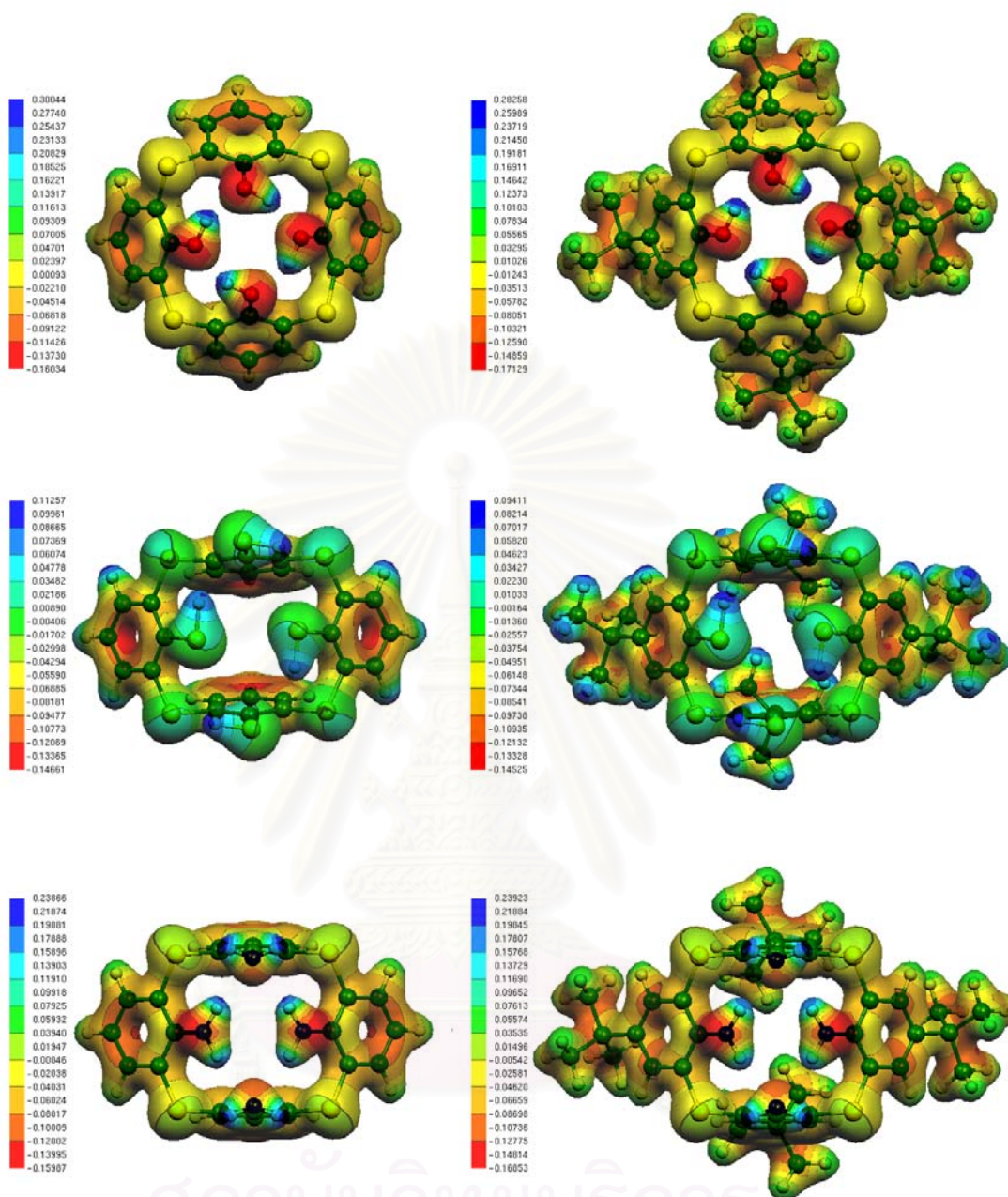


**Figure 3.24** The molecular electrostatic potential (in au) presented over electronic isodensity,  $\rho=0.05 \text{ e } \text{\AA}^{-3}$  of the *cone* conformers of the thiocalix[4]arene derivatives (**1** to **6**).

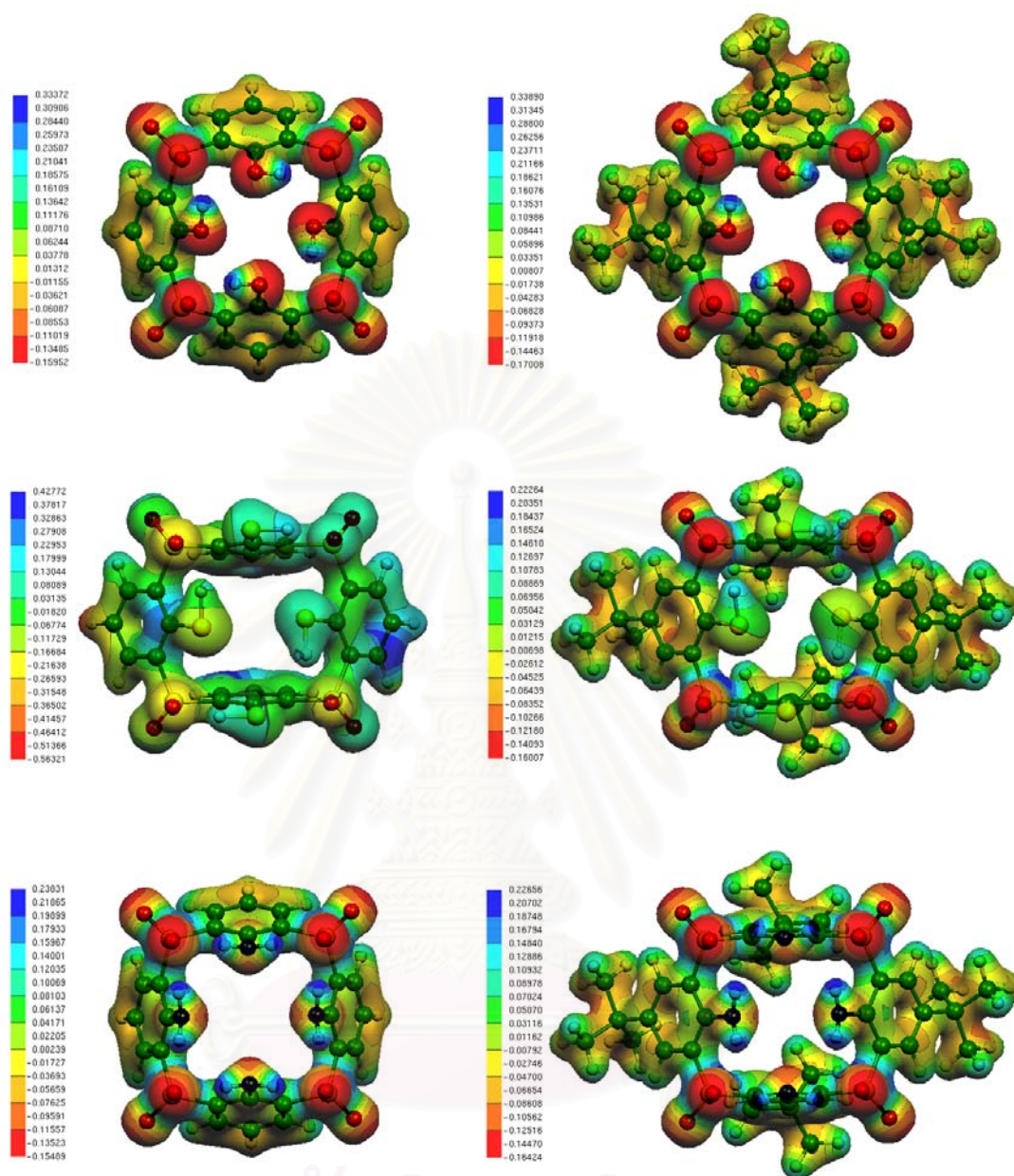


**Figure 3.25** The molecular electrostatic potential (in au) presented over electronic isodensity,  $\rho=0.05 \text{ e } \text{\AA}^{-3}$  of the *cone* conformers of the sulfonylcalix[4]arene derivatives (7 to 12).



### 3.1.7 Proton affinity

The first and second deprotonated forms of sulfonylcalix[4]arene **7** and mercaptosulfonylcalix[4]arene **9** have been optimized at B3LYP/6-31G(d) level. The protonated forms of aminosulfonylcalix[4]arene **11** are also optimized at the same level of theory. The first to second deprotonations of compounds **7** and **9** and the first to fourth protonations of compound **11** of their *cone* conformers are discussed. The deprotonation energy of compounds **7** and **9** will be reported as the protonation energy.

Geometrical structures of all species involved in protonation of cone conformers of compounds **7**, **9** and **11** are shown in Figures 3.26, 3.27 and 3.28 respectively. The proton affinities, PAn (n=1, 2, 3 and 4) of the sulfonylcalix[4]arene **7** (PA1<sub>b</sub>=390.69 and PA2=302.70 kcal/mol), mercaptosulfonylcalix[4]arene **9** (PA1<sub>a1</sub>=385.64 or PA1<sub>a2</sub>=382.55 or PA1<sub>b</sub>=402.65 and PA2=308.57 kcal/mol) and aminosulfonylcalix[4]arene **11** (PA1=224.38, PA2<sub>a</sub>=156.93 or PA2<sub>b</sub>=161.24, PA3<sub>a</sub>=83.96 or PA3<sub>b</sub>=79.64 and PA4=14.92 kcal/mol) are obtained at the B3LYP/6-311G(d,p)//B3LYP/6-31G(d) level of theory (see Table 3.4). Interestingly, the first proton affinities (PA1) of compounds **7** and **9** are approximately twice times higher than that of compound **11**.

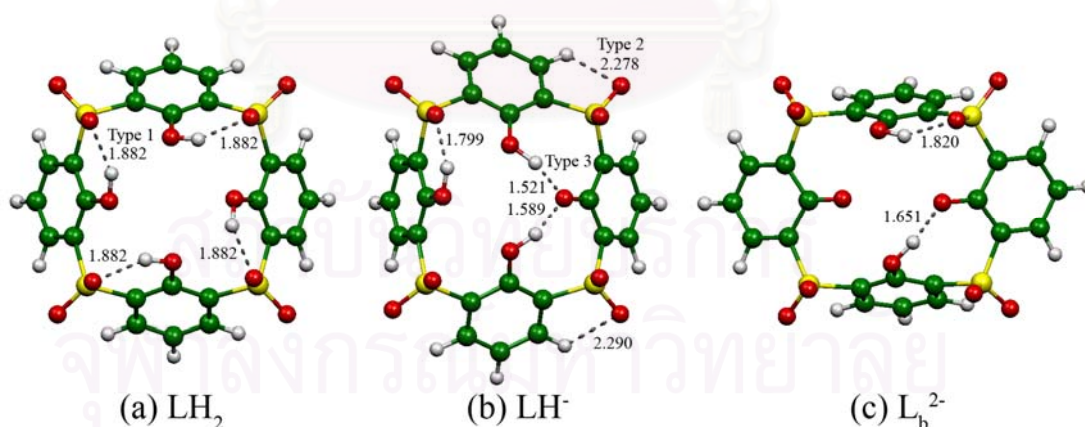


**Figure 3.26** The B3LYP/6-31G(d)-optimized structures of (a) the sulfonylcalix[4]arene (designated as LH<sub>2</sub>), its deprotonated species (b) LH<sup>-</sup> and (c) L<sub>b</sub><sup>2-</sup>. Three types of hydrogen bonds are presented and their bond distances are in Å.

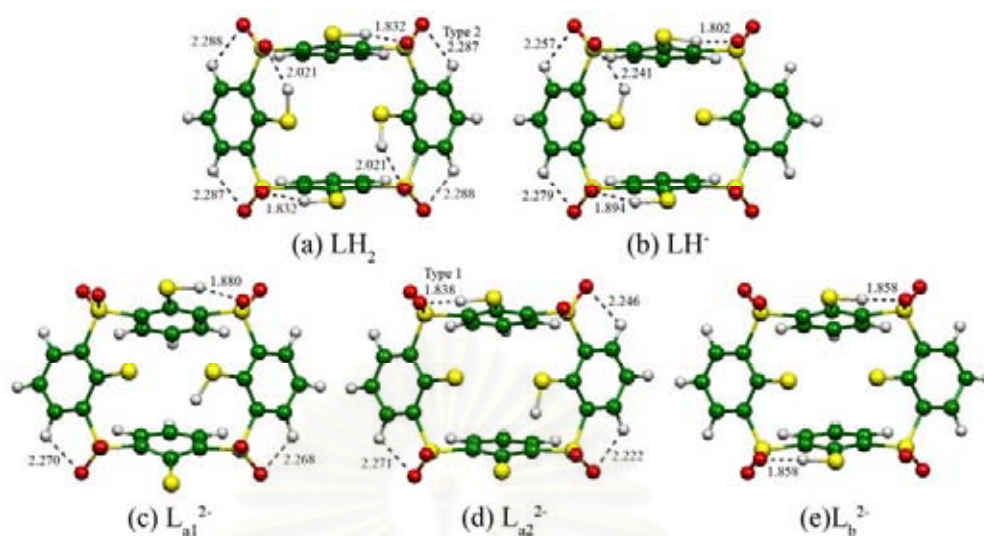


**Figure 3.27** The B3LYP/6-31G(d)-optimized structures of (a) the mercaptosulfonyl calix [4]arene (designated as  $LH_2$ ), its deprotonated species (b)  $LH^+$ , (c)  $L_{a1}^{2-}$ , (d)  $L_{a2}^{2-}$  and (e)  $L_b^{2-}$ . The hydrogen bond distances, Type 1 and 2 are in Å.

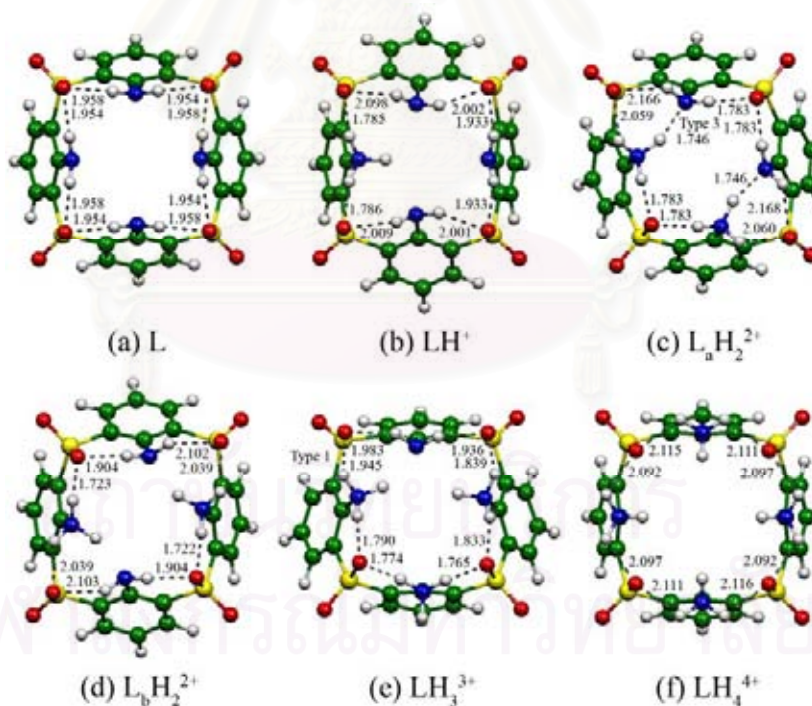


**Figure 3.28** The B3LYP/6-31G(d)-optimized structures of (a) the aminosulfonyl calix[4]arene (designated as  $L$ ), its protonated species (b)  $LH^+$ , (c)  $L_aH_2^{2+}$ , (d)  $L_bH_2^{2+}$ , (e)  $LH_3^{3+}$  and (f)  $LH_4^{4+}$ . The hydrogen bond distances, Type 1 and 3 are in Å.

**Table 3.4** Protonation energies of *cone* conformers of the sulfonylcalix[4]arene (**7**), mercaptosulfonylcalix[4]arene (**9**) and aminosulfonylcalix[4]arene (**11**)

Reactions	Reaction Energies <sup>a</sup>		
	B3LYP/6-31G(d)	B3LYP/6-31G(d,p)	B3LYP/6-311G(d,p)
Protonation: <sup>b</sup>			
Sulfonylcalix[4]arene ( <b>7c</b> )			
$L_b^{2-} + H^+ \rightleftharpoons LH^-$	-394.37	-398.40	-390.69
$LH^- + H^+ \rightleftharpoons LH_2$	-305.79	-308.35	-302.70
Mercaptosulfonylcalix[4]arene ( <b>9c</b> )			
$L_{a1}^{2-} + H^+ \rightleftharpoons LH^-$	-390.07	-392.18	-385.64
$L_{a2}^{2-} + H^+ \rightleftharpoons LH^-$	-386.81	-388.61	-382.55
$L_b^{2-} + H^+ \rightleftharpoons LH^-$	-407.62	-409.62	-402.65
$LH^- + H^+ \rightleftharpoons LH_2$	-312.96	-315.09	-308.57
Aminosulfonylcalix[4]arene ( <b>11c</b> )			
$L + H^+ \rightleftharpoons LH^+$	-229.36	-230.26	-224.38
$LH^+ + H^+ \rightleftharpoons L_aH^{2+}$	-160.83	-162.19	-156.93
$LH^+ + H^+ \rightleftharpoons L_bH^{2+}$	-164.68	-166.08	-161.24
$L_aH^{2+} + H^+ \rightleftharpoons LH^{3+}$	-85.28	-86.84	-83.96
$L_bH^{2+} + H^+ \rightleftharpoons LH^{3+}$	-81.44	-82.95	-79.64
$LH^{3+} + H^+ \rightleftharpoons LH^{4+}$	-15.91	-17.28	-14.92

<sup>a</sup> In kcal/mol. <sup>b</sup>  $L_a$  and  $L_b$  respectively refer to the protonation of neighboring and opposite two-protonated configurations, and 1 and 2 represent a cyclic and non-cyclic array of proton directions, see Figures 3.26, 3.27 and 3.28.

## 3.2 Complexation of thiacalix[4]arene and sulfonylcalix[4]arene derivatives with zinc(II) ion

### 3.2.1 Computational method

The stable structures of zinc(II) complexes with the cone conformers of thiacalix[4]arene and sulfonylcalix[4]arene derivatives have been computed at the B3LYP/6-31G(d) level of theory. The binding energies are calculated as the difference between the total energy of the metal complex and the sum of the total energies of the isolated moieties. The basis set superposition error (BSSE) for all of the Zn(II) complexes has been estimated with the counterpoise method implemented in GAUSSIAN 03 program. Electrostatic potential surfaces, HOMO and LUMO properties of the stable complexes have been calculated at B3LYP/6-31G(d) level. All the calculations have been carried out with the GAUSSIAN 03 program. [52] Graphics of the optimized structures and the electrostatic potential surfaces are produced with the GaussView 3.0 package [54] or the molekel 4.3 package. [55]

### 3.2.2 Complexation properties

Since, there are the different types of narrow rim substituted groups and calix[4]arene bridges of the studied compounds, many binding modes can be investigated. The B3LYP/6-31G(d)-optimized structures of zinc(II) complexes with *cone* conformers of thiacalix[4]arene and sulfonylcalix[4]arene derivatives are presented in Figures 3.29 and 3.30, respectively in which their corresponding geometrical data are tabulated in Tables 3.5 and 3.6. It is found that the symmetrical structures of the zinc(II) complexes with compounds **1** to **4** and **7** to **10** reduce to  $C_1$ -symmetrical structure compared to its corresponding free ligand structures. In contrast to the zinc(II) complexes with amino compounds **5**, **6**, **11** and **12**, the symmetrical structures are not changed when compare to its corresponding free ligand structures in which complexes of compounds **5** and **7** show a  $C_{4V}$ -symmetrical structure and compound **6** and **11** show a  $C_4$ -symmetrical structure, respectively. The complexation energies with ( $\Delta E$ ) and without BSSE correction ( $\Delta E_{BSSE}$ ) of zinc(II) complexes are summarized in Table 3.5. As seen this Table, the BSSE corrections of the complexation energies are in the range of 22.75 to 41.18 kcal/mol whereas the highest and the lowest BSSE corrections are the zinc(II) complexes of aminothiocalix[4]arene (**5**/Zn) and *p-tert*-butylsulfonylcalix[4]arene (**8**/Zn) respectively. Since the zinc(II) complexes of smaller compounds and its *p-tert*-butyl derivatives show a slight difference of the complexation energies, the bulky *p-tert*-butyl groups do not seem to interfere in the stabilization of the zinc(II) complexes. Moreover, the complexation interactions of zinc(II) with thiacalix[4]arene derivatives are stronger than those of sulfonylcalix[4]arene derivatives, in which the strongest complex is **1**/Zn ( $\Delta E_{BSSE} = 645.95$  kcal/mol) and the weakest complex is **11**/Zn ( $\Delta E_{BSSE} = 336.36$  kcal/mol). When considered the narrow rim substituted groups, it is found that the complex ability is in decreasing order; -OH ~ -SH > NH<sub>2</sub> groups. As the complex abilities of amino and mercapto compounds are nearly the same, the plot of complexation energies against average Z-X1 and Z-X2 (X1=X2= O, S or N) distance are considered as shown in Figure 3.31. The plot can be separated the inter-relation into three zones which are three different narrow rim substituted zones. Interestingly, the hydroxy groups play an important role for complex ability more than those of mercapto and amino groups. This can be confirmed by the longer Zn-O

distances when compared to the shorter Zn-N and Zn-S distances and by the highest complexation energy of the **1**/Zn complex.

The HOMO and LUMO of zinc(II) complexes with thiacalix[4]arene and sulfonylcalix[4]arene derivatives are depicted in Figures 3.32 and 3.33, respectively. Obviously, the results show that the HOMO and LUMO shapes of both thiacalix[4]arene and sulfonylcalix[4]arene complexes are very similar in which the difference of calix[4]arene bridges (-S- and SO<sub>2</sub>-) slightly effects to their HOMO and LUMO shapes. By contrast, it is clearly seen that the narrow rim substituted groups strongly effect to HOMO and LUMO shapes of complexes. For example, the HOMO orbitals of zinc(II) complexes with hydroxyl derivatives, compounds **1** and **2**, are located at an adjacent bridge of ligand site whereas its LUMO orbitals are mainly located at zinc atom site. Therefore, it is possible to conclude that electronic transition between these orbitals would take place by predominant metal-ligand charge transfer (MLCT) effect. Then a strong complexation ability is obtained. On the other hand, both HOMO and LUMO orbitals of the zinc(II) complexes with amino derivatives, compounds **5** and **6**, are only located at ligand site. Therefore, the electronic transitions between these orbitals of ligands are occurred only by themselves and the MLCT are quit small. Then weak complexation ability of compounds **5** and **6** is obtained.

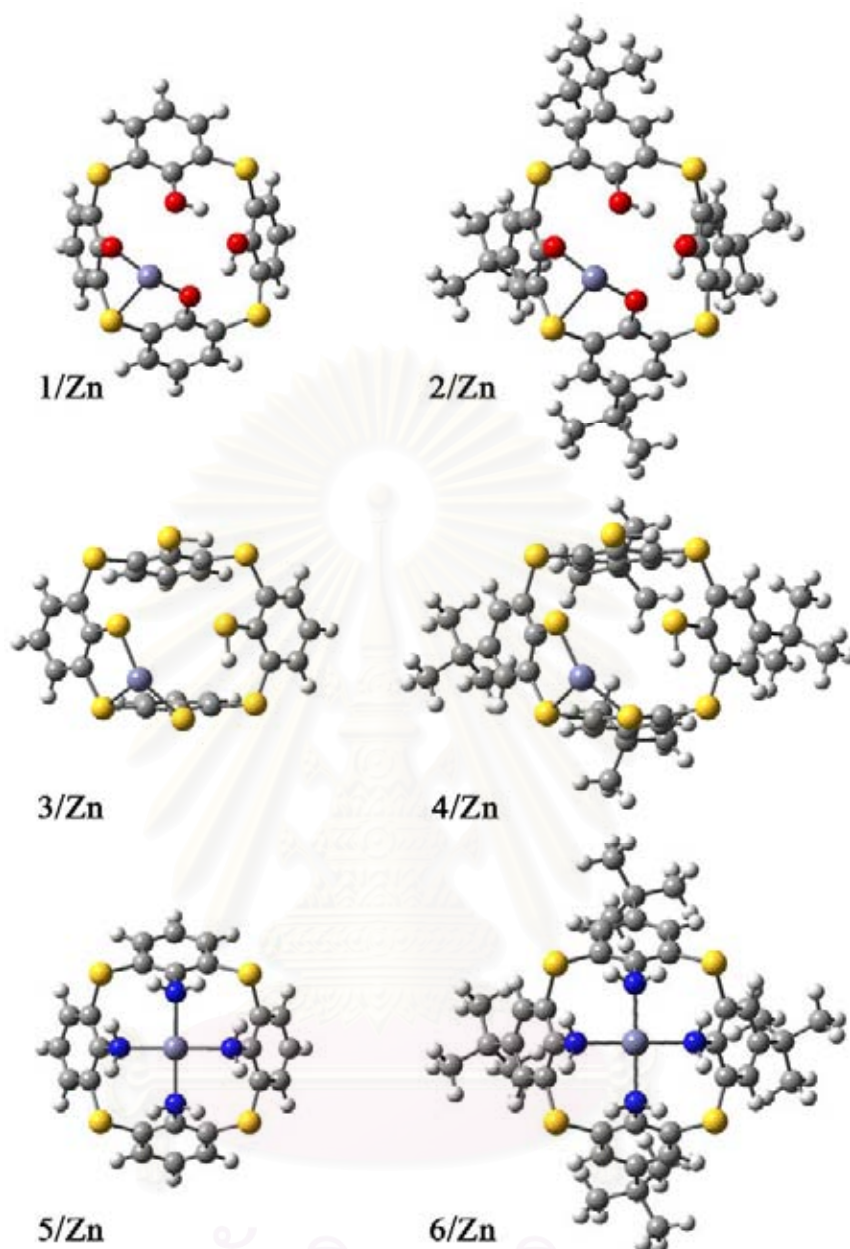


**Figure 3.29** The B3LYP/6-31G(d)-optimized structures of the Zn(II) ion complexes of the cone conformers of thiacalix[4]arene derivatives (**1** to **6**).

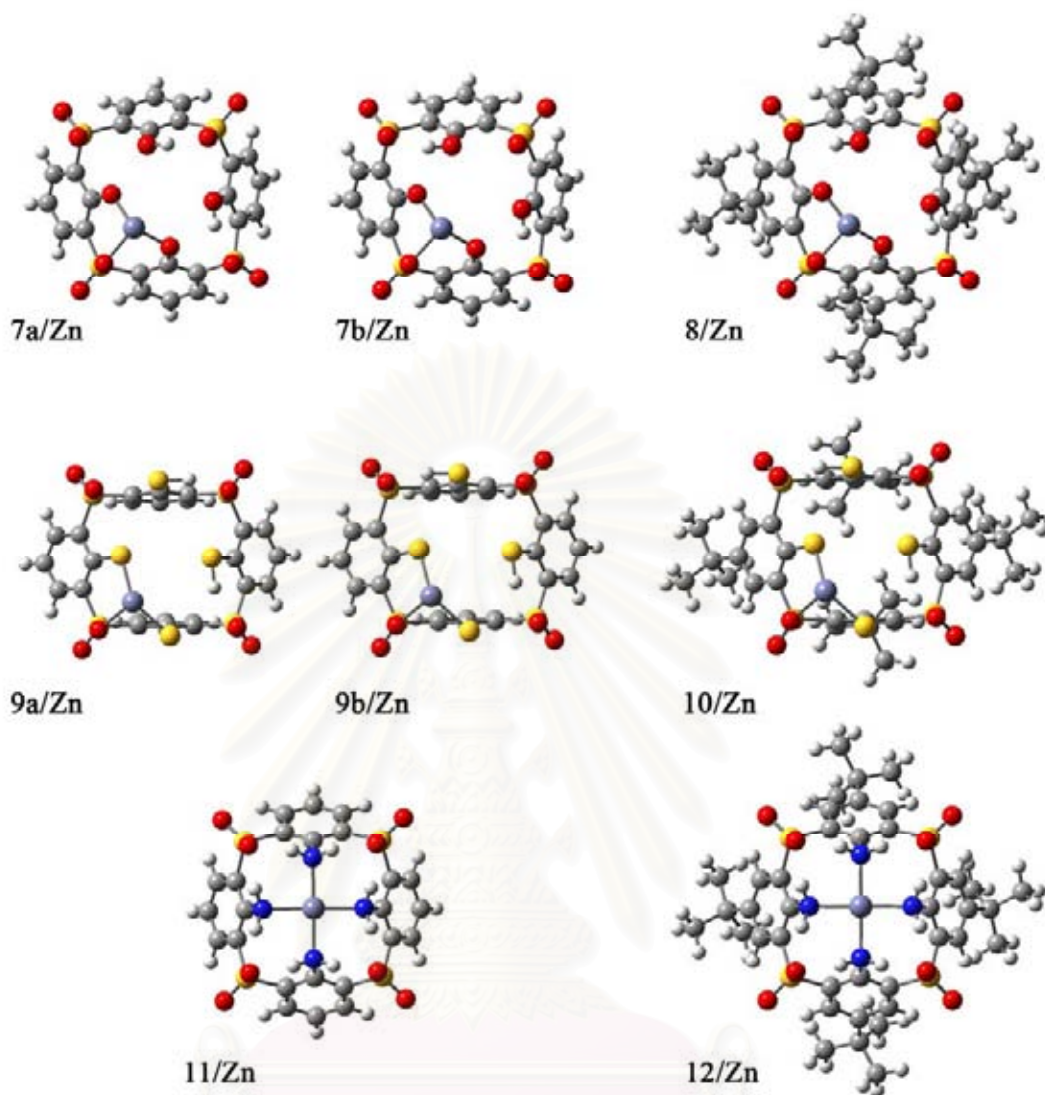


**Figure 3.30** The B3LYP/6-31G(d)-optimized structures of the Zn(II) ion complexes of the *cone* conformers of sulfonylcalix[4]arene derivatives (**7** to **12**).

สถาบันวิทยบริการ  
จุฬาลงกรณ์มหาวิทยาลัย

**Table 3.5** Complexation energies of zinc(II) ion with the cone conformers of thiacalix[4]arene and sulfonylcalix[4]arene derivatives obtained at B3LYP/6-31G(d) level of theory

Complexation <sup>a</sup>	$\Delta E$ <sup>b</sup>	BSSE <sup>b</sup>	$\Delta E_{BSSE}$ <sup>b</sup>
Thiacalix[4]arene (1)			
$L^{2-} + Zn^{2+} \rightleftharpoons ZnL$ (1/Zn)	-683.96	37.99	-645.97
<i>tert</i> -Butylsulfonylcalix[4]arene (2)			
$L^{2-} + Zn^{2+} \rightleftharpoons ZnL$ (2/Zn)	-682.07	38.07	-644.00
Mercaptothiacalix[4]arene (3)			
$L^{2-} + Zn^{2+} \rightleftharpoons ZnL$ (3/Zn)	-673.93	30.14	-643.79
Mercapto- <i>p-tert</i> -butylthiacalix[4]arene (4)			
$L^{2-} + Zn^{2+} \rightleftharpoons ZnL$ (4/Zn)	-674.56	29.72	-644.84
Aminothiacalix[4]arene (5)			
$L + Zn^{2+} \rightleftharpoons ZnL^{2+}$ (5/Zn)	-383.27	22.75	-360.53
Amino- <i>p-tert</i> -butylthiacalix[4]arene (6)			
$L + Zn^{2+} \rightleftharpoons ZnL^{2+}$ (6/Zn)	-397.72	22.92	-374.80
Sulfonylcalix[4]arene (7) <sup>c</sup>			
$L_1^{2-} + Zn^{2+} \rightleftharpoons ZnL_1$ (7a/Zn)	-658.49	41.14	-617.34
$L_2^{2-} + Zn^{2+} \rightleftharpoons ZnL_2$ (7b/Zn)	-652.76	41.03	-611.73
<i>tert</i> -Butylsulfonylcalix[4]arene (8)			
$L^{2-} + Zn^{2+} \rightleftharpoons ZnL$ (1/Zn)	-654.30	41.18	-613.13
Mercaptosulfonylcalix[4]arene (9) <sup>c</sup>			
$L_1^{2-} + Zn^{2+} \rightleftharpoons ZnL_1$ (9a/Zn)	-644.38	34.00	-610.38
$L_2^{2-} + Zn^{2+} \rightleftharpoons ZnL_2$ (9b/Zn)	-641.70	33.95	-607.75
Mercapto- <i>p-tert</i> -butylsulfonylcalix[4]arene (10)			
$L_{a2}^{2-} + Zn^{2+} \rightleftharpoons ZnL_{a2}$ (10/Zn)	-645.56	33.70	-611.86
Aminosulfonylcalix[4]arene (11)			
$L + Zn^{2+} \rightleftharpoons ZnL^{2+}$ (12/Zn)	-359.00	22.64	-336.36
Amino- <i>p-tert</i> -butylsulfonylcalix[4]arene (12)			
$L + Zn^{2+} \rightleftharpoons ZnL^{2+}$ (12/Zn)	-378.43	22.85	-355.59

<sup>a</sup> All ligands or ions are in complexes forms. <sup>b</sup> In kcal/mol. <sup>c</sup> Subscripts 1 and 2 represent a cyclic and non-cyclic array of proton directions, see Figures 3.29 and 3.30. The short names of complexes are in the parenthesis.



**Table 3.6** Geometrical data for zinc(II) complexes of cone conformer of thiacalix[4]arene derivatives computed at B3LYP/6-31G(d) level of theory

Parameter <sup>a</sup>	1/Zn	2/Zn	3/Zn	4/Zn	5/Zn	6/Zn
Bond distances (Å)						
S1-S2	5.616	5.609	5.664	5.659	5.614	5.609
S2-S3	5.566	5.565	5.627	5.648	5.614	5.609
S1-S3	8.111	8.107	8.086	8.102	7.940	7.933
S2-S4	7.693	7.686	7.873	7.883	7.940	7.933
S1-C1	1.801	1.800	1.813	1.815	1.809	1.810
C3-S2	1.807	1.802	1.831	1.828	1.809	1.810
S2-C4	1.821	1.803	1.806	1.812	1.809	1.810
C2-X1	1.344	1.356	1.801	1.799	1.459	1.460
C5-X2	1.339	1.357	1.778	1.780	1.459	1.460
X1-X2	3.572	3.579	4.256	4.257	2.991	2.986
X2-X3	3.085	3.080	3.799	3.718	2.991	2.986
X1-X3	3.597	3.586	6.806	6.536	4.230	4.223
X2-X4	4.840	4.841	4.030	4.180	4.230	4.224
X1-H1	-	-	-	-	1.024	1.024
X2-H2	-	-	-	-	1.024	1.024
Zn-X1	1.826	1.826	2.206	2.200	2.119	2.116
Zn-X2	1.816	1.815	2.185	2.179	2.119	2.116
Bond angles (°)						
S1-C1-C2	120.6	120.6	121.5	121.7	121.6	121.6
C1-C2-X1	119.0	119.4	119.9	120.2	119.9	119.9
C2-C3-S2	121.0	120.9	121.7	121.8	121.6	121.6
C2-X1-H1	-	-	-	-	107.1	107.1
C3-S2-C4	104.9	104.6	102.1	103.2	101.8	101.8
S2-C4-C5	119.0	118.9	122.6	122.6	121.6	121.6
C4-C5-X2	122.4	122.6	126.4	126.5	119.9	119.9
C2-X1-Zn	116.2	115.8	84.0	86.3	116.5	116.5
C5-X2-Zn	101.3	101.1	98.9	97.6	116.5	116.5
X1-Zn-X2	157.5	158.8	151.6	152.9	89.8	89.8
Dihedral Angles (°)						
S1-C1-C2-C3	180.0	-179.7	173.5	172.1	-178.1	-178.4
S1-C1-C2-X1	0.5	0.775	-8.0	-12.1	1.2	0.7
C1-C2-C3-S2	178.7	178.7	-174.6	-171.8	178.1	178.1
C1-C2-X1-H1	-	-	-	-	-147.0	-146.9
C2-C3-S2-C4	84.7	85.6	124.1	116.4	92.9	92.6
C3-S2-C4-C5	-110.9	-110.6	-79.3	-87.9	-92.9	-92.4
S2-C4-C5-C6	175.8	175.1	170.1	172.1	-178.1	-178.3
S2-C4-C5-X2	-2.0	-2.5	-11.6	-11.1	1.2	0.7
C4-C5-C6-S3	-172.9	-172.7	-166.6	-169.3	178.1	178.0
C4-C5-X2-H2	-	-	-	-	-147.0	-146.9
C1-C2-X1-Zn	169.2	167.7	137.0	140.4	90.4	90.6

<sup>a</sup> X = O for **1**, **2**, X= S for **3**, **4**, and X = N for **5**, **6**, see Figure 3.2.

**Table 3.7** Geometrical data for zinc(II) complexes of cone conformer of sulfonylcalix[4]arene derivatives computed at B3LYP/6-31G(d) level of theory

Parameter <sup>a</sup>	7a/Zn	8/Zn	9a/Zn	10/Zn	11/Zn	12/Zn
Bond distances (Å)						
S1-S2	5.669	5.626	5.879	5.861	5.687	5.673
S2-S3	5.626	5.630	5.723	5.729	5.687	5.673
S1-S3	8.373	8.403	8.308	8.387	8.040	8.023
S2-S4	7.652	7.563	8.062	7.975	8.041	8.023
S1-C1	1.811	1.812	1.849	1.851	1.818	1.816
C1-C2	1.421	1.412	1.423	1.422	1.408	1.408
C2-C3	1.432	1.427	1.433	1.428	1.408	1.404
C3-X2	1.811	1.807	1.840	1.838	1.818	1.816
X2-C4	1.801	1.808	1.811	1.816	1.818	1.816
C2-X1	1.316	1.317	1.793	1.795	1.453	1.454
C5-X2	1.313	1.317	1.769	1.768	1.453	1.454
X1-X2	3.315	3.344	4.108	4.110	3.015	2.996
X2-X3	2.734	2.682	3.641	3.564	3.002	2.996
X1-X3	4.471	4.477	6.754	6.627	4.244	4.238
X2-X4	4.400	4.522	3.930	3.916	4.245	4.238
X1-H1	-	-	-	-	1.030	1.029
X2-H2	-	-	-	-	1.030	1.029
O1-O2	5.457	5.410	6.006	6.014	5.362	5.367
O2-O3	5.450	5.402	6.117	6.009	5.363	5.366
S1-O1	1.479	1.481	1.468	1.468	1.488	1.490
S2-O2	1.519	1.517	1.505	1.505	1.488	1.490
H1-O2	-	-	-	-	1.887	1.887
H2-O3	-	-	-	-	1.878	1.887
Zn-X1	1.834	1.822	2.209	2.204	2.116	2.120
Zn-X2	1.817	1.823	2.208	2.206	2.116	2.120
Zn-O2	2.016	2.032	2.024	2.028	-	-
Bond angles (°)						
S1-C1-C2	119.6	118.4	127.1	127.0	123.2	122.9
C1-C2-X1	117.4	117.2	119.8	119.9	121.2	121.6
C2-C3-S2	124.0	123.2	128.6	128.2	123.2	122.8
C2-X1-H1	-	-	-	-	106.9	106.8
C3-S2-C4	113.1	113.3	105.6	106.7	105.3	105.6
S2-C4-C5	123.1	123.3	124.1	124.1	123.2	122.9
C4-C5-X2	127.3	127.3	128.1	128.3	121.2	121.6
O1-S1-C1	110.3	109.9	112.8	112.8	107.0	107.0
O2-S2-C4	105.9	105.6	107.5	106.9	107.0	107.0
C2-X1-Zn	118.6	120.2	87.2	87.0	117.7	118.2
C5-X2-Zn	120.5	120.0	105.6	105.8	117.8	118.2
X1-Zn-X2	130.5	133.1	136.9	137.5	90.9	89.9
Dihedral Angles (°)						
S1-C1-C2-C3	178.3	179.4	174.5	171.6	-179.5	-179.9
S1-C1-C2-X1	-1.3	0.4	-10.2	-14.7	-0.7	-1.8
C1-C2-C3-S2	176.6	175.6	-179.0	-177.2	179.9	179.6
C1-C2-X1-H1	-	-	-	-	-146.9	-146.7
C2-C3-S2-C4	88.4	86.2	116.7	114.0	87.5	87.0
C3-S2-C4-C5	-83.1	-87.3	-65.2	-68.6	-87.4	-86.8
S2-C4-C5-C6	-175.3	-175.6	172.6	176.5	-179.9	-179.9
S2-C4-C5-X2	6.5	5.4	-5.5	-0.4	-1.2	-1.8
C4-C5-C6-S3	178.7	-179.7	-170.8	-174.1	179.7	179.6
C4-C5-X2-H2	-	-	-	-	-147.3	-146.7
O1-S1-C1-C2	41.3	47.0	3.3	10.0	25.5	27.0
O2-S2-C4-C5	31.8	27.6	53.1	49.9	26.2	27.0
C1-C2-X1-Zn	168.0	172.7	140.3	140.3	91.1	91.1
C3-S2-O2-Zn	59.3	60.3	41.1	41.6	-	-

<sup>a</sup> X = O for **7**, **8**, X = S for **9**, **10**, and X = N for **11**, **12**, see Figure 3.3.

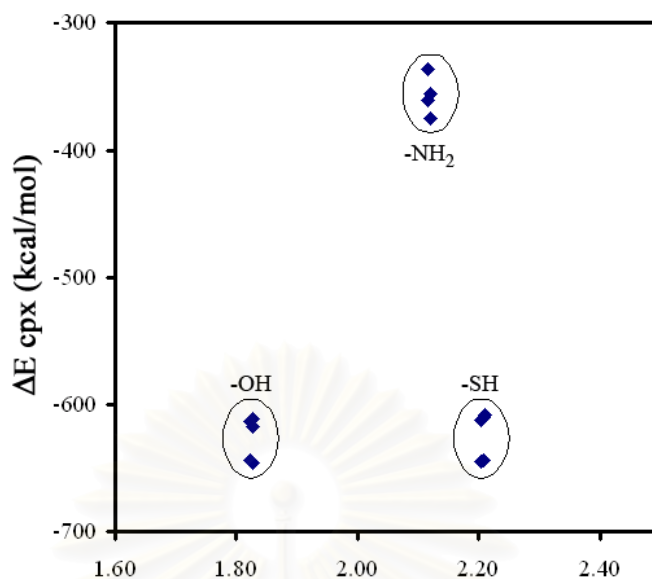


**Figure 3.31** Graphic inter-relationship between the complexation energies ( $\Delta E_{BSSSE}$ ) of thiacalix[4]arene and sulfonylcalix[4]arene complexes and the average distance of Zn-X1 and Zn-X2 bonds (X1 = X2 = O, S or N as shown in Figures 3.2 and 3.3).

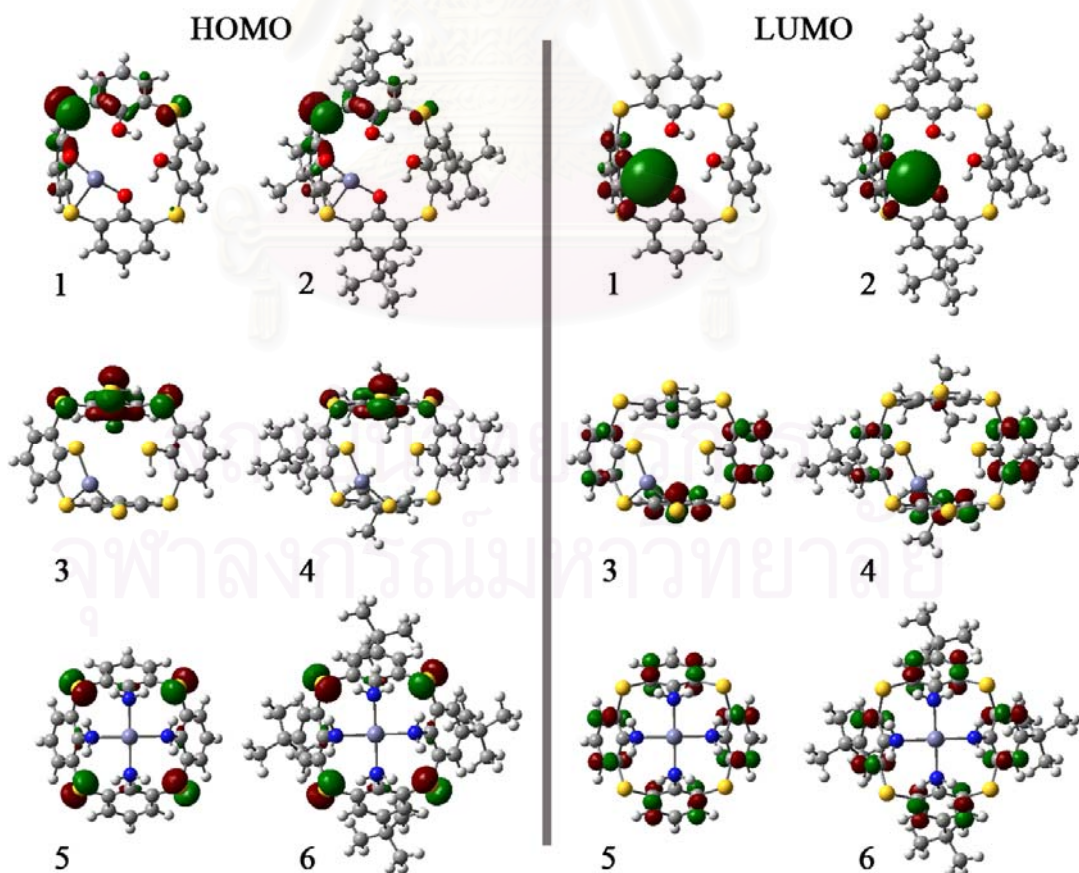


**Figure 3.32** Localization the LUMO and HOMO orbitals in the cone conformers of zinc(II) complexes with thiacalix[4]arene derivatives (1 to 6).

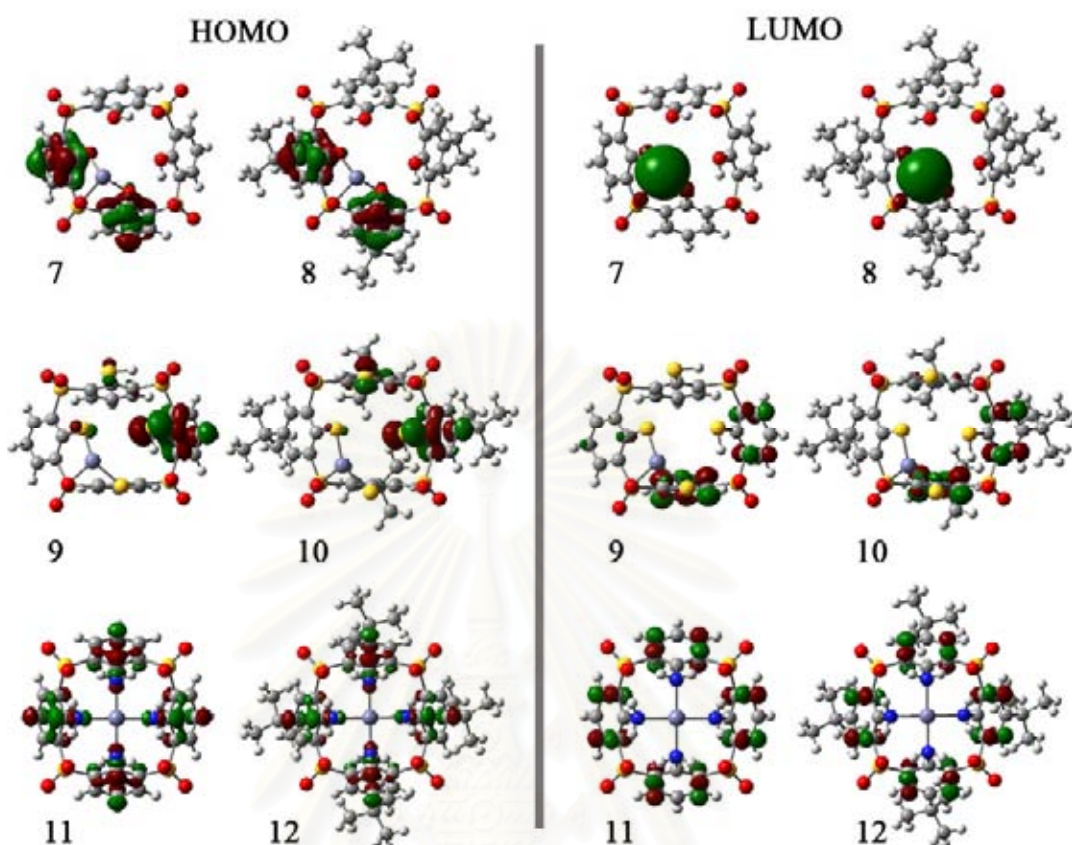


**Figure 3.33** Localization the LUMO and HOMO orbitals (isosurface at 0.05 au) for the cone conformers of sulfonylcalix[4]arene derivatives (7 to 12).

### 3.3 Host–guest complexes with carboxylate and dicarboxylate guest study

Organic anion receptors that contain a chromophore moiety are used for chromogenic sensors for the detection of biological anions. An excellent anion receptor such as thiourea-based chromophores with *p*-nitrophenyl groups is an excellent chromogenic anion receptor for monocarboxylates such as acetate [58]. Anion recognition of two-binding-site receptors lead to the discovery of useful sensors, not only for dicarboxylates but also monocarboxylates. Chromogenic azophenol–thiourea-based anion sensors have been developed for the selective colorimetric detection of acetate and other anions [59–61]. Urea or thiourea groups incorporated in receptors for anion recognition have been studied in a system of various solvents [62–64]. In previous theoretical work, the recognition of carboxylate and dicarboxylates by azophenol–thiourea derivatives are first investigated by the

integrated MO:MO method and show that oxalate is the most favorable ion for forming complexes with both receptors of azophenol–thiourea derivatives [65]. As complex formation of tetraamino-*p-tert*-butylthiacalix[4]arene derivatives with anions is expected, their anion recognitions have led to the development of anion sensors. Information on the binding interactions between the detected anions and their receptors is very important for discovering colorimetric and other detecting sensors. In this part, the binding interactions between carboxylates and different chromophore receptors have therefore been investigated theoretically to obtain their binding energies and thermodynamic data for their interactions. The receptors of tetraamino-*p-tert*-butylthiacalix[4]arene derivatives and anionic guests of acetate, oxalate, malonate, succinate, glutarate, adipate, and pimelate have been investigated.

### 3.3.1 Computational method

Geometries of the host–guest complexes and their host and guest components have been optimized using the hybrid density functional B3LYP method and the two-layered ONIOM(MO:MO) approach (ONIOM) [42, 66] using B3LYP/6-31G(d) as the high-level model and semi-empirical AM1 [67], PM3 [68], and MNDO [69] as low-level models. The reliability of the ONIOM calculations at the integrated levels [70], ONIOM(B3LYP/6-31G(d):AM1), ONIOM2(B3LYP/6-31G(d):PM3), and ONIOM(B3LYP/6-31G(d):MNDO) has been examined for geometry optimizations of the tetraamino-*p-tert*-butylthiacalix[4]arene (tatbtc4a) receptor and its complex with oxalate. Their geometrical data are compared with those of the target geometry optimized at the B3LYP/6-31G(d) level of theory as listed in Table 3.8. Energies and geometries of oxalate/tatctb4a system as the host–guest complex have been performed using the ONIOM(B3LYP/6-31G(d):AM1), ONIOM(B3LYP/6-31G(d):PM3), and ONIOM(B3LYP/6-31G(d):MNDO) methods and also compared with the target B3LYP/6-31G(d) geometry. The ONIOM(B3LYP/6-31G(d):AM1) calculation of the examined system provides reasonable results at a relatively low cost for the present host–guest interactions. The two-layered ONIOM(B3LYP/6-31G(d):AM1) is therefore used for geometry optimization throughout this work. The reliability of the ONIOM(B3LYP/6-31G(d):AM1) for a similar system is discussed in the works of Remko et al. [71, 72]. The real and model systems used in the two-layer ONIOM(MO:MO) calculations for the hosts and host–guest interaction models are

shown in Figure 3.34. The structures of the carboxylate guests and their total energies have been optimized and computed at the B3LYP/6-31G(d) level of theory. All calculations are performed using the GAUSSIAN 03 program [52] and their structures are visualized using the molekel 4.3 program [55].

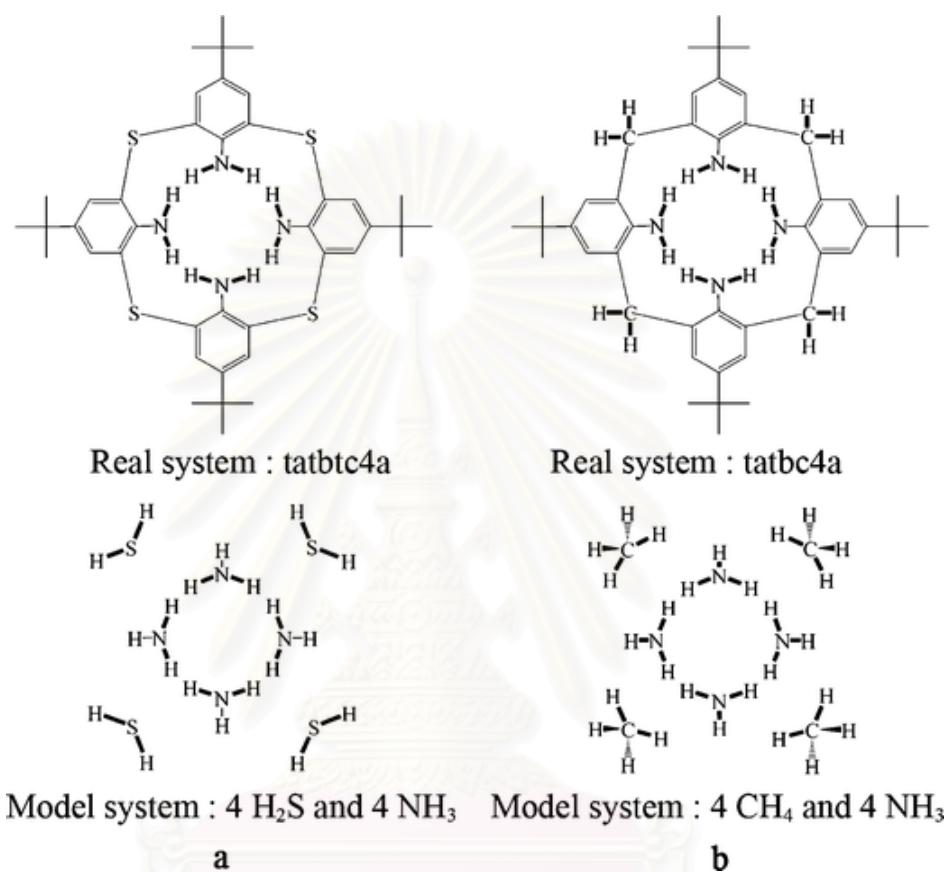


**Figure 3.34** Real molecule (top) and model system (bottom) of hosts (a) tatbtc4a and (b) tatca4a. The bold atoms of the real molecules of hosts were treated at the higher level of theory used in the ONIOM(MO:MO) calculation.

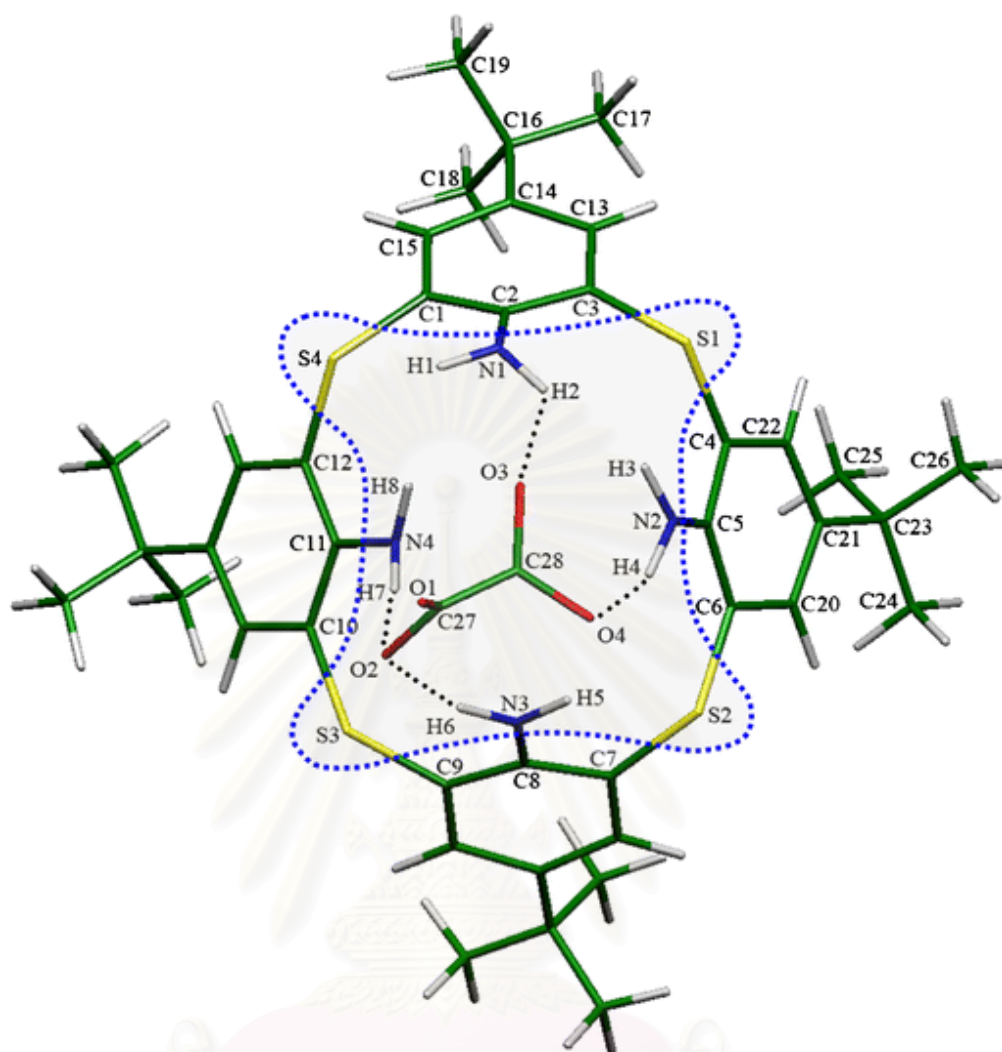


**Figure 3.35** Atom labeling of tatbtc4a/oxalate complex as a representative of a host-guest system.

สถาบันวิทยบริการ  
จุฬาลงกรณ์มหาวิทยาลัย

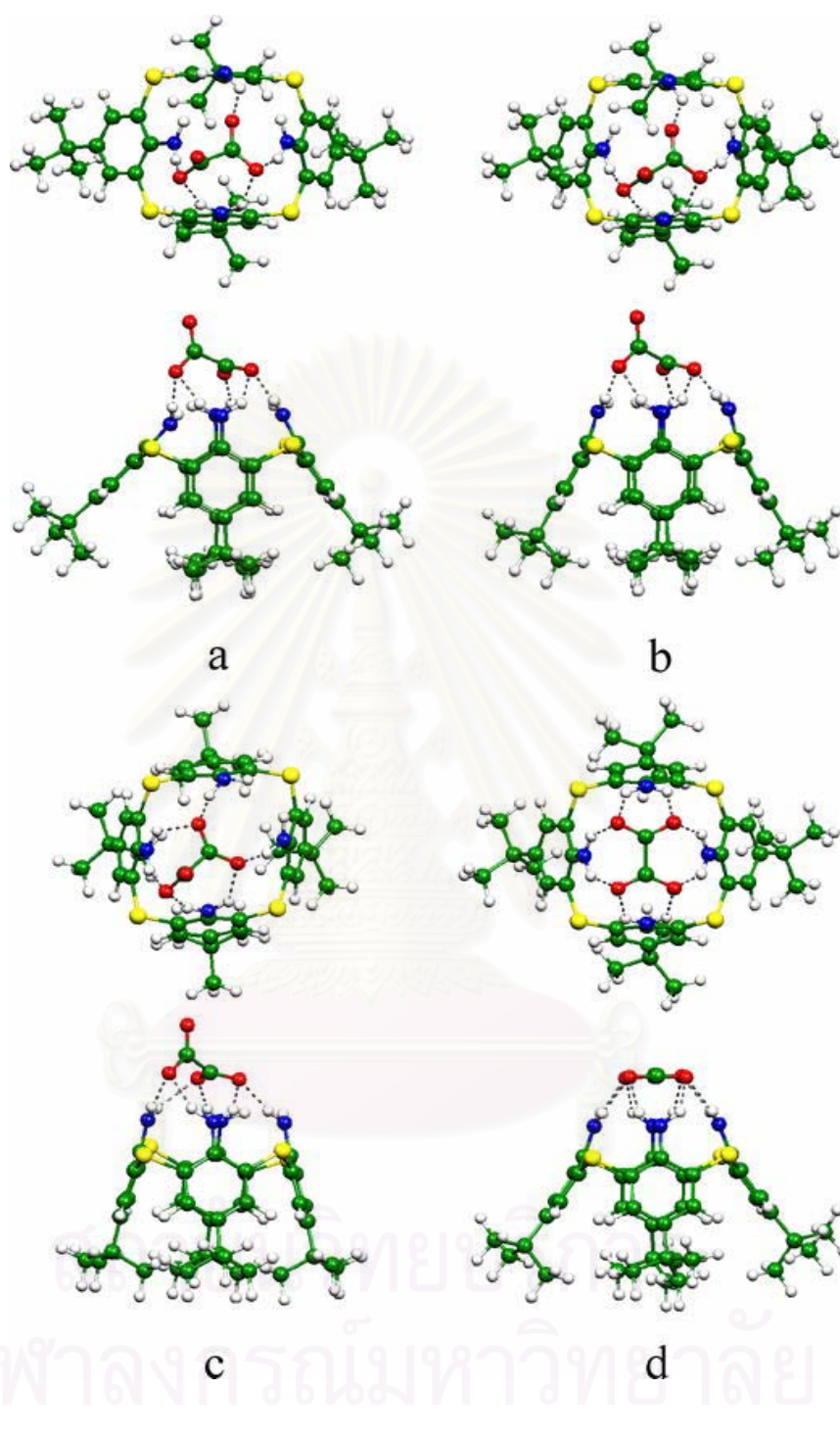


**Figure 3.36** Geometrical structures of tetraamino-*p*-*tert*-butylthiacalix[4]arene (tatbtc4a) complex with oxalate optimized at (a) B3LYP/6-31G, (b) ONIOM(B3LYP/6-31G(d):AM1), (c) ONIOM(B3LYP/6-31G(d):PM3), and (d) ONIOM(B3LYP/6-31G(d):MND0) levels of theory.



**Table 3.8** Geometrical data for the geometries of tetraamino-*p-tert*-butylthiacalix[4]arene (tatbtc4a) complex with oxalate optimized at the B3LYP/6-31G(d), ONIOM(B3LYP/6-31G(d):AM1), ONIOM(B3LYP/6-31G(d):PM3), and ONIOM(B3LYP/6-31G(d):MNDO) levels of theory

Parameter <sup>a</sup>	B3LYP/6-31G(d)	ONIOM(B3LYP/6-31G(d):AM1)	ONIOM(B3LYP/6-31G(d):PM3)	ONIOM(B3LYP/6-31G(d):MNDO)
Host				
Bond distance (Å)				
N1-H1	1.015	1.018	1.040	1.027
N1-H2	1.024	1.031	1.007	1.030
N2-H3	1.011	1.017	1.006	1.027
N2-H4	1.044	1.084	1.040	1.024
N1-C2	1.378	1.406	1.392	1.353
N2-C5	1.333	1.360	1.388	1.360
C1-C2	1.426	1.422	1.425	1.440
C2-C3	1.422	1.419	1.424	1.438
C3-C13	1.397	1.392	1.391	1.400
C13-C14	1.398	1.396	1.390	1.417
C14-C15	1.401	1.400	1.397	1.421
C1-C15	1.392	1.389	1.385	1.398
C14-C16	1.539	1.504	1.513	1.538
C16-C17	1.540	1.524	1.531	1.558
C4-C5	1.439	1.437	1.425	1.435
C5-C6	1.434	1.434	1.426	1.433
C6-C20	1.395	1.385	1.385	1.401
S1-C3	1.815	1.732	1.787	1.731
S1-C4	1.805	1.725	1.787	1.733
S2-C6	1.804	1.724	1.785	1.733
S2-C7	1.816	1.729	1.778	1.732
Bond angle (°)				
H1-N1-H2	107.1	103.9	110.0	107.3
H3-N2-H4	110.0	109.6	110.3	107.1
H5-N3-H6	107.8	106.8	110.8	107.4
H7-N4-H8	110.8	111.6	110.8	107.1
C1-C2-C3	116.1	117.2	118.5	117.9
C3-S1-C4	102.2	99.3	97.5	104.7
C4-C5-C6	115.6	115.8	118.4	118.7
C6-S2-C7	102.2	100.2	101.0	104.6
Dihedral angle (°)				
N1-C2-C3-C13	-173.3	-172.6	-172.9	-163.1
C3-C13-C14-C16	179.0	-179.4	-176.4	175.9
C13-C14-C16-C17	0.2	-1.0	26.0	-5.8
C2-C3-S1-C4	113.7	111.8	93.5	95.6
C3-S1-C4-C5	-88.2	-91.4	-91.5	-107.8
N2-C5-C6-C20	-168.8	-162.5	-173.7	-164.0
C6-C20-C21-C23	177.7	179.7	-176.1	177.3
C20-C21-C23-C24	-1.0	-2.1	-33.2	-10.7
C5-C6-S2-C7	88.8	98.1	114.2	106.0
C6-S2-C7-C8	-116.2	-118.0	-112.0	-95.0
H2-N1-C2-C3	-49.2	-59.1	-6.0	-9.4
H4-N2-C5-C6	-7.4	-28.4	-38.9	-14.7
H6-N3-C8-C9	-22.6	-24.6	-5.6	-9.5
H8-N4-C11-C12	3.5	-22.6	-16.4	-14.7
Guest				
Bond distance (Å)				
C27-C28	1.550	1.553	1.557	1.592
O1-C27	1.241	1.239	1.239	1.264
O2-C27	1.292	1.292	1.294	1.267
O3-C28	1.278	1.288	1.271	1.264
O4-C28	1.268	1.258	1.270	1.268
Bond angle (°)				
O1-C27-O2	126.6	126.9	126.7	125.5
O3-C28-O4	125.7	125.3	126.8	125.5
Dihedral angle (°)				
O1-C27-C28-O3	96.1	93.9	90.6	-176.4
N1-H2...O3	1.981	2.039	2.376	2.376
N3-H6...O2	1.905	1.856	2.013	2.013
N4-H7...O2	1.726	1.732	1.980	1.980

<sup>a</sup> Atomic labeling is shown in Figure 3.35.

### 3.3.2 Complexation properties of tetraamino-*p*-*tert*-butylthiacalix[4]arene

For examination the reliability of the two-layered ONIOM(MO:MO) method, the geometries of the tatbtc4a/oxalate complex have been optimized at four different levels of theory. Its geometries optimized at the B3LYP/6-31G(d), ONIOM(B3LYP/6-31G(d):AM1), ONIOM(B3LYP/6-31G(d):PM3), and ONIOM(B3LYP/6-31G(d):MND0) levels of theory are shown in Figure 3.36 and their corresponding geometrical data are given in Table 3.8. The comparison of the hydrogen bonds of the tatbtc/oxalate complex is found that the ONIOM(B3LYP/6-31G(d):AM1)-optimized hydrogen-bond distances are in good agreement with the B3LYP/6-31G(d)-optimized data. The ONIOM(B3LYP/6-31G(d):AM1)-optimized geometry of the tatbtc/oxalate complex is very similar to the target B3LYP/6-31G(d)-optimized geometry. Thus, the reliability test of the ONIOM(MO:MO) approach for this host–guest system shows the ONIOM2(B3LYP/6-31G(d):AM1) method to be the most reliable with respect to the full B3LYP/6-31G(d) level of theory.

Tetraamino-*p*-*tert*-butylthiacalix[4]arene (tatbtc4a) can form the stable complexes with acetate, oxalate, malonate, succinate, glutarate, and pimelate guests, but not with adipate. The most stable complex is formed with malonate which is stabilized by  $-117.60$  kcal/mol. The stability of the tatbtc4a/carboxylate complex system in decreasing order is malonate > oxalate > succinate > pimelate > glutarate > acetate (see Table 3.9). The ONIOM(B3LYP/6-31G(d):AM1)-optimized geometries of the tatbtc4a complexes with carboxylate guests are shown in Figure 3.37. The geometries of malonate/tatbtc4a and succinate/tatbtc4a are found to have high symmetry, belonging to the point group  $C_2$ . The selectivity coefficient of the tatbtc4a towards malonate with respect to acetate also confirms that the tatbtc4a forms favorably a very stable complex with malonate. As the selectivity coefficient of tatbtc4a toward malonate with respect to oxalate (the second most stable complex with tatbtc4a) is quite large ( $9.90 \times 10^2$ ), the receptor tatbtc4a may well recognize malonate. Table 3.10 shows that the total preorganization energies of the host tatbtc4a and the guest malonate are the lowest energy ( $=4.31$  kcal/mol). The highest guest-preorganization energy is given by adipate ( $=83.28$  kcal/mol). Plots of the preorganization energies of tatbtc4a, its complexation, and binding energies against the size of the carboxylate guests, based on the ONIOM(B3LYP/6-31G(d):AM1) method, are shown in Figure 3.38. Binding energies with and without BSSE

corrections, BSSE-corrected preorganization energies of the association of the tetraamino-*tert*-butylthiacalix[4]arene (tatbtc4a), and various anionic guests derived at the B3LYP/6-31G(d)//ONIOM (B3LYP/6-31G(d):AM1) level of theory are shown in Table 3.11. The binding energies with and without the BSSE corrections indicate that the tatbtc4a/malonate complex is the most stable species with the lowest BSSE-corrected preorganization energy (110.68 kcal/mol).

**Table 3.9** Binding energies, enthalpies, and free energies of association of amino-*p*-*tert*-butylthiacalix[4]arene (**6**, tatbtc4a) and various anionic guests

Guest	$\Delta E_{\text{binding}}^{\text{a}}$	$\Delta H^{298 \text{ a}}$	$\Delta G^{298 \text{ a}}$	$K_B^{\text{acetate} \text{ b}}$
acetate	-43.32	-43.61	-28.03	$1.00 \times 10^{00}$
oxalate	-103.77	-104.26	-80.92	$8.12 \times 10^{38}$
malonate	-117.60	-41.35	-84.99	$8.04 \times 10^{41}$
succinate	-86.91	-87.71	-68.80	$9.83 \times 10^{29}$
glutarate	-75.06	-75.64	-58.19	$1.54 \times 10^{22}$
adipate	-4.93	- <sup>c</sup>	- <sup>c</sup>	- <sup>d</sup>
pimelate	-58.98	-60.26	-42.38	$3.62 \times 10^{10}$

<sup>a</sup> In kcal/mol, derived from the ONIOM(B3LYP/6-31G(d):AM1) energies with ZPE corrections. <sup>b</sup> Selectivity coefficient of guests with respect to acetate. <sup>c</sup> Unreliable results due to the ONIOM(B3LYP/6-31G(d):AM1) frequency calculations.

<sup>d</sup> Indetermination.

**Table 3.10** Preorganization energies, corresponding thermodynamics of amino-*p*-*tert*-butylthiacalix[4]arene (**6**, tatbtc4a) receptor (host), carboxylates (guest), and their complexation energies derived from the ONIOM (B3LYP/6-31G(d):AM1) calculations

Host/guest	Host			Guest			$\Delta E_{\text{preorg}}^{\text{total} \text{ a}}$	$\Delta E_{\text{preorg}}^{\text{a}}$
	$\Delta E_{\text{preorg}}^{\text{host} \text{ a}}$	$\Delta H^{298 \text{ a}}$	$\Delta G^{298 \text{ a}}$	$\Delta E_{\text{preorg}}^{\text{guest} \text{ b}}$	$\Delta H^{298 \text{ b}}$	$\Delta G^{298 \text{ b}}$		
tatbtc4a/acetate	10.65	10.67	10.99	0.86	0.26	2.79	11.51	-54.83
tatbtc4a/oxalate	22.54	21.56	25.01	1.54	1.03	8.66	24.08	-127.85
tatbtc4a/malonate	1.84	1.53	2.10	2.47	64.59	3.81	4.31	-138.72
tatbtc4a/succinate	18.06	16.55	22.32	13.07	12.91	13.69	31.13	-118.04
tatbtc4a/glutarate	17.75	16.31	20.27	17.05	15.87	19.24	34.8	-109.86
tatbtc4a/adipate	17.54	16.74	19.03	83.28	83.02	85.53	100.82	-105.75
tatbtc4a/pimelate	17.87	17.04	19.85	26.49	25.00	27.93	44.36	-103.34

<sup>a</sup> In kcal/mol, derived at the ONIOM (B3LYP/6-31G(d):AM1) level with ZPE corrections <sup>b</sup> In kcal/mol, derived at the B3LYP/6-31G(d) level with ZPE corrections

**Table 3.11** Binding energies of association of the amino-*p*-*tert*-butylthiacalix[4]arene (**6**, tatbtc4a) and various anionic guests and their BSSE corrections values derived from the B3LYP/6-31G(d)//ONIOM (B3LYP/6-31G(d):AM1) calculations and their BSSE corrected values

Guest	$\Delta E_{\text{binding}}^a$	$\Delta E_{\text{complex}}^a$	BSSE <sup>a,b</sup>	$\Delta E_{\text{preorg}}^{\text{BSSE } a}$	$\Delta E_{\text{preorg}}^{\text{BSSE } a}$	$\Delta E_{\text{preorg}}^{\text{BSSE } a}$
tatbtc4a/acetate	-45.35	-86.82	- <sup>c</sup>	-	-	-
tatbtc4a/oxalate	-98.07	-209.13	31.92	-66.16	-177.22	111.06
tatbtc4a/malonate	-100.16	-210.84	31.37	-68.79	-179.47	110.68
tatbtc4a/succinate	-83.33	-204.17	31.54	-51.79	-172.63	120.84
tatbtc4a/glutarate	-67.54	-191.06	24.94	-42.60	-166.12	123.52
tatbtc4a/adipate	-61.70	-189.21	- <sup>d</sup>	-	-	-
tatbtc4a/pimelate	- <sup>e</sup>	- <sup>e</sup>	13.69	- <sup>f</sup>	- <sup>f</sup>	132.50

<sup>a</sup> In kcal/mol. <sup>b</sup> The BSSE energy. <sup>c</sup> No convergence. <sup>d</sup> Unreliable results. <sup>e</sup> No convergence of energies. <sup>f</sup> Indetermination.

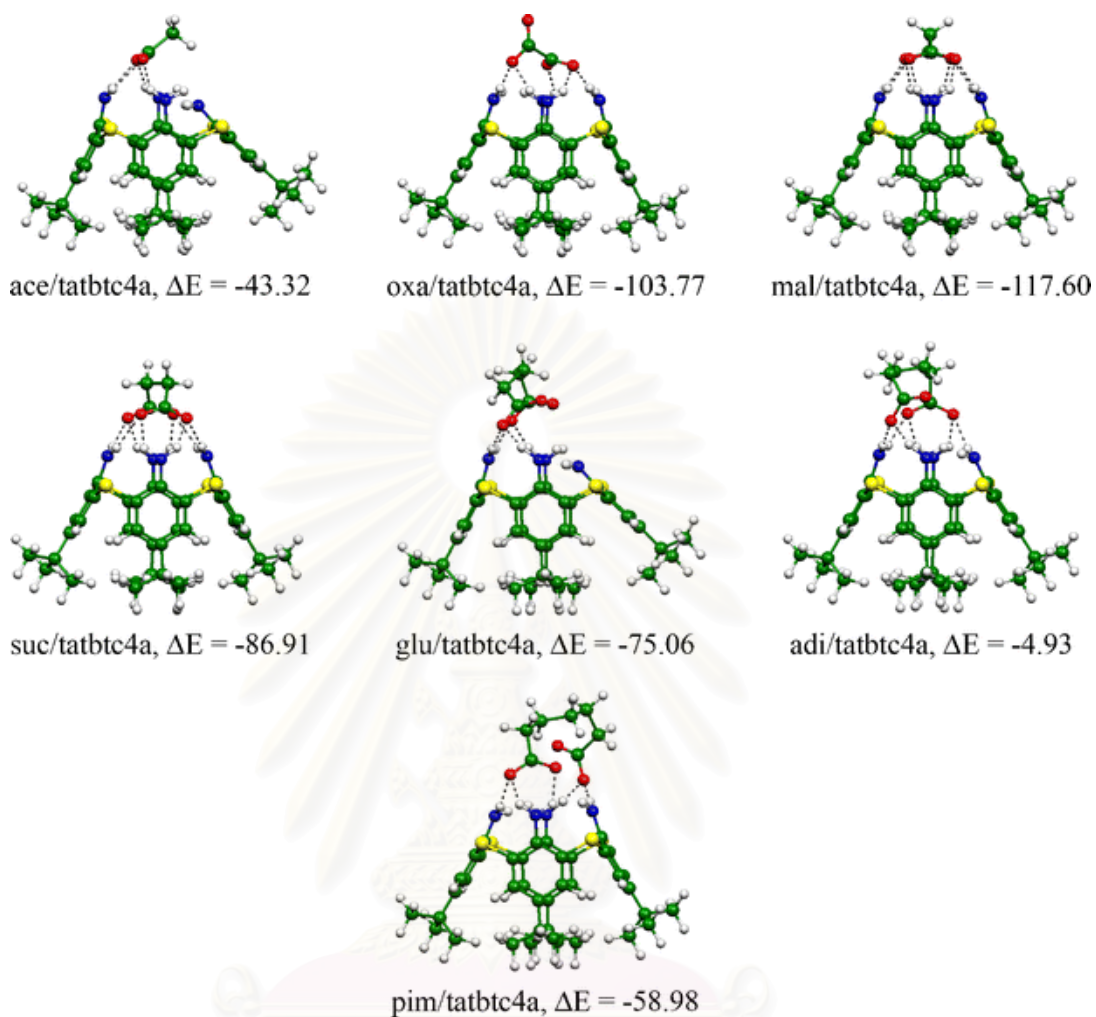


**Figure 3.37** ONIOM(B3LYP/6-31G(d):AM1)-optimized geometries of tetraamino-*p*-*tert*-butylthiacalix[4]arene (tatbtc4a) with carboxylate guests. Binding energies  $\Delta E$  are in kcal/mol.

สถาบันวิทยบริการ  
จุฬาลงกรณ์มหาวิทยาลัย

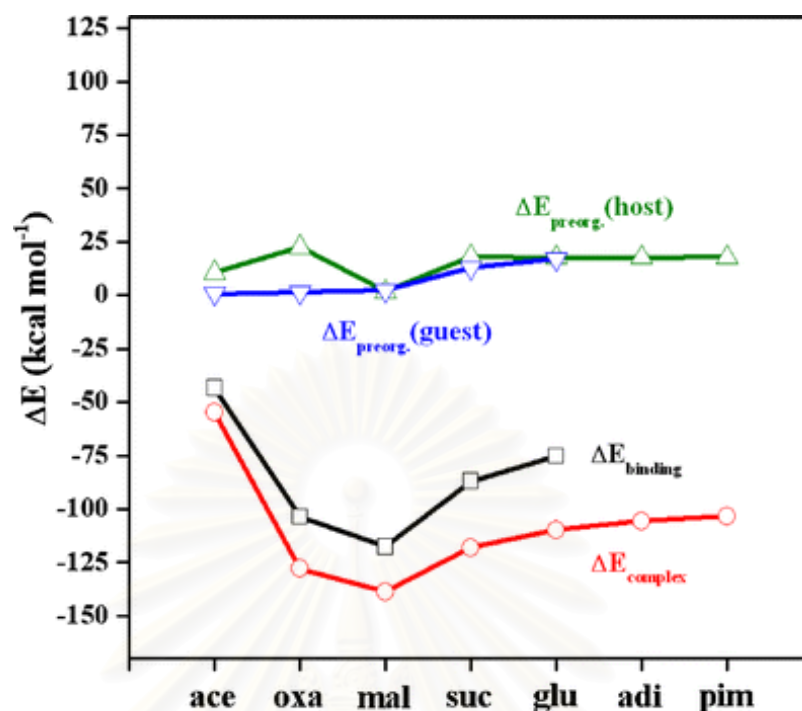


**Figure 3.38** Plots of preorganization energies of tatbtc4a receptor and carboxylates (guests) and their complexation and binding energies against the size of the carboxylate guests, based on the ONIOM(B3LYP/6-31G(d):AM1) method.

### 3.3.3 Complexation properties of amino-*p*-tert-butylcalix[4]arene

Amino-*p*-tert-butylcalix[4]arene (tatbc4a) can form stable complexes with oxalate, malonate, succinate, and glutarate but form weak complexes with acetate and pimelate, as indicated by the binding and Gibbs free energies shown in Table 3.12. The most stable complex is formed with oxalate which is stabilized by  $-67.61$  kcal/mol. The stability of the tatbc4a/carboxylate complex system in decreasing order is: oxalate > malonate > succinate > glutarate > pimelate >> acetate. The ONIOM(B3LYP/6-31G(d):AM1)-optimized geometries of the tatbc4a complexes with carboxylate guests are shown in Figure 3.39. Figure 3.39 shows that the geometries of malonate/tatbc4a and succinate/tatbc4a complexes have the same  $C_2$ -symmetry. Table 3.13 also shows an extreme change in the preorganization energies for the host molecules ( $> 30$  kcal/mol except for the acetate ion, whose energy is 19.27 kcal/mol), and a little change for all guests except adipate and pimelate. The total preorganization energies of all the tatbc4a complexes are higher than 45 kcal/mol

except for the acetate ion (19.94 kcal/mol). The adipate/tatbc4a complex is destabilized by its total preorganization energies (=113.9 kcal/mol) as shown Table 3.13). Plots of the preorganization energies of tatbc4a and its complexation and binding energies against the size of carboxylate guests, based upon the ONIOM(B3LYP/6-31G(d):AM1) method, are shown in Figure 3.40. The BSSE-corrected energies of the tatbc4a complexes computed at the B3LYP/6-31G(d)//ONIOM(B3LYP/6-31G(d):AM1) level (shown in Table 3.14) confirm that the oxalate ion forms the most stable complex with the tatbc4a receptor. According to the B3LYP/6-31G(d)//ONIOM(B3LYP/6-31G(d):AM1)-energy with and without BSSE corrections, the stability of the tatbc4a complexes in decreasing order is: oxalate > malonate > succinate > glutarate > adipate > pimelate.

**Table 3.12** Binding energies, enthalpies, and free energies of association of tetraamino-*p-tert*-butylcalix[4]arene (tatbc4a) and various anionic guests

Guest	$\Delta E_{\text{binding}}^{\text{a}}$	$\Delta H^{298 \text{ a}}$	$\Delta G^{298 \text{ a}}$	$K_B^{\text{acetate}}^{\text{b}}$
acetate	-43.32	-43.61	-28.03	$1.00 \times 10^{00}$
oxalate	-103.77	-104.26	-80.92	$8.12 \times 10^{38}$
malonate	-117.60	-41.35	-84.99	$8.04 \times 10^{41}$
succinate	-86.91	-87.71	-68.80	$9.83 \times 10^{29}$
glutarate	-75.06	-75.64	-58.19	$1.54 \times 10^{22}$
adipate	-4.93	- <sup>c</sup>	- <sup>c</sup>	- <sup>d</sup>
pimelate	-58.98	-60.26	-42.38	$3.62 \times 10^{10}$

<sup>a</sup> In kcal/mol, derived from the ONIOM(B3LYP/6-31G(d):AM1) energies with ZPE corrections. <sup>b</sup> Selectivity coefficient of guests with respect to acetate. <sup>c</sup> Unreliable results due to the ONIOM(B3LYP/6-31G(d):AM1) frequency calculations.

<sup>d</sup> Indetermination.

**Table 3.13** Preorganization energies, corresponding thermodynamics of Tetraamino-*p-tert*-butylthiacalix[4]arene (tatbc4a) receptor (host), carboxylates (guest), and their complexation energies derived at ONIOM (B3LYP/6-31G(d):AM1) calculations

Host/guest	Host			Guest			$\Delta E_{preorg}^{total}$ <sup>a</sup>	$\Delta E_{preorg}$ <sup>a</sup>
	$\Delta E_{preorg}^{host}$ <sup>a</sup>	$\Delta H^{298}$ <sup>a</sup>	$\Delta G^{298}$ <sup>a</sup>	$\Delta E_{preorg}^{guest}$ <sup>b</sup>	$\Delta H^{298}$ <sup>b</sup>	$\Delta G^{298}$ <sup>b</sup>		
tatbc4a/acetate	10.65	10.67	10.99	0.86	0.26	2.79	11.51	-54.83
tatbc4a/oxalate	22.54	21.56	25.01	1.54	1.03	8.66	24.08	-127.85
tatbc4a/malonate	1.84	1.53	2.10	2.47	64.59	3.81	4.31	-138.72
tatbc4a/succinate	18.06	16.55	22.32	13.07	12.91	13.69	31.13	-118.04
tatbc4a/glutarate	17.75	16.31	20.27	17.05	15.87	19.24	34.8	-109.86
tatbc4a/adipate	17.54	16.74	19.03	83.28	83.02	85.53	100.82	-105.75
tatbc4a/pimelate	17.87	17.04	19.85	26.49	25.00	27.93	44.36	-103.34

<sup>a</sup> In kcal/mol, derived at the ONIOM (B3LYP/6-31G(d):AM1) level with ZPE corrections. <sup>b</sup> In kcal/mol, derived at the B3LYP/6-31G(d) level with ZPE corrections.

**Table 3.14** Binding energies of association of the tetraamino-*p-tert*-butylcalix[4]arene (tatbc4a) and various anionic guests and their BSSE corrections values derived from the B3LYP/6-31G(d)//ONIOM (B3LYP/6-31G(d):AM1) calculations and their BSSE corrected values

Guest	$\Delta E_{binding}$ <sup>a</sup>	$\Delta E_{complex}$ <sup>a</sup>	BSSE <sup>a,b</sup>	$\Delta E_{preorg}^{BSSE}$ <sup>a</sup>	$\Delta E_{preorg}^{BSSE}$ <sup>a</sup>	$\Delta E_{preorg}^{BSSE}$ <sup>a</sup>
tatbc4a/acetate	-34.10	-85.60	- <sup>c</sup>	-	-	-
tatbc4a/oxalate	-93.17	-240.76	31.92	-61.26	-208.84	147.59
tatbc4a/malonate	-91.53	-246.99	47.97	-43.56	-199.02	155.46
tatbc4a/succinate	-77.36	-243.25	50.25	-27.11	-193.00	165.90
tatbc4a/glutarate	-70.55	-208.86	34.18	-36.38	-174.68	138.30
tatbc4a/adipate	-64.15	-206.13	34.81	-29.34	-171.32	141.98
tatbc4a/pimelate	-54.41	-213.32	43.75	-10.66	-169.57	158.91

<sup>a</sup> In kcal/mol. <sup>b</sup> The BSSE energy. <sup>c</sup> No convergence. <sup>d</sup> Unreliable results. <sup>e</sup> No convergence of energies. <sup>f</sup> Indetermination.

สถาบันวิทยบริการ  
จุฬาลงกรณ์มหาวิทยาลัย



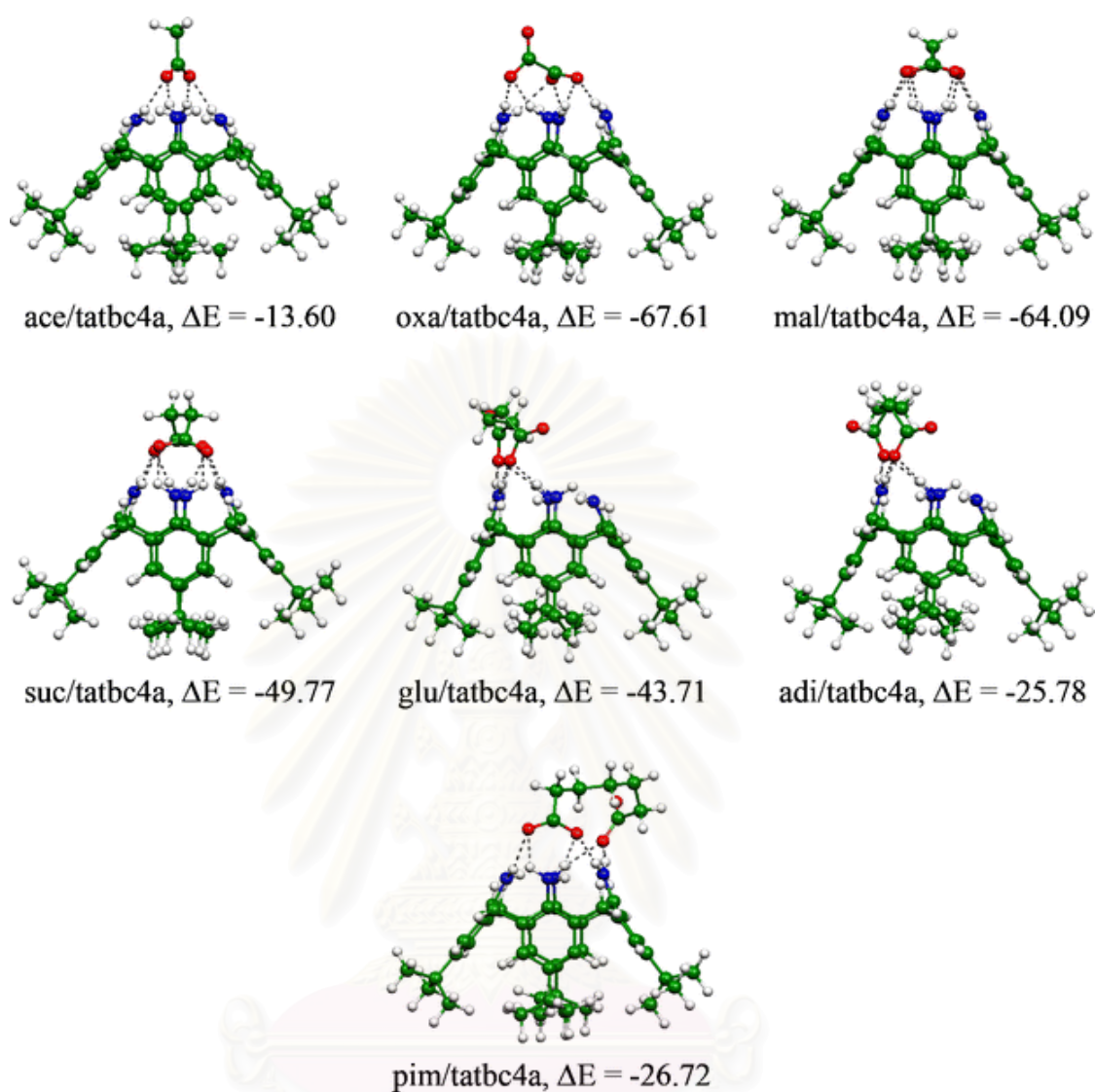


**Figure 3.39** ONIOM(B3LYP/6-31G(d):AM1)-optimized geometries of tetraamino-*p*-*tert*-butylcalix[4]arene (tatbc4a) with carboxylate guests. Binding energies  $\Delta E$  are in kcal/mol.

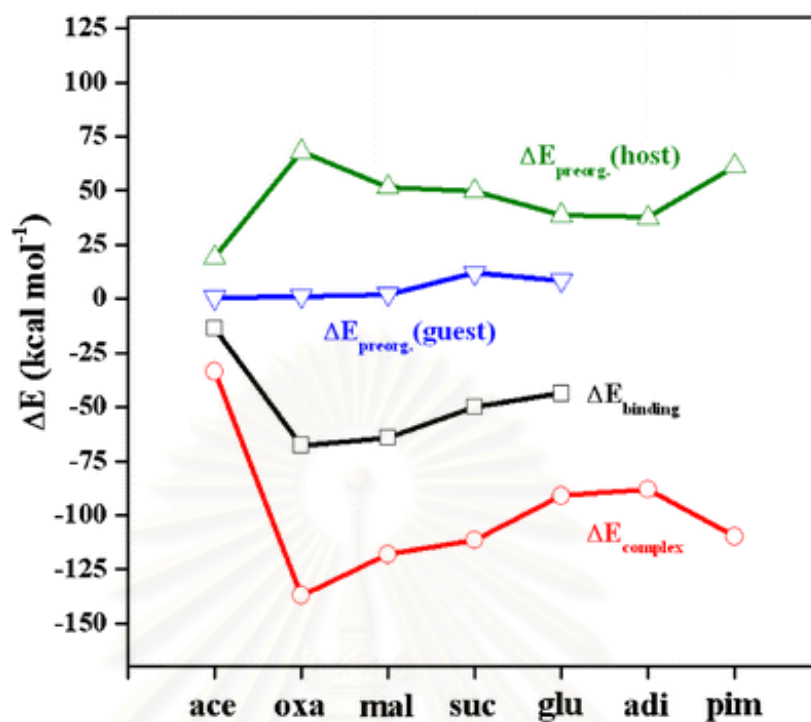


**Figure 3.40** Plots of preorganization energies of tatbc4a receptor and carboxylates (guests) and their complexation and binding energies against the size of the carboxylate guests, based on the ONIOM(B3LYP/6-31G(d):AM1) method.

## CHAPTER IV

### CONCLUSIONS AND SUGGESTIONS

The four typical conformers of thiacalix[4]arene derivatives namely, thiacalix[4]arene **1**, *p-tert*-butylthiacalix[4]arene **2**, mercaptothiacalix[4]arene **3**, mercapto-*p-tert*-butylthiacalix[4]arene **4**, aminothiacalix[4]arene **5**, and amino-*p-tert*-butylthiacalix[4]arene **6** and sulfonylcalix[4]arene derivatives namely sulfonylcalix[4]arene **7**, *p-tert*-butylsulfonylcalix[4]arene **8**, mercaptosulfonylcalix [4]arene **9**, mercapto-*p-tert*-butylsulfonylcalix[4]arene **10**, aminosulfonylcalix[4]arene **11**, and amino-*p-tert*-butylsulfonylcalix[4]arene **12**, have been studied by using the DFT calculation at the B3LYP/6-31G(d) level of theory. The results show that for all thiacalix[4]arene derivatives, the most stable conformers (**1** to **6**) are *cone* and only compound **4** has similar stability of *cone*, *partial cone* and *1,3-alternate* conformers. For sulfonylcalix[4]arene derivatives (**7** to **12**), *1,3-alternate* is found to be the most stable conformer in nearly all derivatives, whereas both *cone* and *partial cone* conformers are found to be the most stable in compound **7**. A number of intramolecular hydrogen bonds at narrow rim are an important factor for the conformational stability. On the other hand, narrow rim substituted groups and *tert*-butyl substituted groups are slightly effective to the conformational stability. The *cone* – *partial cone* interconversions of compound **1**, **3**, **5**, **7**, **9** and **11** have been studied at the B3LYP/6-31G(d) level of theory. The results show that the lower rim substituted groups slightly effect to the rotational barrier of *cone* – *partial cone* interconversions but the bridge types strongly effect. The rotational barrier of thiacalix[4]arene derivatives is higher approximately twice times than sulfonylcalix[4]arene derivatives. As the result, the smaller sulfur (-S-) bridges tent to rotate easier than the bigger sulfonyl (-SO<sub>2</sub>-) bridges. For the HOMO and LUMO orbitals obtained at B3LYP/6-31G(d) level of theory, their shapes and localizations in the cone conformers of both thiacalix[4]arene and sulfonylcalix[4]arene derivatives are finely disperse and very similar.

The stability of selected compounds **7**, **9** and **11**, in solvents (water, chloroform and dichloromethane) has been computed at B3LYP/6-31G(d) level of theory by using the CPCM model. It is found that solvents are slightly effective to

their stabilities, in which the highest stability difference in various solvents at about 2 kcal/mol. is cone conformer for compound **7** and partial cone conformer for compound **9**.

The complexations between zinc(II) ion and the cone conformer of thiacalix[4]arene and sulfonylcalix[4]arene derivatives have been investigated at B3LYP/6-31G(d) level of theory. The result shows that all of complexations are an exothermic process. Furthermore, the complexation between the Zinc(II) ion and thiacalix[4]arene (**1/Zn**) yields the highest energy (ca. -645.97 kcal/mol) which results from the metal-ligand charge transfer (MLCT) effect found on its complex.

The preorganization and binding energies of the receptors tatbtc4a and tatbc4a and seven carboxylate guests (acetate, oxalate, malonate, succinate, glutarate, adipate, and pimelate) and complexation energies of their complexes have been computed using the ONIOM (B3LYP/6-31G(d):AM1) and B3LYP/6-31G(d)//ONIOM(B3LYP/6-31G(d):AM1) methods. Thermodynamic quantities of these complexes have been computed at the ONIOM (B3LYP/6-31G(d):AM1) level of theory. The results show that the relative stability of the tatbtc4a complexes with carboxylates in decreasing order is malonate > oxalate > succinate > glutarate. The relative stability of the tatbc4a complexes with carboxylates in decreasing order is oxalate > malonate > succinate > glutarate > adipate > pimelate. The complexes tatbtc4a/malonate and tatbc4a/oxalate are found to be the most stable species. The selectivity of the tatbtc4a receptor toward to malonate with respect to oxalate, in terms of selectivity coefficient,  $K_{malonate}^{oxalate}$  is  $9.90 \times 10^2$ .

#### **Suggestions for further work:**

The further works should be theoretically studied in the following topics:

1. The spectroscopic properties of thiacalix[4]arene and sulfonylcalix[4]arene derivatives and their zinc(II) complexes.

2. The complexation properties between thiacalix[4]arene and sulfonylcalix[4]arene derivatives and the other metal ions such as alkali, transition metal, lanthanides and actinides.

## REFERENCES

- [1] Vicens, J.; Bohmer, V.; Calixarenes: A Versatile class of compounds; Eds., Kluwer Academic Publishers: Dordrecht, **1991**.
- [2] Asfari, Z.; Böhmer, V.; Harrowfield, J.; Vicens, J. Calixarenes 2001, Eds., Kluwer Academic Publishers, Dordrecht, **2001**.
- [3] Gutsche, C.D.; Stoddart, J.F.; Calixarenes, Monographs in Supramolecular chemistry Vol. 1, Eds. The Royal Society of Chemistry, Cambridge, **1989**.
- [4] Böhmer, V. Calixarenes, macrocycles with (almost) unlimited possibilities, *Angew. Chem. Int. Ed. Engl.* **1995**, 34, 713.
- [5] Ikeda, A.; Shinkai, S. Novel cavity design using calix[n]arene skeletons: Toward molecular recognition and metal binding, *Chem. Rev.* **1997**, 97, 1713.
- [6] Grootenhuis, P.D.J.; Kollman, P.A.; Groenen, L.C.; Reinhoudt, D.N.; van Hummel, G.J.; Ugozzoli, F.; Andreetti, G.D.J. Computational study of the structural, energetic and acid-base properties of calix[4]arenes, *J. Am. Chem. Soc.* **1990**, 112, 4165.
- [7] Sone, T.; Ohba, Y.; Moriya, K.; Kumada, H.; Ito, K. Synthesis and properties of sulfur-bridged analogs of *p-tert*-butylcalix[4]arene, *Tetrahedron* **1997**, 53, 10689.
- [8] Kumagai, H.; Hasegawa, M.; Miyanari, S.; Sugawa, Y.; Sato, Y.; Hori, T.; Ueda, S.; Kamiyama, H. Miyano, S. Facile synthesis of *p-tert*-butylthiacalix[4]arene by the reaction of *p-tert*-butylphenol with elemental sulfur in the presence of a base, *Tetrahedron Lett.* **1997**, 38, 3971.
- [9] Mislin, G.; Graf, E.; Hosseini, M.W.; de Cian, A.; Fischer, J. Sulfone-calixarenes: a new class of molecular building block, *Chem. Commun.* **1998**, 1345.
- [10] Middel, O.; Greff, Z.; Taylor, N.J.; Verboom, W.; Reinhoudt, D.N.; Snieckus, V. The First lateral functionalization of calix[4]arenes by a homologous anionic Ortho-Fries rearrangement, *J. Org. Chem.* **2000**, 65, 667.
- [11] König, B.; Fonseca, M.H. Heteroatom-bridged calixarenes, *Eur. J. Inorg. Chem.* **2000**, 2303.

- [12] Iki, N.; Kumagai, H.; Morohashi, N.; Ejima, K.; Hasegawa, M.; Miyanari, S.; Miyano, S. Selective oxidation of thiacalix[4]arenes to the sulfinyl- and sulfonylcalix[4]arenes and their coordination ability to metal ions Tetrahedron Lett. **1998**, 39, 7559.
- [13] Katagiri, H.; Iki, N.; Hattori, T.; Kabuto, C.; Miyano, S. Calix[4]arenes comprised of aniline units, J. Am. Chem. Soc. **2001**, 123, 779.
- [14] Akdas, H.; Bringel, L.; Graf, E.; Hosseini, M.W.; Mislin, G.; Pansanel, J.; De Cian, A.; Fischer, J. Thiacalixarenes: Synthesis and structural analysis of thiacalix[4]arene and of *p-tert*-butylthiacalix[4]arene, Tetrahedron Lett. **1998**, 39, 2311.
- [15] Iki, N.; Kabuto, C.; Fukushima, T.; Kumagai, H.; Takeya, H.; Miyanari, S.; Miyano, S. Synthesis of *p-tert*-butylthiacalix[4]arene and its inclusion property, Tetrahedron **2000**, 56, 1437.
- [16] Iki, N.; Morohashi, N.; Narumi, F.; Miyano, S.; High complexation ability of thiacalixarene with transition metal ions. the effects of replacing methylene bridges of tetra(*p-t*-butyl)calix[4]arenetetrol by epithio groups” Bull. Chem. Soc. Jpn. **1998**, 71, 1597.
- [17] Iki, N.; Morohashi, N.; Kabuto, C.; Miyano, S. Coordination of epithio groups of *p-tert*-butylthiacalix[4]arene in a  $Zn^{2+}$  complex studied by X-ray crystallography, Chem. Lett. **1999**, 219.
- [18] Mislin, G.; Graf, E.; Hosseini, M.W.; Bilyk, A.; Hall, A.K.; Harrowfield, J.Mc.B.; Skelton, B.W.; White, A.H.; Thiacalixarenes as cluster keepers: synthesis and structural analysis of a magnetically coupled tetracopper(II) square, Chem. Commun. **1999**, 373.
- [19] Lamartine, R.; Bavoux, C.; Vocanson, F.; Martin, A.; Senlis, G.; Perrin, M. Synthesis, X-ray crystal structure and complexation properties towards metal ions of new thiacalix[4]arenes, Tetrahedron Lett. **2001**, 42, 1021.
- [20] Morohashi, N.; Hattori, T.; Yokomakura, K.; Kabuto, C.; Miyano, S., Dinuclear titanium(IV) complex of *p-tert*-butylthiacalix[4]arene as a novel bidentate Lewis acid catalyst, Tetrahedron Lett. **2002**, 43, 7769.

- [21] Morohashi, N.; Iki, N.; Sugawara, A.; Miyano, S. Selective oxidation of thiacalix[4]arenes to the sulfinyl and sulfonyl counterparts and their complexation abilities toward metal ions as studied by solvent extraction Tetrahedron, **2001**, 57, 5557.
- [22] Kajiwara, T.; Yokozawa, S.; Ito, T.; Iki, N.; Morohashi, N.; Miyano, S. Zinc(II) slides on a ligand surface: The X-ray crystal structure and dynamic behavior in solution of [Zn(H2L)(tacn)] Angew. Chem. Int. Ed., **2002**, 41, 2076.
- [23] Morohashi, N.; Iki, N.; Kijiwara, T.; Ito, T.; Miyano, S. Synthesis and structural characterization of a Pd<sup>2+</sup> complex with *p-tert*-butylsulfonylcalix[4]arene Chem. Lett. **2001**, 66.
- [24] Kabuto, C.; Higuchi, Y.; Niimi, T.; Hamada, F.; Iki, N.; Morohashi, N.; Miyano, S. Crystal structures of mono-, di-, and tri(*p-tert*-butyl)-thiacalix[4]arenes: Dimeric self-inclusion behavior, J. Incl. Phenom. Macro. **2002**, 42, 89.
- [25] Atwood, J.L., Barbour, L.J., Jerga, A. Storage of methane and freon by interstitial van der Waals confinement, Science **2002**, 296, 2367.
- [26] Bernardino, R.J.; Cabral, B.J.; Structure and conformational equilibrium of thiacalix[4]arene by density functional theory, J. Mol. Struct. (Theochem), **2001**, 549, 253.
- [27] Ruangpornvisuti, V. Conformational structures, proton affinity of *p-tert*-butylthiacalix[4]arene and its zinc complex" J. Mol. Struct. (Theochem) **2004**, 683, 103.
- [28] Wannoo, B.; Sang-aroon, W.; Tuntulani, T.; Pulpoka, B.; Ruangpornvisuti, V.; Conformational and energetical structures of sulfonylcalix[4]arene, *p-tert*-butylsulfonylcalix[4]arene and their zinc complexes, J. Mol. Struct. (Theochem), **2003**, 629, 137.
- [29] Suwattanamala, A.; Magalhães, A.L.; Gomes, J.A.N.F. Structure and conformational equilibrium of new thiacalix[4]arene derivatives, Chem. Phys. Lett. **2004**, 385, 368.
- [30] Grant, G.H.; Richards W.G. Computational chemistry, Oxford, **1995**.
- [31] Jensen, F. Introduction to computational chemistry, John Wiley & Sons, **1999**.

- [32] Young, D. Computational chemistry: A Practical guide for applying techniques to real world problems, John Wiley & Sons, **2001**.
- [33] Cramer, C.J. Essentials of computational chemistry, John Wiley & Sons, **2002**.
- [34] Rogers, D. Computational chemistry using the PC, 3<sup>rd</sup> Ed. John Wiley & Sons, **2003**.
- [35] Atkins, P.W. Quanta 2<sup>nd</sup> ed. Oxford University, **1991**.
- [36] Levine, I. N. Quantum chemistry, Prentice Hall, **1991**.
- [37] Atkins, P.W.; Friedman R.S. Molecular quantum mechanics, Oxford, **1997**.
- [38] Ziegler, T. Approximate density functional theory as a practical tool in molecular, Chem. Rev. **1991**, 91, 651.
- [39] Matsubara, T.; Sieber, S.; Morokuma, K. A test of the new integrated MO + MM (IMOMM) method for the conformational energy of ethane and *n*-butane, Int. J. Quant. Chem. **1996**, 60, 1101.
- [40] Musaev, D.G.; Froese, R.D.J.; Morokuma, K. Molecular orbital and IMOMM studies of the chain transfer mechanisms of the diimine-M(II), (M=Ni, Pd) catalyzed ethylene polymerization reaction, Organometallics, **1998**, 17, 1850.
- [41] Froese, R.D.J.; Musaev, D.G.; Morokuma, K. A theoretical study of substituent effects in the diimine-M(II) catalyzed ethylene polymerization reaction using the IMOMM method, J. Am. Chem. Soc. **1998**, 120, 1581.
- [42] Humbel, S.; Sieber, S.; Morokuma, K. The IMOMO method: integration of different levels of molecular orbital approximations for geometry optimization of large systems. Test for *n*-butane conformation and SN<sub>2</sub> reaction: RCl + Cl<sup>-</sup>, J. Chem. Phys. **1996**, 105, 1959.
- [43] Svensson, M.; Humbel, S.; Froese, R.D.J.; Matsubara, T.; Sieber, S.; Morokuma, K. ONIOM: A multilayered integrated MO+MM method for geometry optimizations and single point energy predictions. A test for Diels-Alder reactions and Pt(P(*t*-Bu)<sub>3</sub>)<sub>2</sub> + H<sub>2</sub> oxidative addition, J. Phys. Chem. **1996**, 100, 19357.
- [44] Froese, R.D.J.; Morokuma, K. Accurate calculations of bond breaking energies in C<sub>60</sub> using the three-layered ONIOM method, Chem. Phys. Lett. **1999**, 305, 419.



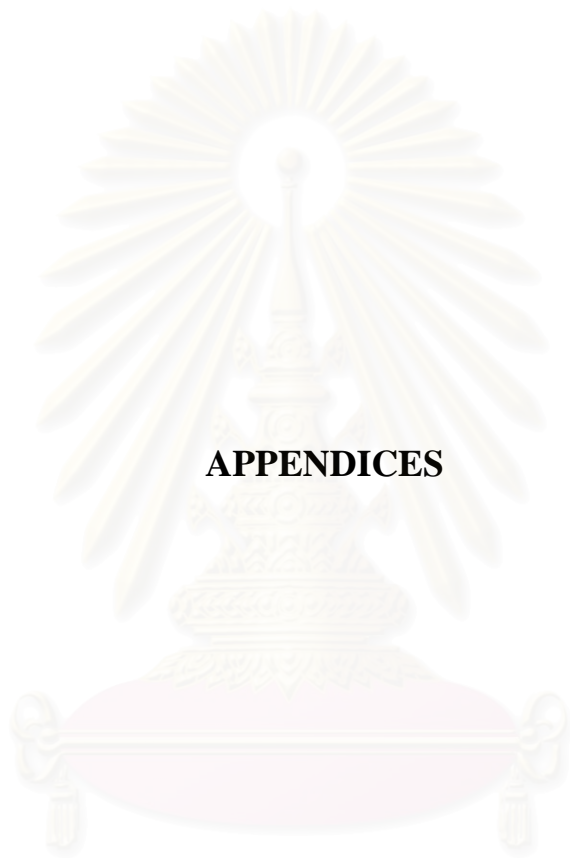
- [45] Boys, S.F., Bernardi, F. The calculations of small molecular interaction by the difference of separate total energies - some procedures with reduced error, *Mol. Phys.* **1970**, 19, 553.
- [46] Atkins, P.W. *Physical chemistry*, 5<sup>th</sup> ed. Oxford University Press, Oxford, UK, **1994**.
- [47] McQuarrie, D.A. *Statistical mechanics*, Harper & Row, New York, 1973.
- [48] Becke, D. Density-functional exchange-energy approximation with correct asymptotic behavior, *Phys. Rev. A*, **1988**, 38, 3098.
- [49] Lee, C.; Yang, W.; Parr, R.G. Development of the Colle-Salvetti correlation-energy formula into a functional of the electron density, *Phys. Rev. B*, **1988**, 37, 785.
- [50] Barone, V.; Cossi, M.; Tomasi, J. Analytical second derivatives of the free energy in solution by polarizable continuum models, *J. Comput. Chem.* **1998**, 19, 404.
- [51] Cossi, M.; Barone, V. Analytical second derivatives of the free energy in solution by polarizable continuum models, *J. Chem. Phys.* **1998**, 109, 6246.
- [52] Frisch M.J. et al., *Gaussian 03*, Revision D.02, Gaussian, Inc., Wallingford, CT, **2006**.
- [53] Schaftenaar, G. *MOLDEN 4.2*: CAOS/CAMM Center Nijmegen, Toernooiveld, Nijmegen, Netherlands, **1991**.
- [54] Dennington II, R.; Keith, T.; Millam, J.; Eppinnett, K.; Hovell W.L.; Gilliland, R. *GaussView*, Version 3.00, Semichem Inc., Shawnee Mission, KS, **2003**.
- [55] Flükiger, P.; Lüthi, H.P.; Portmann S.; Weber, J. *Molekel 4.3*: Swiss Center for Scientific Computing, Manno, Switzerland, **2000**.
- [56] Sabin, J.R.; Trickey, S.B.; Apell, S.P.; Oddershede, J. Molecular shape, capacitance, and chemical hardness, *Int. J. Quantum Chem.* **2000**, 77(1), 358.
- [57] Koopmans, T. Ordering of wave functions and eigenenergies to the individual electrons of an atom, *Physica*, **1933**, 1, 104.

- [58] Kato, R.; Nishizawa, S.; Hayashita, T.; Teramae, N. A thiourea-based chromoionophore for selective binding and sensing of acetate. *Tetrahedron Lett.* **2001**, 42, 5053.
- [59] Lee, D.H.; Lee, K.H., Hong, J.-I. An azophenol-based chromogenic anion sensor, *Org. Lett.* **2001**, 3, 5.
- [60] Lee, D.H.; Lee, H.Y., Lee, K.H., Hong, J.-I. Selective anion sensing based on a dual-chromophore approach, *Chem. Comm.* **2001**, 13, 1188.
- [61] Lee, D.H.; Lee, H.Y., Hong, J.-I. Anion sensor based on the indoaniline–thiourea system, *Tetrahedron Lett.* **2002**, 43, 7273.
- [62] Baerriqter, H.; Grave, L.; Nissink, WM.; Chrisstoffels, L.A.J.; Vander Maas, J.H.; Verboom, W.; de Jong, F.; Reindoudt, D.N. (Thio)urea resorcinarene cavitands. complexation and membrane transport of halide anions, *Org. Chem.* **1998**, 63, 4174.
- [63] Fan, E.; Van, Arman S.A.; Kincaid, D.; Hamilton, A.D. Molecular recognition: hydrogen-bonding receptors that function in highly competitive solvents, *J. Am. Chem. Soc.* **1993**, 115, 369.
- [64] Lee, K.H.; Hong, J.-I. C<sub>3</sub>-Symmetric metacyclophane-based anion receptors with three thiourea groups as linkers between aromatic groups, *Tetrahedron Lett.* **2000**, 41, 6083.
- [65] Ruangpornvisuti, V. Recognition of carboxylate and dicarboxylates by azophenol–thiourea derivatives: a theoretical host–guest investigation, *J. Mol. Struct. (Theochem)* **2004**, 686, 47.
- [66] Maseras F.; Morokuma, K. IMOMM: A new integrated ab initio + molecular mechanics geometry optimization scheme of equilibrium structures and transition states, *J. Comput. Chem.* **1995**, 16, 1170.
- [67] Dewar, M.J.S.; Reynolds, C.H. An improved set of mndo parameters for sulfur, *J. Comput. Chem.* **1986**, 2, 140.
- [68] Stewart, J.J.P. Optimization of parameters for semiempirical methods I. Method, *J. Comput. Chem.*, **1989**, 10, 209.
- [69] Dewar M.J.S.; Thiel W. Ground states of molecules. 38. The MNDO method. Approximations and parameters, *J. Am. Chem. Soc.* **1977**, 99, 4899.

- [70] Dapprich, S.; Komaromi, I.; Byun, K.S.; Morokuma, K.; Frisch, M.J. A new ONIOM implementation in Gaussian98. Part I. The calculation of energies, gradients, vibrational frequencies and electric field derivatives, *J. Mol. Struct. (Theochem)* **1999**, 461, 1.
- [71] Remko, M.; Walsh, O.A.; Richards, W.G. Theoretical study of molecular structure, tautomerism, and geometrical isomerism of moxonidine: Two-layered ONIOM calculations, *J. Phys. Chem. A* **2001**, 105, 6926.
- [72] Remko, M. The gas-phase acidities of substituted hydroxamic and silahydroxamic acids: A Comparative *ab initio* study, *J. Phys. Chem. A* **2002**, 106, 5005.



สถาบันวิทยบริการ  
จุฬาลงกรณ์มหาวิทยาลัย



**APPENDICES**

สถาบันวิทยบริการ  
จุฬาลงกรณ์มหาวิทยาลัย

## APPENDIX I

**Table S1** Relative energies,  $\Delta E_{rel}$  of thiacalix[4]arene derivatives obtained at the B3LYP/6-31G(d)//B3LYP/6-31G(d) level of theory

Compound/conformer	$\Delta E_{rel}$ (kcal/mol)
thiacalix[4]arenes (1)	
<i>cone</i>	0.00 (-2817.84147076)
<i>partial cone</i>	10.69
1,2- <i>alternate</i>	14.80
1,3- <i>alternate</i>	14.82
<i>p-tert</i> -butylthiacalix[4]arenes (2)	
<i>cone</i>	0.00 (-3446.86233936)
<i>partial cone</i>	10.67
1,2- <i>alternate</i>	14.51
1,3- <i>alternate</i>	15.86
tetramercaptothiacalix[4]arenes (3)	
<i>cone</i>	0.00 (-4109.65826205)
<i>partial cone</i>	1.76
1,2- <i>alternate</i>	5.16
1,3- <i>alternate</i>	1.97
tetramercapto- <i>p-tert</i> -butylthiacalix[4]arenes (4)	
<i>cone</i>	0.04
<i>partial cone</i>	0.41
1,2- <i>alternate</i>	3.30
1,3- <i>alternate</i>	0.00 (-4738.67759456)
tetraaminothiacalix[4]arenes (5)	
<i>cone</i>	0.00 (-2738.37295369)
<i>partial cone</i>	1.39
1,2- <i>alternate</i>	6.51
1,3- <i>alternate</i>	4.00
tetraamino- <i>p-tert</i> -butylthiacalix[4]arenes (6)	
<i>cone</i>	0.00 (-3367.39294758)
<i>partial cone</i>	1.28
1,2- <i>alternate</i>	6.17
1,3- <i>alternate</i>	3.86

**Table S2** Relative energies,  $\Delta E_{rel}$  of sulfonylcalix[4]arene derivatives obtained at the B3LYP/6-31G(d)//B3LYP/6-31G(d) level of theory derivatives

Compound/conformer	$\Delta E_{rel}$ (kcal/mol)
sulfonylcalix[4]arenes ( <b>7</b> )	
<i>cone</i>	0.16
<i>partial cone</i>	0.00 (-3419.34518)
1,2- <i>alternate</i>	1.49
1,3- <i>alternate</i>	5.83
<i>p-tert</i> -butylsulfonylcalix[4]arenes ( <b>8</b> )	
<i>cone</i>	4.55
<i>partial cone</i>	4.84
1,2- <i>alternate</i>	12.32
1,3- <i>alternate</i>	0.00 (-4048.37773)
tetramercaptosulfonylcalix[4]arenes ( <b>9</b> )	
<i>cone</i>	6.79
<i>partial cone</i>	1.49
1,2- <i>alternate</i>	5.03
1,3- <i>alternate</i>	0.00 (-4711.15198)
tetramercapto- <i>p-tert</i> -butylsulfonylcalix[4]arenes ( <b>10</b> )	
<i>cone</i>	10.79
<i>partial cone</i>	4.65
1,2- <i>alternate</i>	8.02
1,3- <i>alternate</i>	0.00 (-5340.18536)
mercaptosulfonylcalix[4]arenes ( <b>11</b> )	
<i>cone</i>	9.13
<i>partial cone</i>	3.03
1,2- <i>alternate</i>	13.75
1,3- <i>alternate</i>	0.00 (-3339.91320)
tetraamino- <i>p-tert</i> -butylsulfonylcalix[4]arenes ( <b>12</b> )	
<i>cone</i>	3.19
<i>partial cone</i>	1.15
1,2- <i>alternate</i>	10.58
1,3- <i>alternate</i>	0.00 (-3968.93349)

**Table S3** Relative energies,  $\Delta E_{rel}$  (in kcal/mol) of the B3LYP/6-31G(d)-optimized conformers of sulfonylcalix[4]arene derivatives obtained at different levels of theory, the total energies (in au) of the most stable conformer are shown in parentheses

Compound /conformer	B3LYP/6-31G(d) <sup>a</sup>	B3LYP/6-31G(d,p) <sup>a</sup>	B3LYP/6-311G(d,p) <sup>a</sup>	H <sub>2</sub> O <sup>b</sup>	CHCl <sub>3</sub> <sup>b</sup>	CH <sub>2</sub> Cl <sub>2</sub> <sup>b</sup>
sulfonylcalix[4]arenes (7)						
<i>cone</i>	0.16	0.24	0.11	1.82	0.84	1.21
<i>partial cone</i>	0.00 (-3419.34518)	0.00 (-3419.38727)	0.00 (-3419.92755)	0.53	0.11	0.78
1,2- <i>alternate</i>	1.49	1.53	1.38	0.00	0.00	0.00
1,3- <i>alternate</i>	5.83	5.54	5.01	3.87	4.26	4.58
tetramercaptosulfonylcalix[4]arenes (9)						
<i>cone</i>	6.79	7.18	6.53	7.32	7.82	8.21
<i>partial cone</i>	1.49	1.86	1.72	3.00	2.87	3.40
1,2- <i>alternate</i>	5.03	5.41	4.87	5.88	5.93	6.45
1,3- <i>alternate</i>	0.00 (-4711.15198)	0.00 (-4711.18625)	0.00 (-4711.73952)	0.00	0.00	0.00
mercaptosulfonylcalix[4]arenes (11)						
<i>cone</i>	9.13	9.40	9.17	9.18	9.19	9.00
<i>partial cone</i>	3.03	3.15	3.53	2.17	2.64	2.65
1,2- <i>alternate</i>	13.75	13.87	14.17	11.53	12.14	11.52
1,3- <i>alternate</i>	0.00 (-3339.91320)	0.00 (-3339.96131)	0.00 (-3340.47141)	0.00	0.00	0.00

<sup>a</sup> The single-point calculation of the B3LYP/6-31G(d)-optimized geometry. <sup>b</sup> The single-point CPCM calculations ( $\epsilon=78.4$  for water,  $\epsilon=4.9$  for chloroform and  $\epsilon=8.94$  for dichloromethane) at the B3LYP/6-31G(d) level.

## APPENDIX II

**Table S4** Dipole moments (in debye) of the B3LYP/6-31G(d)-optimized conformers of sulfonylcalix[4]arene derivatives obtained at different levels of theory

Compound /conformer	Dipole moment					
	B3LYP/6- 31G(d) <sup>a</sup>	B3LYP/6- 31G(d,p) <sup>a</sup>	B3LYP/6- 311G(d,p) <sup>a</sup>	H <sub>2</sub> O <sup>b</sup>	CHCl <sub>3</sub> <sup>b</sup>	CH <sub>2</sub> Cl <sub>2</sub> <sup>b</sup>
sulfonylcalix[4]arenes (7)						
<i>cone</i>	11.236	11.188	11.982	15.892	14.715	15.290
<i>partial cone</i>	7.464	7.438	7.902	10.463	9.699	10.053
<i>1,2-alternate</i>	0.001	0.001	0.001	0.005	0.011	0.017
<i>1,3-alternate</i>	0.000	0.000	0.000	0.005	0.006	0.008
mercaptosulfonylcalix[4]arenes (9)						
<i>cone</i>	9.387	9.327	9.593	14.950	13.422	14.112
<i>partial cone</i>	5.375	5.349	5.528	8.366	7.527	7.932
<i>1,2-alternate</i>	1.353	1.352	1.326	1.891	1.745	1.809
<i>1,3-alternate</i>	0.001	0.001	0.001	0.038	0.053	0.0367
mercaptosulfonylcalix[4]arenes (11)						
<i>cone</i>	5.431	5.445	6.098	7.4583	6.943	7.177
<i>partial cone</i>	2.912	2.904	3.252	4.042	3.854	3.979
<i>1,2-alternate</i>	0.004	0.004	0.004	0.006	0.012	0.005
<i>1,3-alternate</i>	0.001	0.001	0.001	0.002	0.018	0.029

<sup>a</sup> The single-point calculation of the B3LYP/6-31G(d)-optimized geometry. <sup>b</sup> The single-point CPCM calculations ( $\epsilon=78.4$  for water,  $\epsilon=4.9$  for chloroform and  $\epsilon=8.94$  for dichloromethane) at the B3LYP/6-31G(d) level.

สถาบันวิทยบริการ  
จุฬาลงกรณ์มหาวิทยาลัย



**Table S5** The  $E_{LUMO}$  and  $E_{HOMO}$  energies and frontier molecular orbital energy gap,  $\Delta E_{HOMO-LUMO}$  of typical conformers of thiacalix[4]arene derivatives computed at B3LYP/6-311G(d,p)//B3LYP/6-31G(d) level of theory

Compound/conformer	$E_{LUMO}^a$	$E_{HOMO}^a$	$\Delta E_{HOMO-LUMO}^a$	$\eta^{a,b}$	$\mu^{a,c}$	$\chi^{a,d}$
thiacalix[4]arenes (1)						
<i>cone</i>	-1.116	-6.368	5.252	2.626	-3.742	3.742
<i>partial cone</i>	-1.088	-6.041	4.953	2.476	-3.565	3.565
<i>1,2-Alternate</i>	-1.007	-5.687	4.680	2.340	-3.347	3.347
<i>1,3-Alternate</i>	-1.007	-6.068	5.061	2.531	-3.538	3.538
<i>p-tert-butylthiacalix[4]arenes (2)</i>						
<i>cone</i>	-0.980	-6.068	5.089	2.544	-3.524	3.524
<i>partial cone</i>	-0.952	-5.823	4.871	2.435	-3.388	3.388
<i>1,2-Alternate</i>	-0.980	-5.633	4.653	2.327	-3.306	3.306
<i>1,3-Alternate</i>	-0.871	-5.823	4.953	2.476	-3.347	3.347
mercaptothiacalix[4]arenes (3)						
<i>cone</i>	-1.252	-5.823	4.572	2.286	-3.538	3.538
<i>partial cone</i>	-1.170	-5.932	4.762	2.381	-3.551	3.551
<i>1,2-Alternate</i>	-1.170	-5.905	4.735	2.367	-3.538	3.538
<i>1,3-Alternate</i>	-1.088	-6.068	4.980	2.490	-3.578	3.578
<i>p-tert-butylmercaptothiacalix[4]arenes (4)</i>						
<i>cone</i>	-1.116	-5.633	4.517	2.259	-3.374	3.374
<i>partial cone</i>	-1.034	-5.742	4.708	2.354	-3.388	3.388
<i>1,2-Alternate</i>	-1.007	-5.769	4.762	2.381	-3.388	3.388
<i>1,3-Alternate</i>	-0.952	-5.823	4.871	2.435	-3.388	3.388
aminothiacalix[4]arenes (5)						
<i>cone</i>	-0.871	-5.361	4.490	2.245	-3.116	3.116
<i>partial cone</i>	-0.925	-5.252	4.327	2.163	-3.089	3.089
<i>1,2-Alternate</i>	-1.007	-5.361	4.354	2.177	-3.184	3.184
<i>1,3-Alternate</i>	-1.088	-5.714	4.626	2.313	-3.401	3.401
<i>p-tert-butylaminothiacalix[4]arenes (6)</i>						
<i>cone</i>	-0.789	-5.197	4.408	2.204	-2.993	2.993
<i>partial cone</i>	-0.844	-5.116	4.272	2.136	-2.980	2.980
<i>1,2-Alternate</i>	-0.898	-5.197	4.299	2.150	-3.048	3.048
<i>1,3-Alternate</i>	-0.980	-5.551	4.572	2.286	-3.265	3.265

<sup>a</sup> In eV. <sup>b</sup> Chemical hardness,  $\eta = \Delta E_{HOMO-LUMO}/2$ . <sup>c</sup> Electronic chemical potential,  $\mu = (E_{HOMO} + E_{LUMO})/2$ . <sup>d</sup> The Mulliken electronegativity,  $\chi = -(E_{HOMO} + E_{LUMO})/2$ .

**Table S6** The  $E_{LUMO}$  and  $E_{HOMO}$  energies and frontier molecular orbital energy gap,  $\Delta E_{HOMO-LUMO}$  of typical conformers of thiacalix[4]arene derivatives computed at B3LYP/6-311G(d,p)//B3LYP/6-31G(d) level of theory

Compound/conformer	$E_{LUMO}^a$	$E_{HOMO}^a$	$\Delta E_{HOMO-LUMO}^a$	$\eta^{a,b}$	$\mu^{a,c}$	$\chi^{a,d}$
sulfonylcalix[4]arenes (7)						
<i>cone</i>	-2.395	-7.075	4.680	2.340	-4.735	4.735
<i>partial cone</i>	-2.395	-7.048	4.653	2.327	-4.721	4.721
<i>1,2-Alternate</i>	-2.422	-7.184	4.762	2.381	-4.803	4.803
<i>1,3-Alternate</i>	-2.449	-7.238	4.789	2.395	-4.844	4.844
<i>p-tert-butylsulfonylcalix[4]arenes (8)</i>						
<i>cone</i>	-2.177	-6.694	4.517	2.259	-4.435	4.435
<i>partial cone</i>	-2.123	-6.748	4.626	2.313	-4.435	4.435
<i>1,2-Alternate</i>	-2.123	-6.830	4.708	2.354	-4.476	4.476
<i>1,3-Alternate</i>	-2.095	-6.776	4.680	2.340	-4.435	4.435
mercaptosulfonylcalix[4]arenes (9)						
<i>cone</i>	-2.313	-6.776	4.463	2.231	-4.544	4.544
<i>partial cone</i>	-2.286	-6.830	4.544	2.272	-4.558	4.558
<i>1,2-Alternate</i>	-2.395	-6.803	4.408	2.204	-4.599	4.599
<i>1,3-Alternate</i>	-2.286	-6.966	4.680	2.340	-4.626	4.626
<i>p-tert-butylmercaptosulfonylcalix[4]arenes (10)</i>						
<i>cone</i>	-2.095	-6.395	4.299	2.150	-4.245	4.245
<i>partial cone</i>	-2.068	-6.558	4.490	2.245	-4.313	4.313
<i>1,2-Alternate</i>	-2.095	-6.422	4.327	2.163	-4.259	4.259
<i>1,3-Alternate</i>	-1.986	-6.721	4.735	2.367	-4.354	4.354
aminosulfonylcalix[4]arenes (11)						
<i>cone</i>	-2.204	-6.177	3.973	1.986	-4.191	4.191
<i>partial cone</i>	-2.068	-6.449	4.381	2.191	-4.259	4.259
<i>1,2-Alternate</i>	-2.150	-6.395	4.245	2.123	-4.272	4.272
<i>1,3-Alternate</i>	-2.123	-6.422	4.299	2.150	-4.272	4.272
<i>p-tert-butylaminosulfonylcalix[4]arenes (12)</i>						
<i>cone</i>	-1.905	-6.204	4.299	2.150	-4.055	4.055
<i>partial cone</i>	-1.905	-6.177	4.272	2.136	-4.041	4.041
<i>1,2-Alternate</i>	-1.959	-6.177	4.218	2.109	-4.068	4.068
<i>1,3-Alternate</i>	-1.905	-6.150	4.245	2.123	-4.027	4.027

<sup>a</sup> In eV. <sup>b</sup> Chemical hardness,  $\eta = \Delta E_{HOMO-LUMO}/2$ . <sup>c</sup> Electronic chemical potential,  $\mu = (E_{HOMO} + E_{LUMO})/2$ . <sup>d</sup> The Mulliken electronegativity,  $\chi = -(E_{HOMO} + E_{LUMO})/2$ .

## BIOGRAPHY

**NAME, NICKNAME** : Mr. Banchob Wanno, BJ  
**BIRTH DATE** : August 16<sup>th</sup>, 1972  
**BIRTH PLACE** : Roi-Et Province, Thailand  
**EDUCATION** : 

YEAR	INSTITUTION	DEGREE
1990	Suwannaphumtayapaisarn	High School
1994	Maharakham Univ.	B.Sc. (Chemistry)
1999	Mahidol Univ.	M.Sc. (Physical Chemistry)
2007	Chulalongkorn Univ.	Ph.D. (Chemistry)

  
**ADDRESS** : 8 Moo 1, Baan Hang-Wah, Huachang Subdistrict,  
Suwannaphum District, Roi-Et, 45130, Thailand.  
**E-MAIL** : banchobw@gmail.com, banchobw@hotmail.com

## PUBLICATIONS

- [1] Ruangpornvisuti V.; Supakornchailert, K.; Tungchitpienchai, C.; **Wanno B.** Struct. Chem. **2007**, *In Press*.
- [2] **Wanno, B.**; Du, A.J.; Ruangpornvisuti, V.; Smith, S.C. Chem. Phys. Lett. **2007**, 436, 218-223.
- [3] Ruangpornvisuti, V.; **Wanno, B.** J. Mol. Model. **2007**, 13, 65-77.
- [4] **Wanno, B.**; Ruangpornvisuti, V. J. Mol. Struct. (*Theochem*) **2006**, 775, 113-120.
- [5] **Wanno, B.**; Ruangpornvisuti, V. J. Mol. Struct. (*Theochem*) **2006**, 766, 159-164.
- [6] Ruangpornvisuti, V.; Supakornchailert, K.; Tungchitpienchai, C.; **Wanno B.** Struct. Chem. **2006**, 17, 27-34.
- [7] **Wanno, B.**; Ruangpornvisuti, V. J. Mol. Struct. **2006**, 787, 76-89.
- [8] **Wanno, B.**; Ruangpornvisuti, V. Chem. Phys. Lett. **2005**, 415, 176-182.
- [9] Thipyapong, K.; Yasarawan, N.; Wanno, B.; Arano, Y.; Ruangpornvisuti, V. J. Mol. Struct. (*Theochem*) **2005**, 755, 45-53.
- [10] **Wanno, B.**; Ruangpornvisuti, V. J. Mol. Struct. (*Theochem*) **2004**, 685, 57-71.
- [11] Ruangpornvisuti, V.; Wanno, B. J. Mol. Model. **2004**, 10, 418-426.
- [12] **Wanno, B.**; Sang-aroon, W.; Tuntulani, T.; Polpoka, B.; Ruangpornvisuti, V. **2003**, 629, 137-150.